NASA Technical Paper 2933

1989

Static Internal Performance of a Nonaxisymmetric Vaned Thrust Reverser With Flow Splay Capability

Linda S. Bangert
and Laurence D. Leavitt
Langley Research Center
Hampton, Virginia

NASA
National Aeronautics and Space Administration
Office of Management
Scientific and Technical Information Division

Summary

An investigation was conducted in the static-test facility of the Langley 16-Foot Transonic Tunnel on a dual-port, nonaxisymmetric, block-and-turn type thrust reverser model. Vane cascades in the reverser ports turned the flow in the splay (or lateral) direction and aided in turning the flow in the reverse direction. Splaying reverser flow is a method of delaying to lower landing ground roll speeds the reingestion of hot exhaust flow into the inlets. Exhaust flow splay can also help prevent the impingement of hot exhaust gases on the empennage surfaces when the reverser is integrated into an actual airframe. The vane cascades consisted of two sets of perpendicular vanes with a variable number of reversing and splay vanes. A skewed vane cascade was also tested which had only one set of vanes angled to provide both reversing and splay. Vane cascades were designed to provide different amounts of flow splay in the top and bottom ports. Inner doors, trim tabs, and an orifice plate all provided means of varying the port area for reverser flow modulation. The outer door position was varied as a means of influencing the flow reverse angle. Nozzle pressure ratio was varied from 1.75 to approximately 6.

Results of this study indicate that reverse and splay vector angles achieved were higher than the corresponding geometric angles. The larger reverse angles are caused by the exhaust flow attaching to the outer door. As a result, the normal force generated is smaller than expected because it is traded for a larger than expected axial force. The computed splay vector angles are larger than expected since the normal force was smaller (than expected) relative to the side force generated. Both reverse and splay angles were a function of nozzle pressure ratio (NPR). Decreasing the port area with flow modulation devices (the inner door, the trim tabs, or the orifice plate) had very little effect on the reverse and splay vector angles but did have a marked effect on discharge coefficient and static pressure ratios in the reverser port. Decreasing the number of splay vanes decreased the splay vector angle with essentially no effect on reverse vector angle or overall performance. The skewed vane cascade provided less splay vectoring than the baseline configuration but a higher discharge coefficient. If high discharge coefficients are a requirement in the reverser port, nearly equal areas in the port and vanes is a design condition that should be avoided. If sidewalls are present and the splay vector angle is high enough for the flow to impinge on these sidewalls, turning losses can cause a loss in resultant thrust ratio as well as a decreased splay vector angle. The outer door does provide an effective means of making minor adjustments to the reverse vector angle, but the number and spacing of reversing vanes in the vane cascade has little effect on reverse vector angle.

Introduction

The design requirements for the next generation of fighter aircraft may include the ability to land on short or bomb-damaged runways. This capability will likely require the addition of thrust reversing to nozzle designs. Not only will this thrust reversing be used for reduction of landing ground roll distances but also will be needed for effective control of aircraft flight path during the landing/approach phase to allow for precision touchdown. Partial deployment of thrust reversers allows the engine to remain at high thrust levels (eliminating the need for extra engine spool-up time) immediately prior to touchdown in case wave-off or some other major flight-path adjustment is necessary.

Several research programs have addressed the central problems associated with the use of thrust reversers at landing/approach conditions (refs. 1 to 10). In general, thrust reverser effects on airplane stability and control are somewhat configuration dependent but may often be attributed to specific occurrences such as reverser flow blockage of the free-stream flow over tail surfaces, impingement of reverser flow on empennage surfaces, and entrainment of the free-stream flow by reverser exhaust flow.

In addition to the stability and control problems mentioned, consideration must be given to the possible reingestion of hot exhaust gases into the engine inlets. (See ref. 11.) Reingested gases can generate temperature and pressure distortion levels at the compressor face which could stall the compressor and cause possible engine damage. Susceptibility to reingestion of reverser exhaust flow is a function of such parameters as aircraft forward airspeed, height above the ground, inlet suction characteristics (hence local aerodynamic characteristics adjacent to the inlet), proximity of reverser port to the inlet, engine mass flow, and of course, reverser efflux angle (angle of the projection of reverser exhaust flow in the normal/axial force plane). The aircraft velocity at which the reingestion of reverser exhaust flow occurs dictates the amount of useful reverse thrust available for the reduction of landing ground roll. Obviously, the longer full reverse thrust can be maintained during the ground roll phase, the shorter the landing ground roll distance.

One method, which has been shown to be very effective in reducing the velocity at which reverser exhaust ingestion occurs (for a given efflux angle), is to splay (or cant) the reverser flow. In fact, without

the ability to splay reverser flow, ingestion speeds can be on the order of touchdown speeds for some configurations as reported in reference 11. Benefits of splaying reverser flow are partially the result of increased lateral separation of the reverser jets which would tend to eliminate the fountain effect found for many unsplayed (0°) cases once the reverser flow impinges upon the ground.

The U.S. Air Force STOL and Maneuver Demonstration Program (refs. 12 and 13) is the most recent program aimed at demonstrating landing/approach performance of thrust vectoring/reversing exhaust nozzles. This program will demonstrate, through flight test, short take-off and landing capability on a modified F-15 fighter while enhancing its maneuverability. This will be accomplished through the use of two-dimensional thrust vectoring/reversing nozzles. However, these nozzles do not utilize the benefits of splaying the reverser flow, so that optimum reverser performance will likely not be obtained.

Although many studies have addressed reverser installed and internal performance (refs. 1 to 31), few (if any) internal performance data are available on reverser configurations with both efflux and splay capabilities. As a result an investigation was conducted in the static-test facility of the Langley 16-Foot Transonic Tunnel on a subscale, nonaxisymmetric thrust reverser model. The model hardware simulated a dual-port, block-and-turn type thrust reverser with vane cascades in the reverser ports which turned the flow in both the reverse and splay directions. The configurations tested were designed for application in a close-spaced twin-engine afterbody system. However, since individual port performance was desired, only one engine/nozzle (of the twin-engine system) was simulated. The vane cascades consisted of two sets of perpendicular vanes with a variable number of reversing and splay vanes. A skewed vane cascade was also tested which had only one set of vanes angled to provide both reversing and splay. Vane cascades were designed to provide different amounts of flow splay in the top and bottom ports. Inner doors, trim tabs, and an orifice plate all provided means of varying the port area for reverser flow modulation. The outer door position was varied as a means of influencing the flow reverse angle. Jet exhaust was simulated by high-pressure air at a controlled temperature of about 530°R, and nozzle pressure ratio was varied from 1.75 to approximately 6.

Symbols

All forces (with the exception of resultant gross thrust) and angles are referred to the model centerline (body axis). A detailed discussion of the data reduction and calibration procedures as well as definitions of forces, angles, and propulsion relationships used herein can be found in reference 29.

A_p	minimum area of reverser port, in^2
A_v	minimum area of vane cascades, in^2
F	measured thrust along body axis, lbf
F_i	ideal isentropic gross thrust, $w_p\sqrt{\frac{RT_{t,j}}{g^2}\left(\frac{2\gamma}{\gamma-1}\right)\left[1-\left(\frac{p_a}{p_{t,j}}\right)^{(\gamma-1)/\gamma}\right]}$, lbf
F_N	measured normal force, lbf
F_r	resultant gross thrust, $\sqrt{F^2+F_N^2+F_Y^2}$, lbf
F_Y	measured side force, lbf
g	gravitational constant, 32.174 ft/sec^2
NPR	nozzle pressure ratio, $p_{t,j}/p_a$
p	local static pressure, psi
p_a	ambient pressure, psi
$p_{t,j}$	jet total pressure, psi
R	gas constant for air, 1716 ft^2/sec^2-°R
$T_{t,j}$	total temperature, °R
w_i	ideal weight-flow rate based on measured minimum area (either A_v or A_p), lbf/sec
w_p	measured weight-flow rate, lbf/sec
x	distance along surface of outer door and nozzle boattail fairing, in. (see fig. 4(h))
α	geometric splay vane angle, measured counterclockwise from vertical reference line for top port and clockwise for bottom port, deg
γ	ratio of specific heats for air, 1.4
δ	measured reverser vector angle in reverse direction, measured up from horizontal reference plane, $\tan^{-1}(F_N/F)-180$, deg

ϕ	measured reverser vector angle in splay direction, positive measured counterclockwise (as seen from aft) from vertical reference plane for top port, $-\tan^{-1}(F_Y/F_N)$, and clockwise (as seen from aft) for bottom port, $\tan^{-1}(F_Y/F_N)$, deg

Subscripts:

B	bottom
sum	weighted sum of top and bottom ports
T	top

Abbreviations:

Config.	configuration
Sta.	model station, in.

Apparatus and Methods

Static-Test Facility

This investigation was conducted in the static-test facility of the Langley 16-Foot Transonic Tunnel. All tests were conducted in a room with a high ceiling with the jet exhausting to the atmosphere. The control room was remotely located from the test area and a closed-circuit television camera was used to observe the model. This facility utilizes the same clean, dry-air supply as that used in the 16-Foot Transonic Tunnel (ref. 32) and a similar air-control system including valves, filters, and a heat exchanger to operate the jet flow at a constant stagnation temperature.

Single-Engine Propulsion Simulation System

A sketch of the single-engine, air-powered nacelle model on which various thrust reverser configurations were mounted is presented in figure 1 with a dual-port reverser configuration installed. An external high-pressure air system provided a continuous flow of clean, dry air at a controlled temperature of about 530°R and was varied up to approximately 90 psi at the instrumentation section. This high-pressure air was brought through the dolly-mounted support strut by six tubes, which connect to a high-pressure plenum chamber. As shown in figure 1, the air was then discharged perpendicularly into the model low-pressure plenum through eight multiholed sonic nozzles equally spaced around the high-pressure plenum. This method was designed to minimize any forces imposed by the transfer of axial momentum as the air passed from the nonmetric high-pressure plenum to the metric (mounted to the force balance) low-pressure plenum. Two flexible metal bellows were used as seals and served to compensate for axial forces caused by pressurization. The air was then passed from the model low-pressure plenum through a choke plate/screen combination and instrumentation section which were circular in cross section. The reverser model was attached at model station 43.59.

Model Description

The model hardware downstream of station 43.59 simulates the aerodynamic flow path of a non-axisymmetric block-and-turn type thrust reverser concept shown schematically in figure 2. Photographs of the subscale model hardware are shown in figure 3. It should be noted that the model hardware represented the left-hand nozzle of a twin-engine installation. Both the top and bottom vane cascades directed the exhaust flow to the left (or outboard for the twin-engine case). Sketches of the model hardware are shown in figure 4.

As indicated in the concept schematic (fig. 2), transition from forward flight to reverse thrust mode is accomplished by rotating the convergent nozzle flaps inward to simultaneously block the flow and to open the reverser port. An outer door opens to allow the flow from the reverser port to exhaust through the vane cascades to the free stream. The position of the upper portion of the blocker (called the inner door) is variable as a means of guiding the flow into the vane cascades and controlling the area of the port upstream of the vanes. The vane cascades, which are fixed (not actuated), turn the flow in the lateral or splay direction and aid in turning the flow in the reverse direction. The position of the outer door is variable as a means of influencing the angle of the reverser flow in the axial direction.

The reverser model, shown in figure 4, had an integral transition section (axisymmetric to non-axisymmetric flow path, fig. 4(a)), which connected to the single-engine propulsion simulation system at model station 43.59. The baseline configuration consisted of inner door A (fig. 4(b)) and vane cascades A1 (fig. 4(c)). As seen in figure 4(c), the top and bottom vane cascades were designed to provide differing amounts of exhaust flow splay (α = 9° for the top port and 19° for the bottom). These differing splay levels are generally a requirement for twin-engine nozzle/reverser installations to limit hot gas ingestion and flow impingement problems discussed previously. The vane cascades were designed such that the minimum flow area occurs in the cascades. This is an important requirement for efficient flow turning because it allows reverser port flow to be turned in both the reverse and

splay directions at more efficient subsonic conditions. Inner doors B and C (fig. 4(b)) provided a parametric port area variation upstream of the vane cascades. Inner door B provided a small port flow-path area decrease while inner door C provided a small increase. Neither of these passage areas were designed to move the minimum area out of the vane cascades, but they did provide small variations in port passage Mach number upstream of the vane cascades. The minimum vane areas (A_v) and minimum port areas (A_p) are tabulated in figure 4.

Detailed sketches of the vane cascades tested with inner doors A, B, and C (hereafter called flow paths A, B, and C) are shown in figures 4(c) and (d). Vane cascades designated A, B, and C were tested with flow paths A, B, and C, respectively. As seen (figs. 4(c) and (d)), each vane cascade consists of two sets of perpendicular vanes. One set aids in turning the flow in the reverse (fore and aft) direction and the other provides turning in the splay (or side) direction. All vanes were designed by customizing an 18-percent-thick cambered airfoil section to satisfy both structural and aerodynamic requirements. Truncation of the airfoil trailing edges was necessary to satisfy the structural requirements, and the camber of the mean chord line was designed to provide the desired amount of flow turning without flow separation.

Vane cascades A1, B1, and C1 had identical splay vane arrangements. All were designed to have the reversing vanes provide 129° of turning. (See fig. 4(a).) The reversing vanes were respaced slightly to accommodate the upstream port area differences provided by flow paths A, B, and C. Vane cascades A2 and A3 provided a comparison (with A1) of the number of splay and reversing vanes, respectively. Cascades A2 had only 9 splay vanes compared with the 12 found in A1. Cascade A3, which was designed for the top port only, had three reversing vanes compared with the two found in A1. As would be expected, vane areas increased for A2 and decreased for A3 relative to the baseline vane cascades A1; thus, a vane area comparison as well as a vane number comparison was provided.

A skewed vane cascade (A4), designed for the bottom port only, was also examined. As seen in figure 4(d), this concept provided both reversing and splay of the flow with only one set of vanes. The vane stiffeners existed only for structural support of the skewed turning vanes.

One advantage of this type of reverser concept lies in the ability to modulate the levels of reverse thrust by directing a portion of the exhaust flow through the reverser ports and a portion through the main exhaust nozzle. The resulting capability to "fine tune" the airplane approach path is especially important in terms of achieving a precision touchdown. Several means of modulating the reverser port area were investigated. Inner doors D and E (fig. 4(b)) simulated port area variations that would be obtained if the primary nozzle flaps were actuated to regulate flow to the reverser port and main nozzle. For this investigation, however, the main nozzle flow was fully blocked. As would be expected, the minimum area moves from the vane cascade upstream to the inner doors as the inner doors are closed. In addition to variations in inner door position, an orifice plate (fig. 4(e)), representing a series of fully open butterfly valves, was examined for its impact on reverser performance. Here also the minimum port area is formed upstream of the vane cascades. A third mass-flow modulation technique examined was the use of trim tabs as shown in figure 4(f). This method simply reduced vane area while allowing the reverser minimum area to remain in the vane cascades where exhaust flow turning is more efficient.

In some aircraft installations, it may not be realistic to have a sidewall which moves with the outer door so that it is not in the reverser exhaust path. Reverser port performance characteristics were therefore determined for an installation in which sidewalls could not be moved (fig. 4(g)). Obviously if the splayed reverser flow were to impinge on these sidewalls, reductions in splay turning angle would be measured and could have a significant impact on overall reverser performance and suitability for a particular application.

As mentioned previously, the outer door position was varied as a means of influencing flow reverse angle. The sketch in figure 4(a) shows the baseline (142.2°) external door position and the alternate (147.8°) door position. Note also that a portion of the nozzle boattail fairing forms a short additional ramp at an angle of 171.7° for the baseline and 172.2° for the alternate.

The only way to determine and evaluate the performance increments resulting from the various configuration variables is to determine that performance for a single port only. It was recognized that the flow characteristics into a single reverser port (for example, the top port) might be considerably different if the bottom port was closed than if both ports were operating. A technique developed in reference 15 allows the isolated testing of either the top or bottom port. The technique involves using a splitter plate (fig. 4(h)) with a generous leading-edge radius. This splitter plate acts as a bellmouth and results in single-port flow characteristics which more nearly duplicate those obtained with both ports flowing.

Instrumentation

A six-component strain-gauge balance was used to measure forces and moments on the model downstream of station 20.50. (See fig. 1.) Jet total pressure was measured at a fixed station in the instrumentation section by a five-probe rake. A thermocouple, also located in the instrumentation section, measured jet total temperature. Flow rate of the high-pressure air supplied to the nozzle was measured by a pair of critical flow venturis. Diagnostic static-pressure orifices were located in the transition section and on the blocker, inner doors, and outer doors. Static-pressure-orifice locations are indicated in sketches included with the plotted pressure data.

Data Reduction

The basic performance parameters used for the presentation of results were $F/F_i, F_N/F_i, F_Y/F_i$, F_r/F_i, δ, ϕ, and w_p/w_i. With the exception of resultant gross thrust F_r, all force data in this report are referenced to the body axis (centerline). The component internal thrust ratios, $F/F_i, F_N/F_i$, and F_Y/F_i, represent the ratio of actual nozzle thrust (along the body axis, vertical axis, and lateral axis, respectively) to ideal nozzle thrust, where ideal nozzle thrust is based on measured weight-flow rate and total temperature and pressure conditions in the nozzle throat, as defined by the equations in the symbol definitions. The balance force measurements, from which actual nozzle thrust is subsequently obtained, are initially corrected for model weight tares and balance interactions. Although the bellows arrangement was designed to eliminate pressure and momentum interactions with the balance, small bellows tares on all balance components still exist. These tares result from a small pressure difference between the ends of the bellows when internal velocities are high and also small differences in the forward and aft bellows spring constants when the bellows are pressurized. As discussed in reference 29, these bellows tares were determined by running calibration nozzles with known performance over a range of expected normal- and side-force and yawing-, pitching-, and rolling-moment loadings. The balance data were then corrected in a manner similar to that discussed in reference 29 to obtain final forces. The resultant gross thrust F_r used in the resultant thrust ratio F_r/F_i was then determined from these corrected balance data as were the individual force ratios, $F/F_i, F_N/F_i$, and F_Y/F_i. Significant differences between F_r/F_i and F/F_i occur when jet-exhaust flow is directed away from the axial direction. The individual force ratios are presented to allow a direct comparison of normal- and side-force magnitudes relative to axial-force values.

The vector angles δ and ϕ were also determined from the corrected balance data. The reverse vector angle δ is measured up from a horizontal reference plane so that $\delta = 0°$ represents thrust in the forward flight mode and $|\delta| > 90°$ represents reverse thrust. For a dual-port thrust reverser, 90° of reverse thrust would give $\delta = -90°$ for the top port and $\delta = 90°$ for the bottom port. Reverser splay vector angle is measured counterclockwise (as seen from aft) from a vertical reference plane for the top port and clockwise (as seen from aft) for the bottom port so that flow splayed to the pilot's left would have a positive ϕ on both the top and bottom ports. These conventions were retained even when individual port configurations were tested in the top port.

Reverser discharge coefficient w_p/w_i is the ratio of measured weight-flow rate to ideal weight-flow rate, where ideal weight-flow rate is based on jet total pressure $p_{t,j}$, jet total temperature $T_{t,j}$, and a throat area, which was the measured minimum area, whether it occurred in the vane cascade or in the reverser port.

As discussed in the section "Model Description," individual port performance was determined by blocking off the lower port and using a splitter plate in an attempt to duplicate the flow characteristics of that port when both ports are flowing. To check the performance of the splitter plate, component thrust ratios and discharge coefficients with both ports flowing were compared with the sum of top- and bottom-port thrust ratios and discharge coefficients weighted by measured weight flow. The force ratio F/F_i with both ports flowing is compared with

$$\left(\frac{F}{F_i}\right)_{\text{sum}} = \left\{\left(\frac{F}{F_i}\right)_T \left[\frac{(w_p)_T}{(w_p)_T + (w_p)_B}\right]\right\} + \left\{\left(\frac{F}{F_i}\right)_B \left[\frac{(w_p)_B}{(w_p)_T + (w_p)_B}\right]\right\} \quad (1)$$

These comparisons are presented in figure 5. Since all individual port configurations were tested in the top port, F_N/F_i is negative, so that the weighted difference (instead of the sum) was compared with F_N/F_i with both ports flowing:

$$\left(\frac{F_N}{F_i}\right)_{\text{sum}} = \left\{\left(\frac{F_N}{F_i}\right)_T \left[\frac{(w_p)_T}{(w_p)_T + (w_p)_B}\right]\right\} - \left\{\left(\frac{F_N}{F_i}\right)_B \left[\frac{(w_p)_B}{(w_p)_T + (w_p)_B}\right]\right\} \quad (2)$$

Also F_Y/F_i is positive for top-port configurations and negative for bottom-port configurations tested

in the top port, so that the weighted difference was compared with F_Y/F_i with both ports flowing:

$$\left(\frac{F_Y}{F_i}\right)_{\text{sum}} = \left\{\left(\frac{F_Y}{F_i}\right)_T \left[\frac{(w_p)_T}{(w_p)_T + (w_p)_B}\right]\right\} - \left\{\left(\frac{F_Y}{F_i}\right)_B \left[\frac{(w_p)_B}{(w_p)_T + (w_p)_B}\right]\right\} \quad (3)$$

And lastly, discharge coefficient for both ports flowing is compared with

$$\left(\frac{w_p}{w_i}\right)_{\text{sum}} = \left\{\left(\frac{w_p}{w_i}\right)_T \left[\frac{(w_p)_T}{(w_p)_T + (w_p)_B}\right]\right\} + \left\{\left(\frac{w_p}{w_i}\right)_B \left[\frac{(w_p)_B}{(w_p)_T + (w_p)_B}\right]\right\} \quad (4)$$

In all cases, the sum of the discharge coefficients of the individual ports is within 2 percent of the discharge coefficient of the dual-port configurations, whereas the worst sum of the component thrust ratios is within 5 percent of the dual-port thrust ratios, generally 3 percent or less. Individual port comparisons presented herein are not affected by the splitter plate, but care should be exercised in combining individual port performance to estimate dual-port performance because results should be weighted by weight-flow ratios.

Results and Discussion

The results of this investigation are presented in both tabular and plotted form. The configurations tested are presented in table 1 along with the pertinent data tables and figures. Table 2 contains the basic data for all configurations tested. Plotted data for the individual port reverser configurations are presented in figures 6 through 14 where resultant thrust ratio F_r/F_i, the component thrust ratios $F/F_i, F_N/F_i$, and F_Y/F_i, discharge coefficient w_p/w_i, and the vector angles δ and ϕ are presented as a function of NPR. Selected static pressures (expressed as the ratio $p/p_{t,j}$) are also presented. The ratio of minimum vane area to minimum port area (A_v/A_p) is presented for each configuration to indicate where the choke region for the reverser occurs; $A_v/A_p > 1$ indicates that the throat forms in the reverser port, whereas $A_v/A_p < 1$ indicates that the throat forms in the vane cascade.

Basic Data

The basic internal performance exhibits characteristics typical of other convergent-divergent nozzles (ref. 29). Discharge coefficient increases to a maximum, generally occurring at NPR = 3, and then remains nearly constant for further increases in NPR. The internal thrust ratio increases up to a maximum, which usually occurs at the NPR for fully expanded flow (for these configurations, generally at NPR ≈ 5), and then decreases for higher NPR's. (Note that an increase in reverser performance is distinguished by a larger negative value of F/F_i.) However, the same observation is not true when considering F_r/F_i. Resultant thrust ratio generally increased throughout the test range of NPR. This feature, coupled with the results of the internal thrust ratio, indicates that performance is being influenced by an external expansion process taking place on the outer door. Since resultant thrust ratio tends to climb throughout the test range of NPR, it is apparent that the fully expanded flow condition (on the outer door) has not been reached.

Exceptions to this trend can be noted for configurations where vane cascades A1 were run with door E (fig. 10) or with the orifice plate (fig. 11). In these cases, performance increased (F/F_i became more negative and F_r/F_i became more positive) throughout the test range of NPR; this indicates a change in the effective internal expansion ratio of the port. In both cases, the physical throat has relocated from the vane cascade to door E or to the orifice plate. This resulted in an increase in the effective expansion ratio (ratio of exit area to throat area of the port). Apparently the expansion ratio change was large enough so that design NPR was above 6, and beyond the range tested.

Both reverse and splay thrust vector angles were larger than the corresponding geometric vane angles. In fact, the measured reverse vector angles were between $-140°$ and $-150°$ compared with the geometric reverser vane angle of 129°. These large reverse angles are a result of the exhaust flow attaching to the outer door. The net result is that a larger than expected axial force (reverse thrust) is generated along with a smaller than expected normal force. The flow expansion on the outer door is discussed in more detail later. Measured splay vector angles varied between 15° and 30° for the top port and between 35° and 55° for the bottom port. Compared with the geometric splay angles of 9° and 19° for the top and bottom ports, respectively, the measured splay vector angles are large. Again, these larger than expected splay angles can be explained in part by the fact that the normal-force component being generated was smaller (than expected) relative to the side-force component being generated.

Both reverse and splay vector angles were a function of NPR for all configurations. For configurations

without reverser flow modulation devices (figs. 6–9 and 13–14), the reverse vector angle δ was generally constant for NPR < 5 then decreased 3°–5°. Recall that a less negative δ indicates a decrease in reverse angle. Similarly, for all unmodulated configurations except the skewed cascade and the configurations with the sidewalls, the splay vector angle ϕ remained generally constant for NPR < 3 and decreased for further increases in NPR. This effect has been observed before (ref. 15). A possible explanation for this trend is that each passage between the reversing or splay vanes forms a single-expansion-ramp nozzle with one solid jet boundary and one free jet boundary downstream of the vane exit. As discussed in reference 23, this type of nozzle tends to turn the exhaust flow, where the direction of the flow turning is a function of NPR and the orientation of the external expansion surface with respect to the model. For underexpanded flow (values of NPR greater than required for fully expanded flow), the flow tends to be turned away from the external expansion surface. Loss of turning performance in either the reverse or splay directions would be expected at underexpanded flow conditions (NPR > 3 for splay and NPR > 5 for reverse). The NPR for fully expanded flow is different for reverse and splay because the vane spacing in each direction created passages with different expansion ratios.

Static pressure ratios presented for each configuration are provided for a nozzle pressure ratio of 5. While not extensive enough for quantitative use (pressure integration, etc.), these static-pressure taps located on the forward lip, sidewalls, inner doors, and external ramp do provide qualitative information which aids in the understanding of the force balance results. It should be noted that the dashed-line fairings indicate that the exact fairing is not known. For example, the dashed fairing found between orifices 4 and 5 exists because it is believed that for many of the configurations, the physical throat forms in the vane cascades. As a result, static pressure downstream of orifice 4 probably increases to levels above 0.5283 (static pressure ratio indicating sonic flow) before expanding to the lower pressures measured on the ramp.

In general these static pressure ratio data indicate subsonic flow in the reverser port (upstream of the vane cascades) except in the region of the forward lip (orifices 2 through 4); this indicates a region of supersonic flow. It is believed that the sharp corner produces a very localized region of overexpansion as the flow negotiates the turn. Exceptions to the port subsonic flow do exist and are discussed later.

Individual Port Performance Comparisons

Effect of port flow-path area. The effect of port flow-path area on reverser port performance characteristics is presented in figure 6. Recall that configurations B1 and C1 had smaller and larger flow-path areas (area of flow path leading into the vane cascades), respectively, than the baseline flow path A1. The reversing vanes in cascades B1 and C1 were respaced to accommodate the flow-path area changes. With the exception of discharge coefficient, reverser port flow-path area had little effect on reverser performance or turning characteristics. As seen discharge coefficient increased as vane area decreased and decreased as vane area increased. The smaller port area associated with configuration B1 reduced internal velocities in the reverser, as verified by the higher static pressures observed in the reverser port. This allowed more efficient passage of the mass flow, thereby increasing w_p/w_i relative to the baseline. The effects were, of course, opposite for the C1 configuration with the larger flow path.

Effect of number of reversing vanes. The effect of varying the number of reversing vanes in the vane cascade on internal performance is shown in figure 7. Configuration A3, which was designed for the top port only, has three reversing vanes, whereas the baseline cascade A1 has only two. Increasing the number of reversing vanes had little effect on thrust ratio or the flow turning angle performance. A 1- to 2-percent increase in discharge coefficient was measured because the addition of the extra reversing vane resulted in a smaller port area. Based on the previous port area discussion, this was expected.

Effect of number of splay vanes. The effect on internal performance of removing 3 of the 12 splay vanes (configuration A2) is shown in figure 8. This 25-percent decrease in the number of splay vanes resulted in a decrease in splay vector angle ϕ of 3° to 6° for the top port and 6° to 9° for the bottom port, depending on NPR, whereas flow reverse vector angle δ and resultant thrust ratio F_r/F_i were essentially unchanged. This indicates that the reverser efflux angle rotated in the axial-side plane only, so that F and F_N both increased to make up for the decrease in F_Y. Removing splay vanes resulted in a larger port area; consequently, the discharge coefficient decreased for both the top and bottom ports. This observation is again consistent with previous flow-path area results.

Effect of skewed vane cascade. Figure 9 compares the performance of the skewed vane cascade A4B, which was designed for the bottom port only, with that of the baseline vane cascade A1B. The skewed cascade provided slightly larger reverse vector angles

but as much as a 4° loss of flow splay vector angle as compared with the baseline cascade. As discussed previously, a larger reverse vector angle should result in a larger splay vector angle for a given amount of side force produced by the flow turning; therefore the skewed cascade is actually providing even less flow turning in the splay direction than the splay vector angle would indicate. Also ϕ decreased over the entire test range of NPR, indicating that the flow in the splay direction was probably underexpanded (NPR greater than design). Discharge coefficient of the skewed vane concept was as much as 5 percent higher than the baseline, an effect partially due to the reduced vane area, but it may also indicate that the blockage due to the uncambered stiffeners and effects of the oblique corners was less than the blockage provided by intersecting vanes.

Effect of reverser mass-flow modulation devices. The effect on internal performance of varying inner door position, as a means of modulating mass flow, is shown in figure 10. All inner door comparisons are made with the baseline vane cascades A1T and A1B. As seen, inner door position had a very significant impact on reverser characteristics. As the inner doors closed down (reducing port area, mass flow, etc.) from door A to door E, ideal thrust, as well as the component thrust forces generated, is reduced. Resultant thrust ratio and the component thrust ratios ($F/F_i, F_N/F_i$, and F_Y/F_i) also decreased; this indicates that the efficiencies with which forces are being generated have decreased. The net result of these decreases is a small net increase in both the reverse and splay vector angles generated. However, these angular increases do not provide a true assessment of the forces available for flight-path control.

The primary reason for changing inner door position is to provide a means of modulating mass flow entering the reverser port. As seen in figures 10(c) and (f), the inner door had significant effects on port static pressures. As expected, static pressure ratios increased in the region upstream of the vane cascades as the inner door (hence throat area) was closed down and the throat relocated from the vanes to the port ($A_v/A_p > 1$). Although the static-pressure orifice data were not detailed enough to provide conclusive evidence, it is believed that the door E case resulted in the physical minimum area (throat) being at the downstream edge of the inner door. This throat apparently forms downstream of orifice 4 on the forward lip. The flow then probably expands into the vane cascades, where the supersonic flow is deflected by the vanes. It has long been recognized that subsonic turning of exhaust flow results in more efficient turning than supersonic deflection.

Nozzle discharge coefficient results are less clear. The only general comment that can be made is that door D resulted in the lowest discharge coefficients. Reasons for this are not known; however, this result is believed to be associated with the fact that for door D the ratio of measured vane area to port area (A_v/A_p) is approximately 1. More is said about this in subsequent discussions.

A second reverser port mass-flow modulation scheme investigated was the orifice plate, shown in figure 4(e). As stated previously, the orifice plate represented a series of five fully open butterfly valves. In an actual installation, these butterfly valves would be modulated to provide proper open areas for the specific approach or landing situation. As for the inner door cases, the orifice plate, which is expected to be the minimum area in the port, caused reductions in resultant, axial, normal, and side force ratios as shown in figure 11. Reverse and splay vector angle trends also followed a pattern similar to those noted for the inner door position. The orifice plate increased both reverse and splay angles relative to the baseline (no orifice plate) case. As seen in figures 11(c) and (f), the orifice plate produced a larger region of supersonic flow in the reverser port, so that flow turning losses were higher than the baseline.

The third method for modulating mass flow was through the use of trim tabs. The effect of these trim tabs, which were tested with vane cascade A1T only, is presented in figure 12. As shown in figure 4(f), the tabs were installed immediately upstream of the vane cascades and were designed to block off some of the passages. These tabs provided an effective way of modulating weight flow (by changing the vane area) with negligible effects on performance or flow angles. As with other variations in the vane area, a decrease in vane area resulted in an increase in discharge coefficient. Note in figure 12(f) that the short and long trim tabs on the right side had essentially the same effect on w_p/w_i and static pressure ratios. This is as expected; since the flow is splayed to the left, blocking the flow on the right side should have little effect.

The relationship between nozzle discharge coefficient w_p/w_i and the ratio of measured vane area to port area A_v/A_p is presented in figure 13 for all individual port configurations tested. As seen, nozzle discharge coefficient was not so much a function of the throat position (in the vanes or in the port) as it was a function of whether the vane-to-port area ratio approached unity. At that condition, nozzle discharge coefficient reached a minimum. Unfortunately, detailed pressure instrumentation in the reverser port and vane cascades was not available; thus, exact reasons for this trend are not known. If high discharge

coefficients are a requirement, $A_v/A_p = 1$ is a design condition that should be avoided.

Effect of sidewalls. The addition of sidewalls downstream of the exit of vane cascades A1 had no effect on discharge coefficient (fig. 14), as would be expected, since they had no effect on the port throat area. The sidewalls also had very little effect on the reverse or splay vector angles for the top port; this indicates that the splayed flow was not impinging on the sidewalls. However, for the bottom port, which was designed to have a higher splay angle than the top port, the sidewalls decreased both the reverse and splay vector angles. These losses in both side- and axial-force coefficients are reflected in the loss in resultant thrust coefficient, indicating that flow impingement on the sidewalls causes turning losses.

Effect of outer door position. Figure 15 shows the effect of the outer door position on the performance of vane cascades A1. As with the sidewalls, the outer door position had little effect on discharge coefficient, since it was downstream of the throat. The outer door and a portion of the external boattail fairing upstream of the outer door hinge formed a dual-angle expansion surface for the flow exiting the vane cascade. The baseline outer door angles/nozzle boattail fairing angles were 142.2°/171.7°, and the alternate positions were 147.8°/172.2° as shown in figure 4(a). Reverse thrust vector angles of −140° to −150° were achieved with the baseline outer door, and the alternate door position increased the reverse vector angle 3° to 5° with an accompanying increase in splay vector angle of as much as 4°. As seen in figure 15, this increase in splay vector angle is more a result of the reduction in normal force than increased side-force generation. This reduction in normal force would be expected as the outer door angle increased from 142.2° to 147.8° as normal force is being traded for larger axial force.

Static pressure ratios along the centerline of the outer doors are presented in figure 16. Comparison of pressure ratios for the baseline outer door with those measured on the alternate door reveals that for a given NPR the pressure ratios are generally lower on the alternate door. The net result of this lower pressure on the aft-facing ramp would be an increase in the amount of reverse thrust generated and a decrease in the downward normal force. These results are consistent with the static data presented in figure 15. Varying the position of the outer door could be a simple and effective way to make minor adjustments to the reverse flow angle and therefore the flow splay angle.

Conclusions

An investigation was conducted in the static-test facility of the Langley 16-Foot Transonic Tunnel on a dual-port, nonaxisymmetric, block-and-turn type thrust reverser model. Vane cascades in the reverser ports turned the flow in the splay (or lateral) direction and aided in turning the flow in the reverse direction. Splaying reverser flow is a method of delaying to lower landing ground roll speeds the reingestion of hot exhaust flow into the inlets. Exhaust flow splay can also help prevent the impingement of hot exhaust gases on the empennage surfaces when the reverser is integrated into an actual airframe. The vane cascades consisted of two sets of perpendicular vanes with a variable number of reversing and splay vanes. A skewed vane cascade was also tested which had only one set of vanes angled to provide both reversing and splay. Vane cascades were designed to provide different amounts of flow splay in the top and bottom ports. Inner doors, trim tabs, and an orifice plate all provided means of varying the port area for reverser flow modulation. The outer door position was varied as a means of influencing the flow reverse angle. Nozzle pressure ratio was varied from 1.75 to approximately 6.00. Results of this study indicate the following conclusions:

1. In general, both the reverse and splay vector angles were larger than the corresponding geometric angles. The larger reverse angles are caused by the exhaust flow attaching to the outer door. As a result, the normal force relative to the side force is smaller than expected; this resulted in larger computed splay vector angles.

2. Both reverse and splay vector angles were a function of NPR. A possible explanation is that each passage of the vane cascade forms a single-expansion-ramp nozzle with one solid jet boundary and one free jet boundary. Nozzles of this type tend to turn the exhaust flow, and the flow turning is a function of NPR.

3. Decreasing the port area with flow modulation devices (the inner door, the trim tabs, or the orifice plate) had very little effect on the reversing and splay vector angles. Port area changes did have a marked effect on discharge coefficient and static pressure ratios in the reverser port.

4. Decreasing the number of splay vanes decreased the splay vector angle with essentially no effect on reverse vector angle or overall performance.

5. The skewed vane cascade provided less splay vectoring than the baseline configuration but a higher discharge coefficient. This may indicate that the blockage due to the uncambered stiffeners and effects

of the oblique corners was less than the blockage provided by intersecting vanes.

6. If high discharge coefficients are a requirement in the reverser port, nearly equal areas in the port and vanes is a design condition that should be avoided.

7. If sidewalls are present and the splay vector angle is large enough for the flow to impinge on the sidewalls, turning losses can cause a loss in resultant thrust ratio as well as a decreased splay vector angle.

8. The outer door provides an effective means of making minor adjustments to the reverse vector angle. The number and spacing of reversing vanes in the vane cascade has little effect on reverse vector angle.

NASA Langley Research Center
Hampton, VA 23665-5225
July 26, 1989

References

1. Capone, Francis J.; and Berrier, Bobby L.: *Investigation of Axisymmetric and Nonaxisymmetric Nozzles Installed on a 0.10-Scale F-18 Prototype Airplane Model.* NASA TP-1638, 1980.
2. Bare, E. Ann; Berrier, Bobby L.; and Capone, Francis J.: *Effect of Simulated In-Flight Thrust Reversing on Vertical-Tail Loads of F-18 and F-15 Airplane Models.* NASA TP-1890, 1981.
3. Capone, Francis J.; Re, Richard J.; and Bare, E. Ann: Thrust Reversing Effects on Twin-Engine Aircraft Having Nonaxisymmetric Nozzles. AIAA-81-2639, Dec. 1981.
4. Carson, George T., Jr.; Capone, Francis J.; and Mason, Mary L.: *Aeropropulsive Characteristics of Nonaxisymmetric-Nozzle Thrust Reversers at Mach Numbers From 0 to 1.20.* NASA TP-2306, 1984.
5. Banks, Daniel W.; and Paulson, John W., Jr.: *Aerodynamic Characteristics and Predicted Landing Performance of an F-15 Fighter With Two Thrust-Reverser Configurations.* NASA TP-2466, 1985.
6. Glezer, A.; Hughes, R. V.; and Hunt, B. L.: Thrust Reverser Effects on the Tail Surface Aerodynamics of an F-18 Type Configuration. AIAA-83-1860, July 1983.
7. Chiarelli, Charles; Lorincz, Dale; and Hunt, Brian: Thrust Reverser Induced Flow Interference on Tactical Aircraft Stability and Control. AIAA-82-1133, June 1982.
8. Chiarelli, Charles; and Compton, Michael: Wind Tunnel Evaluation of Tactical Aircraft Stability and Control as Affected by Nozzle Thrust Reverser Parameter Variations. AIAA-83-1228, June 1983.
9. Burger, Karl Heinz: In-Flight Short Field Landing Investigations on a Combat Aircraft With Thrust Reverser. AIAA-83-2693, Nov. 1983.
10. Eigenmann, M. F.; Kitzmiller, D. E.; and Hakim, A. D.: Axisymmetric Approach and Landing Thrust Reverser Concepts: In-Ground Effects Wind Tunnel Test Results. AIAA-84-1215, June 1984.
11. Amin, N. F.; and Richards, C. J.: Thrust Reverser Exhaust Plume Reingestion Tests for a STOL Fighter Model. AIAA-83-1229, June 1983.
12. Mello, J. F.; and Kotansky, D. R.: Aero/Propulsion Technology for STOL and Maneuver. AIAA-85-4013, Oct. 1985.
13. Selegan, David R.: STOL and Maneuver Technology Program. *Powered Lift Systems Plus an Overview of the JVX Program,* SP-555, Soc. of Automotive Engineers, Inc., Dec. 1983, pp. 1–7. (Available as SAE Paper 831425.)
14. Bitterick, W. C.: Axisymmetric Approach and Landing Thrust Reversers for Single Engine Fighters. AIAA-84-1214, June 1984.
15. Leavitt, Laurence D.; and Burley, James R., II: *Static Internal Performance of a Single-Engine Nonaxisymmetric-Nozzle Vaned-Thrust-Reverser Design With Thrust Modulation Capabilities.* NASA TP-2519, 1985.
16. Berrier, Bobby L.; and Capone, Francis J.: *Effect of Port Corner Geometry on the Internal Performance of a Rotating-Vane-Type Thrust Reverser.* NASA TP-2624, 1986.
17. Leavitt, Laurence D.; and Re, Richard J.: *Static Internal Performance Characteristics of Two Thrust-Reverser Concepts for Axisymmetric Nozzles.* NASA TP-2025, 1982.
18. Rowe, R. Kevin; Dusa, D. J.; and Leavitt, Laurence D.: Static Internal Performance Evaluation of Several Thrust Reversing Concepts for 2D-CD Nozzles. AIAA-84-1174, June 1984.
19. Obye, R. C.; and Hakim, A. D.: Axisymmetric Approach and Landing Thrust Reverser Concepts: Hot Flow Test Results. AIAA-84-1176, June 1984.
20. McLafferty, George H.; and Peterson, Jeffrey L.: Results of Tests of a Rectangular Vectoring/Reversing Nozzle on an F100 Engine. AIAA-83-1285, June 1983.
21. Nelson, B. D.; and Nicolai, L. M.: Application of Multi-Function Nozzles to Advanced Fighters. AIAA-81-2618, Dec. 1981.
22. Banks, D. W.; Quinto, P. F.; and Paulson, J. W., Jr.: Thrust-Induced Effects on Low-Speed Aerodynamics of Fighter Aircraft. AIAA-81-2612, Dec. 1981.
23. Re, Richard J.; and Berrier, Bobby L.: *Static Internal Performance of Single Expansion-Ramp Nozzles With Thrust Vectoring and Reversing.* NASA TP-1962, 1982.
24. Hiley, P. E.; and Bowers, D. L.: Advanced Nozzle Integration for Supersonic Strike Fighter Application. AIAA-81-1441, July 1981.
25. Re, Richard J.; and Leavitt, Laurence D.: *Static Internal Performance Including Thrust Vectoring and Reversing of Two-Dimensional Convergent-Divergent Nozzles.* NASA TP-2253, 1984.
26. Mercer, Charles E.; and Maiden, Donald L.: *Effects of an In-Flight Thrust Reverser on the Stability and Control Characteristics of a Single-Engine Fighter Airplane Model.* NASA TN D-6886, 1972.
27. Goetz, Gerald F.; Young, John H.; and Palcza, J. Lawrence: A Two-Dimensional Airframe Integrated Nozzle Design With Inflight Thrust Vectoring and Reversing Capabilities for Advanced Fighter Aircraft. AIAA Paper No. 76-626, July 1976.

28. Willard, C. M.; Capone, F. J.; Konarski, M.; and Stevens, H. L.: Static Performance of Vectoring/Reversing Non-Axisymmetric Nozzles. AIAA-77-840, July 1977.

29. Capone, Francis J.: *Static Performance of Five Twin-Engine Nonaxisymmetric Nozzles With Vectoring and Reversing Capability.* NASA TP-1224, 1978.

30. Hiley, P. E.; Kitzmiller, D. E.; and Willard, C. M.: Installed Performance of Vectoring/Reversing Nonaxisymmetric Nozzles. *J. Aircr.*, vol. 16, no. 8, Aug. 1979, pp. 532–538.

31. Capone, Francis J.; Gowadia, Noshir S.; and Wooten, W. H.: Performance Characteristics of Nonaxisymmetric Nozzles Installed on the F-18 Aircraft. AIAA-79-0101, Jan. 1979.

32. Peddrew, Kathryn H., compiler: *A User's Guide to the Langley 16-Foot Transonic Tunnel.* NASA TM-83186, 1981.

Table 1. Configuration Summary

Vane cascade	Flow path or inner door	Reverser modulation	Outer door	Sidewalls	Table	Figures
A1T	A	None	Baseline	Off	2(a)	6–8, 10–16
A1B	A	None	Baseline	Off	2(a)	6, 8–11, 13–16
B1T	B	None	Baseline	Off	2(b)	6, 13
B1B	B	None	Baseline	Off	2(b)	6, 13
C1T	C	None	Baseline	Off	2(c)	6, 13
C1B	C	None	Baseline	Off	2(c)	6, 13
A3T	A	None	Baseline	Off	2(d)	7, 13
A2T	A	None	Baseline	Off	2(f)	8, 13
A2B	A	None	Baseline	Off	2(f)	8, 13
A4B	A	None	Baseline	Off	2(e)	9, 13
A1T	D	Inner door	Baseline	Off	2(g)	10, 13
A1B	D	Inner door	Baseline	Off	2(g)	10, 13
A1T	E	Inner door	Baseline	Off	2(h)	10, 13
A1B	E	Inner door	Baseline	Off	2(h)	10, 13
A1T	A	Orifice plate	Baseline	Off	2(i)	11, 13
A1B	A	Orifice plate	Baseline	Off	2(i)	11, 13
A1T	A	Trim tabs	Baseline	Off	2(j)	12, 13
A1T	A	None	Baseline	On	2(k)	14
A1B	A	None	Baseline	On	2(k)	14
A1T	A	None	Alternate	Off	2(l)	15, 16
A1B	A	None	Alternate	Off	2(l)	15, 16

Table 2. Tabulated Data

(a) Vane cascades A1 (baseline)

NPR	w_p, lbf/sec	w_p / w_i	F_i, lbf	F/F_i	F_r/F_i	F_N/F_i	F_Y/F_i	δ, deg	ϕ, deg
Vane cascade A1T, flow path A (baseline)									
1.755	1.819	0.807	55.0	-0.686	0.861	-0.477	0.208	-145.1	23.5
2.004	2.151	.832	71.6	-.698	.879	-.495	.201	-144.7	22.1
2.500	2.739	.850	103.2	-.721	.911	-.514	.213	-144.5	22.5
3.000	3.306	.854	134.7	-.731	.933	-.530	.236	-144.1	24.0
4.004	4.425	.856	198.5	-.739	.958	-.567	.222	-142.5	21.3
5.004	5.524	.856	263.4	-.756	.966	-.562	.213	-143.4	20.7
6.000	6.632	.856	329.3	-.719	.972	-.621	.204	-139.2	18.1
Vane cascade A1B, flow path A (baseline)									
1.749	1.739	0.859	52.4	-0.620	0.847	-0.366	-0.447	-149.4	50.6
2.002	2.033	.874	67.7	-.632	.873	-.375	-.472	-149.3	51.5
2.509	2.584	.886	97.3	-.647	.903	-.395	-.491	-148.6	51.1
3.003	3.102	.889	126.3	-.664	.921	-.406	-.493	-148.5	50.5
4.003	4.141	.889	185.5	-.687	.947	-.457	-.464	-146.4	45.5
4.998	5.169	.890	245.9	-.708	.953	-.458	-.444	-147.1	44.1
6.002	6.215	.890	308.0	-.683	.958	-.514	-.432	-143.1	40.1

(b) Vane cascades B1

NPR	w_p, lbf/sec	w_p / w_i	F_i, lbf	F/F_i	F_r/F_i	F_N/F_i	F_Y/F_i	δ, deg	ϕ, deg
Vane cascade B1T, flow path B									
1.755	1.742	0.837	52.6	-0.688	0.867	-0.491	0.196	-144.5	21.7
1.997	2.024	.852	67.2	-.703	.887	-.502	.204	-144.5	22.1
2.498	2.575	.867	97.0	-.728	.914	-.513	.207	-144.8	22.0
3.005	3.109	.870	126.7	-.738	.936	-.529	.226	-144.4	23.1
4.007	4.156	.872	186.5	-.744	.959	-.566	.213	-142.8	20.6
5.002	5.186	.872	247.1	-.756	.965	-.564	.203	-143.3	19.8
5.999	6.223	.872	309.0	-.721	.969	-.617	.196	-139.4	17.6
Vane cascade B1B, flow path B									
1.754	1.656	0.870	50.0	-0.627	0.852	-0.339	-0.466	-151.6	54.0
2.009	1.928	.883	64.4	-.641	.880	-.350	-.491	-151.4	54.5
2.503	2.428	.893	91.6	-.654	.905	-.372	-.503	-150.4	53.6
2.996	2.917	.895	118.7	-.669	.924	-.389	-.504	-149.8	52.3
3.994	3.904	.896	174.7	-.691	.948	-.446	-.472	-147.2	46.7
5.008	4.894	.896	232.8	-.711	.955	-.451	-.451	-147.6	45.0
6.010	5.868	.896	291.2	-.685	.957	-.505	-.438	-143.6	40.9

Table 2. Continued

(c) Vane cascades C1

NPR	w_p, lbf/sec	w_p/w_i	F_i, lbf	F/F_i	F_r/F_i	F_N/F_i	F_Y/F_i	δ, deg	ϕ, deg
Vane cascade C1T, flow path C									
1.750	1.805	0.753	54.4	-0.690	0.856	-0.458	0.214	-146.4	25.0
1.998	2.161	.788	71.9	-.696	.870	-.478	.212	-145.5	23.9
2.506	2.825	.821	106.6	-.715	.903	-.511	.208	-144.4	22.1
3.000	3.420	.829	139.3	-.729	.924	-.526	.214	-144.2	22.1
3.995	4.583	.832	205.0	-.735	.951	-.564	.214	-142.5	20.7
4.992	5.718	.833	272.1	-.756	.960	-.555	.205	-143.7	20.3
6.015	6.885	.833	342.2	-.723	.968	-.612	.197	-139.7	17.8
Vane cascade C1B, flow path C									
1.749	1.749	0.813	54.2	-0.620	0.838	-0.346	-0.445	-.150.8	52.1
1.999	2.113	.833	70.3	-.631	.863	-.363	-.464	-150.1	52.0
2.502	2.694	.848	101.3	-.647	.894	-.382	-.485	-149.4	51.7
2.998	3.244	.852	131.9	-.657	.914	-.402	-.492	-148.5	50.7
4.002	4.337	.853	194.3	-.685	.944	-.456	-.463	-146.4	45.5
5.007	5.427	.854	258.3	-.707	.953	-.459	-.444	-147.0	44.1
6.006	6.513	.854	323.0	-.681	.958	-.517	-.433	-142.8	40.0

(d) Vane cascade A3T

NPR	w_p, lbf/sec	w_p/w_i	F_i, lbf	F/F_i	F_r/F_i	F_N/F_i	F_Y/F_i	δ, deg	ϕ, deg
Vane cascade A3T, flow path A									
1.751	1.782	0.831	53.8	-0.687	0.866	-0.479	0.219	-145.1	24.6
2.002	2.087	.848	69.5	-.702	.885	-.489	.224	-145.1	24.6
2.499	2.656	.862	99.7	-.718	.909	-.506	.232	-144.8	24.7
2.994	3.185	.865	129.7	-.737	.929	-.517	.227	-144.9	23.7
4.008	4.270	.866	191.8	-.742	.955	-.561	.219	-142.9	21.3
4.992	5.319	.866	253.3	-.764	.964	-.550	.210	-144.2	20.9
5.998	6.389	.866	317.3	-.734	.969	-.600	.202	-140.8	18.6

(e) Vane cascade A4B

NPR	w_p, lbf/sec	w_p/w_i	F_i, lbf	F/F_i	F_r/F_i	F_N/F_i	F_Y/F_i	δ, deg	ϕ, deg
Vane cascade A4B, flow path A									
1.748	1.685	0.879	50.7	-0.661	0.875	-0.358	-0.448	-151.5	51.4
1.996	1.989	.907	66.1	-.670	.882	-.364	-.443	-151.5	50.6
2.497	2.557	.933	96.3	-.682	.896	-.382	-.438	-150.8	48.9
2.993	3.089	.939	125.6	-.699	.909	-.403	-.420	-150.0	46.1
4.004	4.144	.941	185.9	-.708	.932	-.459	-.397	-147.0	40.9
4.993	5.165	.942	246.1	-.729	.944	-.464	-.380	-147.6	39.4
6.005	6.235	.942	309.0	-.705	.952	-.521	-.371	-143.5	35.5

Table 2. Continued

(f) Vane cascades A2

NPR	w_p, lbf/sec	w_p/w_i	F_i, lbf	F/F_i	F_r/F_i	F_N/F_i	F_Y/F_i	δ, deg	ϕ, deg
Vane cascade A2T, flow path A									
1.757	1.805	0.777	54.6	-0.706	0.863	-0.468	0.169	-146.5	19.9
2.002	2.147	.807	71.4	-.706	.877	-.493	.167	-145.0	18.7
2.496	2.766	.834	104.0	-.727	.908	-.519	.164	-144.5	17.5
2.996	3.346	.840	136.1	-.741	.929	-.532	.174	-144.3	18.1
3.998	4.488	.843	200.8	-.744	.955	-.573	.175	-142.4	17.0
5.001	5.607	.844	267.0	-.757	.961	-.568	.168	-143.1	16.5
6.008	6.737	.844	334.5	-.721	.968	-.625	.161	-139.1	14.4
Vane cascade A2B, flow path A									
1.753	1.775	0.844	53.6	-0.648	0.836	-0.393	-0.352	-148.8	41.8
1.995	2.067	.860	68.6	-.661	.856	-.401	-.367	-148.7	42.5
2.502	2.634	.873	99.1	-.676	.887	-.422	-.390	-148.0	42.7
2.992	3.167	.877	128.6	-.686	.909	-.440	-.403	-147.4	42.5
3.970	4.202	.879	188.2	-.703	.937	-.485	-.386	-145.4	38.6
4.006	4.240	.879	190.5	-.704	.937	-.483	-.386	-145.6	38.6
4.995	5.294	.879	252.0	-.723	.945	-.481	-.372	-146.4	37.7
5.999	6.366	.880	315.7	-.693	.951	-.539	-.366	-142.1	34.2

(g) Inner door D

NPR	w_p, lbf/sec	w_p/w_i	F_i, lbf	F/F_i	F_r/F_i	F_N/F_i	F_Y/F_i	δ, deg	ϕ, deg
Vane cascade A1T, inner door D									
1.753	1.576	0.761	47.5	-0.610	0.780	-0.450	0.184	-143.6	22.2
2.002	1.832	.772	60.9	-.626	.803	-.464	.194	-143.5	22.6
2.509	2.320	.781	87.5	-.651	.841	-.482	.226	-143.5	25.1
3.001	2.785	.783	113.3	-.677	.872	-.500	.231	-143.6	24.8
4.000	3.723	.785	166.8	-.704	.906	-.529	.214	-143.1	22.1
5.005	4.661	.786	221.8	-.730	.920	-.521	.207	-144.5	21.7
6.005	5.595	.786	277.4	-.690	.930	-.591	.198	-139.4	18.5
Vane cascade A1B, inner door D									
1.752	1.498	0.745	45.2	-0.577	0.796	-0.337	-0.434	-149.7	52.2
2.000	1.743	.757	57.9	-.590	.818	-.343	-.451	-149.8	52.8
2.502	2.212	.766	83.2	-.607	.847	-.350	-.476	-150.0	53.6
3.003	2.660	.768	108.2	-.629	.868	-.364	-.475	-149.9	52.5
4.002	3.547	.769	159.2	-.660	.906	-.427	-.451	-147.1	46.5
5.002	4.435	.770	211.3	-.697	.920	-.417	-.433	-149.2	46.1
5.996	5.326	.771	264.3	-.683	.927	-.463	-.422	-145.9	42.3

Table 2. Continued

(h) Inner door E

NPR	w_p, lbf/sec	w_p / w_i	F_i, lbf	F/F_i	F_r/F_i	F_N/F_i	F_Y/F_i	δ, deg	ϕ, deg
Vane cascade A1T, inner door E									
1.755	0.894	0.870	27.0	-0.626	0.772	-0.400	0.209	-147.4	27.6
2.007	1.040	.881	34.6	-.617	.767	-.404	.213	-146.8	27.8
2.499	1.311	.891	49.2	-.626	.795	-.430	.234	-145.5	28.5
3.008	1.583	.895	64.5	-.639	.816	-.449	.236	-144.9	27.7
4.000	2.109	.898	94.7	-.661	.842	-.472	.220	-144.5	25.0
5.001	2.642	.899	125.9	-.672	.861	-.497	.207	-143.5	22.6
5.998	3.177	.901	157.7	-.721	.872	-.445	.207	-148.3	24.9
Vane cascade A1B, inner door E									
1.754	0.851	0.828	25.7	-0.548	0.754	-0.300	-0.421	-151.3	54.5
1.996	.988	.841	32.8	-.557	.763	-.301	-.426	-151.7	54.8
2.492	1.257	.856	47.1	-.564	.783	-.314	-.443	-150.9	54.7
3.004	1.523	.861	62.0	-.582	.799	-.328	-.439	-150.6	53.3
3.993	2.033	.866	91.1	-.618	.827	-.367	-.410	-149.3	48.2
5.004	2.550	.867	121.6	-.620	.849	-.421	-.399	-145.8	43.5
6.003	3.066	.869	152.3	-.674	.856	-.355	-.391	-152.2	47.7

(i) Orifice plate

NPR	w_p, lbf/sec	w_p / w_i	F_i, lbf	F/F_i	F_r/F_i	F_N/F_i	F_Y/F_i	δ, deg	ϕ, deg
Vane cascade A1T, flow path A, orifice plate									
1.749	1.309	0.731	39.4	-0.652	0.804	-0.418	0.217	-147.3	27.4
2.004	1.567	.760	52.1	-.653	.812	-.431	.215	-146.6	26.5
2.499	2.031	.789	76.3	-.660	.833	-.453	.232	-145.5	27.1
2.997	2.474	.803	100.7	-.666	.849	-.471	.233	-144.7	26.3
4.007	3.348	.814	150.6	-.683	.876	-.502	.224	-143.7	24.0
5.003	4.201	.817	200.2	-.690	.893	-.525	.214	-142.7	22.2
6.003	5.049	.817	250.5	-.704	.905	-.529	.207	-143.1	21.3
Vane cascade A1B, flow path A, orifice plate									
1.749	1.280	0.715	38.6	-0.569	0.787	-0.322	-0.439	-150.5	53.8
2.006	1.532	.743	51.1	-.575	.799	-.328	-.448	-150.3	53.7
2.501	1.982	.770	74.6	-.594	.824	-.354	-.449	-149.2	51.8
3.007	2.424	.783	98.6	-.608	.842	-.376	-.446	-148.3	49.9
4.003	3.258	.791	146.1	-.635	.870	-.406	-.435	-147.4	47.0
5.003	4.081	.793	194.4	-.650	.891	-.436	-.426	-146.1	44.3
6.004	4.897	.793	243.3	-.670	.903	-.442	-.415	-146.6	43.2

Table 2. Continued

(j) Trim tabs

NPR	w_p, lbf/sec	w_p / w_i	F_i, lbf	F/F_i	F_r/F_i	F_N/F_i	F_Y/F_i	δ, deg	ϕ, deg
Vane cascade A1T, flow path A, short trim tab on both sides									
1.747	1.581	0.840	47.6	-0.688	0.873	-0.493	0.214	-144.4	23.5
2.003	1.873	.864	62.3	-.701	.890	-.504	.217	-144.3	23.3
2.499	2.382	.880	89.6	-.719	.916	-.520	.229	-144.1	23.8
2.996	2.868	.884	116.6	-.727	.934	-.533	.243	-143.8	24.5
5.011	4.819	.887	229.2	-.736	.961	-.579	.215	-141.8	20.4
6.013	5.809	.888	286.9	-.707	.967	-.626	.206	-138.5	18.2
Vane cascade A1T, flow path A, short trim tab on right side									
1.753	1.692	0.819	51.1	-0.698	0.871	-0.476	0.211	-145.7	23.9
1.997	2.000	.846	66.4	-.704	.884	-.495	.203	-144.9	22.3
2.500	2.564	.865	96.3	-.726	.914	-.514	.208	-144.7	22.1
3.001	3.085	.869	125.6	-.734	.932	-.528	.224	-144.3	23.0
3.997	4.120	.871	184.7	-.747	.954	-.554	.214	-143.4	21.1
5.007	5.168	.871	245.8	-.752	.959	-.560	.203	-143.3	19.9
5.995	6.180	.872	306.8	-.719	.962	-.610	.195	-139.7	17.7
Vane cascade A1T, flow path A, long trim tab on both sides									
1.752	1.317	0.854	39.8	-0.683	0.871	-0.498	0.211	-143.9	22.9
2.003	1.546	.874	51.5	-.694	.885	-.503	.221	-144.1	23.7
2.503	1.970	.890	74.2	-.714	.915	-.521	.236	-143.9	24.3
3.002	2.375	.894	96.6	-.725	.932	-.532	.243	-143.7	24.5
3.992	3.173	.897	142.1	-.742	.952	-.553	.224	-143.3	22.1
4.995	3.969	.899	189.1	-.732	.957	-.578	.214	-141.7	20.3
5.997	4.763	.900	236.9	-.706	.961	-.619	.205	-138.8	18.3
Vane cascade A1T, flow path A, long trim tab on right side									
1.752	1.559	0.822	47.0	-0.679	0.857	-0.483	0.199	-144.6	22.4
1.998	1.842	.850	61.2	-.692	.875	-.499	.195	-144.2	21.3
2.496	2.348	.867	88.4	-.717	.907	-.517	.203	-144.2	21.4
2.995	2.832	.871	115.2	-.728	.926	-.529	.218	-144.0	22.4
4.001	3.799	.874	170.1	-.743	.947	-.549	.207	-143.5	20.7
5.002	4.744	.874	225.9	-.742	.953	-.564	.197	-142.8	19.2
5.999	5.684	.875	282.7	-.713	.960	-.614	.189	-139.3	17.1

Table 2. Concluded

(k) Sidewalls

NPR	w_p, lbf/sec	w_p/w_i	F_i, lbf	F/F_i	F_r/F_i	F_N/F_i	F_Y/F_i	δ, deg	ϕ, deg
Vane cascade A1T, flow path A, sidewalls installed									
1.755	1.790	0.806	54.0	-0.691	0.856	-0.459	0.212	-146.4	24.8
2.002	2.117	.832	70.3	-.698	.876	-.489	.200	-145.0	22.3
2.496	2.701	.851	101.4	-.718	.904	-.511	.201	-144.6	21.4
3.001	3.253	.856	132.7	-.728	.928	-.533	.215	-143.8	22.0
3.994	4.346	.857	194.8	-.738	.955	-.571	.206	-142.3	19.9
4.999	5.453	.857	259.0	-.752	.961	-.567	.189	-143.0	18.4
6.016	6.547	.857	325.2	-.715	.965	-.626	.170	-138.8	15.2
Vane cascade A1B, flow path A, sidewalls installed									
1.754	1.701	0.854	51.4	-0.612	0.809	-0.361	-0.386	-149.4	46.9
2.009	1.991	.869	66.4	-.610	.821	-.379	-.398	-148.2	46.4
2.508	2.524	.882	95.2	-.617	.842	-.409	-.402	-146.5	44.5
2.999	3.034	.886	123.4	-.634	.863	-.430	-.396	-145.9	42.7
4.001	4.058	.889	182.1	-.661	.901	-.479	-.380	-144.1	38.4
5.005	5.094	.890	242.3	-.680	.922	-.503	-.369	-143.5	36.3
6.002	6.101	.890	302.9	-.653	.934	-.563	-.360	-139.2	32.6

(l) Alternate external door

NPR	w_p, lbf/sec	w_p/w_i	F_i, lbf	F/F_i	F_r/F_i	F_N/F_i	F_Y/F_i	δ, deg	ϕ, deg
Vane cascade A1T, flow path A, alternate external door									
1.752	1.803	0.812	54.3	-0.696	0.846	-0.435	0.206	-148.0	25.4
1.998	2.137	.840	70.8	-.711	.860	-.440	.201	-148.3	24.6
2.498	2.724	.857	102.3	-.736	.896	-.460	.221	-148.0	25.6
3.004	3.282	.860	133.6	-.752	.919	-.471	.239	-147.9	26.9
4.002	4.383	.861	196.1	-.778	.940	-.478	.224	-148.4	25.1
5.007	5.467	.861	260.6	-.767	.953	-.525	.213	-145.6	22.1
6.008	6.556	.860	325.9	-.742	.963	-.578	.205	-142.1	19.6
Vane cascade A1B, flow path A, alternate external door									
1.753	1.730	0.866	52.2	-0.627	0.837	-0.320	-0.453	-153.0	54.8
2.001	2.012	.880	67.0	-.641	.861	-.320	-.477	-153.4	56.1
2.494	2.539	.892	95.6	-.659	.894	-.342	-.497	-152.6	55.5
3.002	3.070	.894	124.9	-.683	.916	-.355	-.496	-152.6	54.4
4.001	4.083	.895	183.5	-.715	.936	-.389	-.464	-151.5	50.0
5.012	5.131	.895	244.4	-.726	.945	-.413	-.441	-150.4	46.9
6.001	6.138	.895	304.8	-.702	.949	-.473	-.429	-146.0	42.2

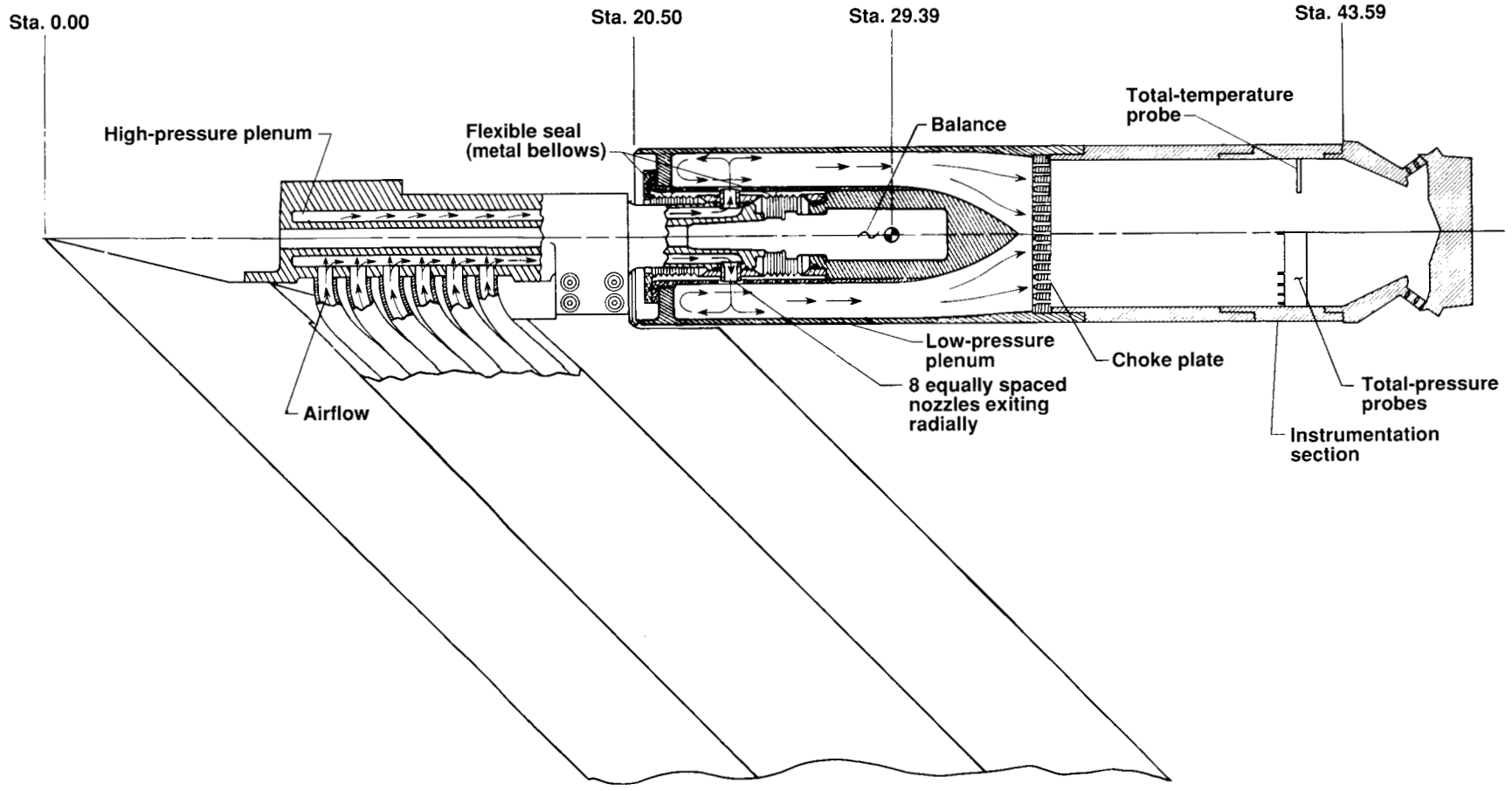

Figure 1. Sketch of air-powered nacelle model with typical dual-port reverser configuration installed.

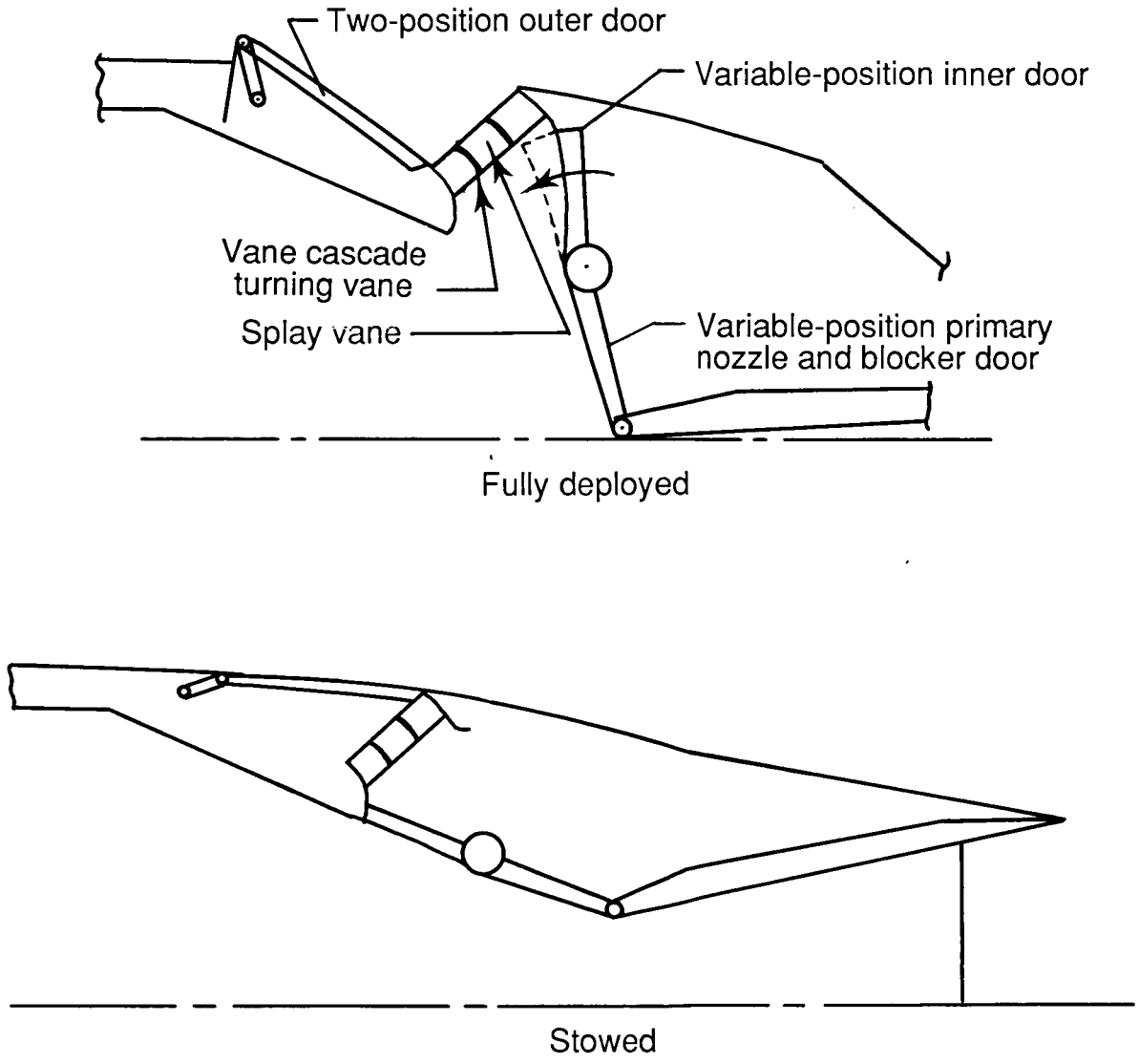

Figure 2. Schematic of thrust reverser concept.

(a) Baseline configuration with sidewall removed. L-89-51

Figure 3. Model hardware.

ORIGINAL PAGE
BLACK AND WHITE PHOTOGRAPH

(b) Close-up of reverser port.

Figure 3. Continued.

L-89-53

(c) Vane cascades.

Figure 3. Continued.

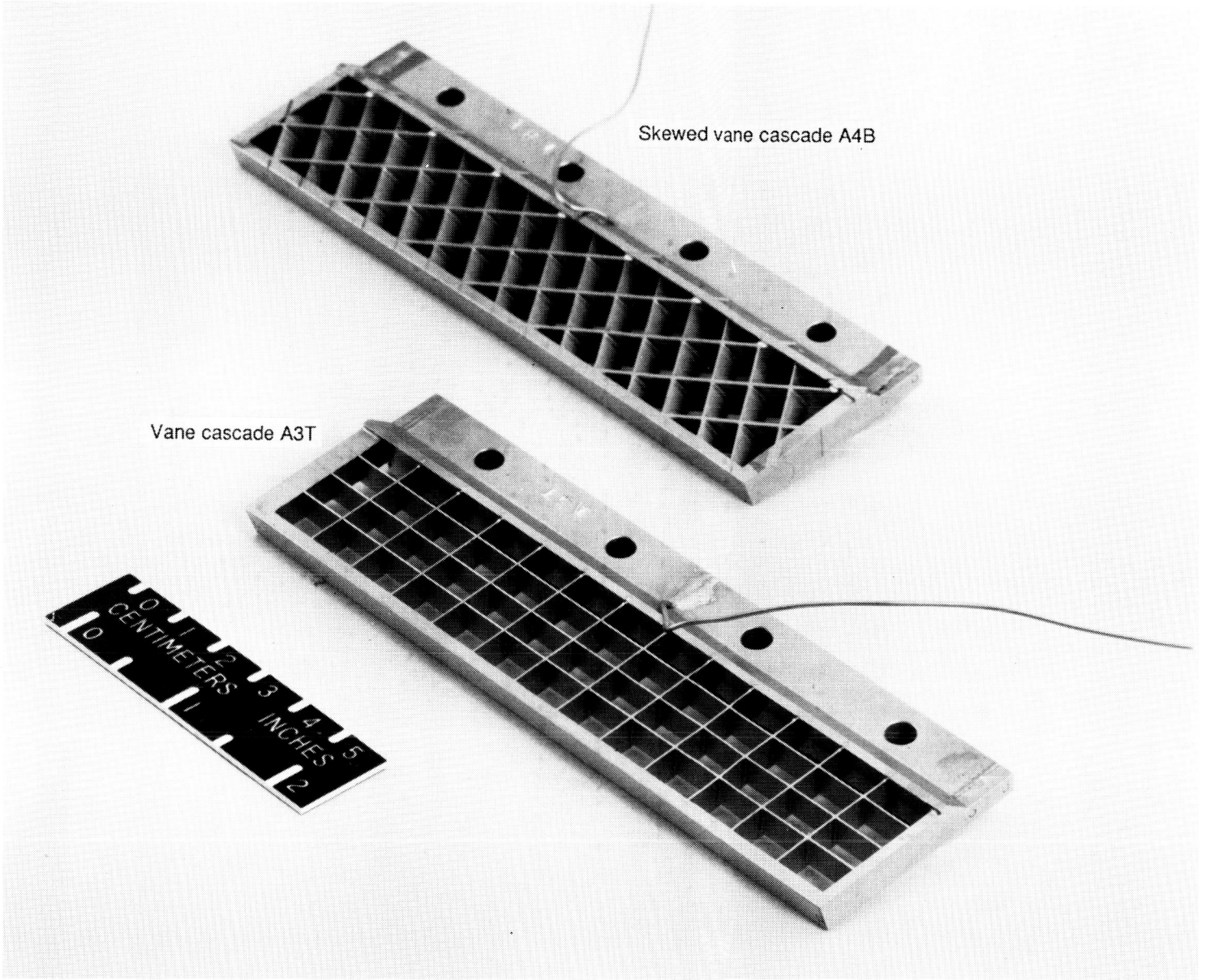

L-89-54

(c) Concluded.

Figure 3. Continued.

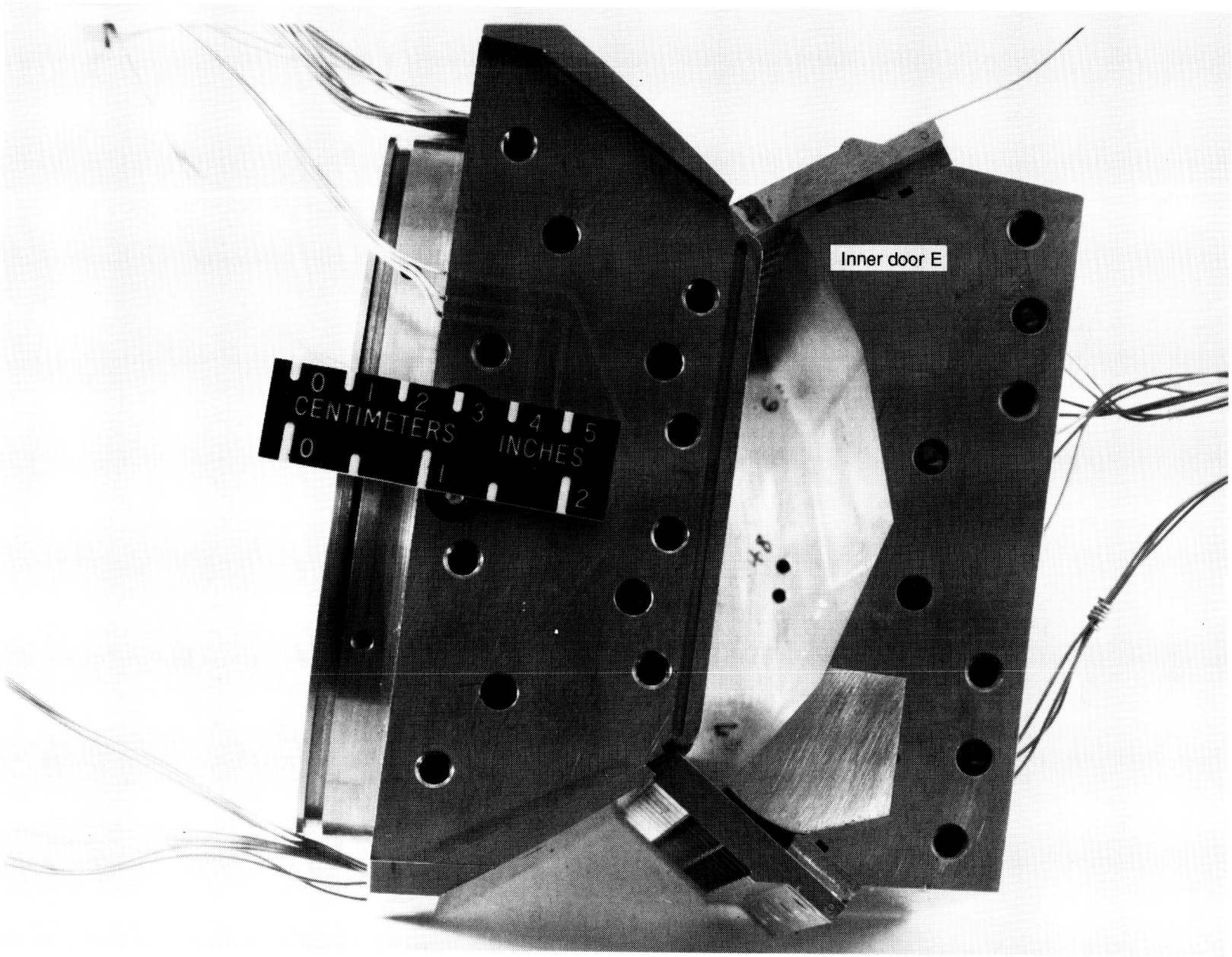

L-89-55

(d) Reverser with inner door E; sidewall and splitter removed.

Figure 3. Concluded.

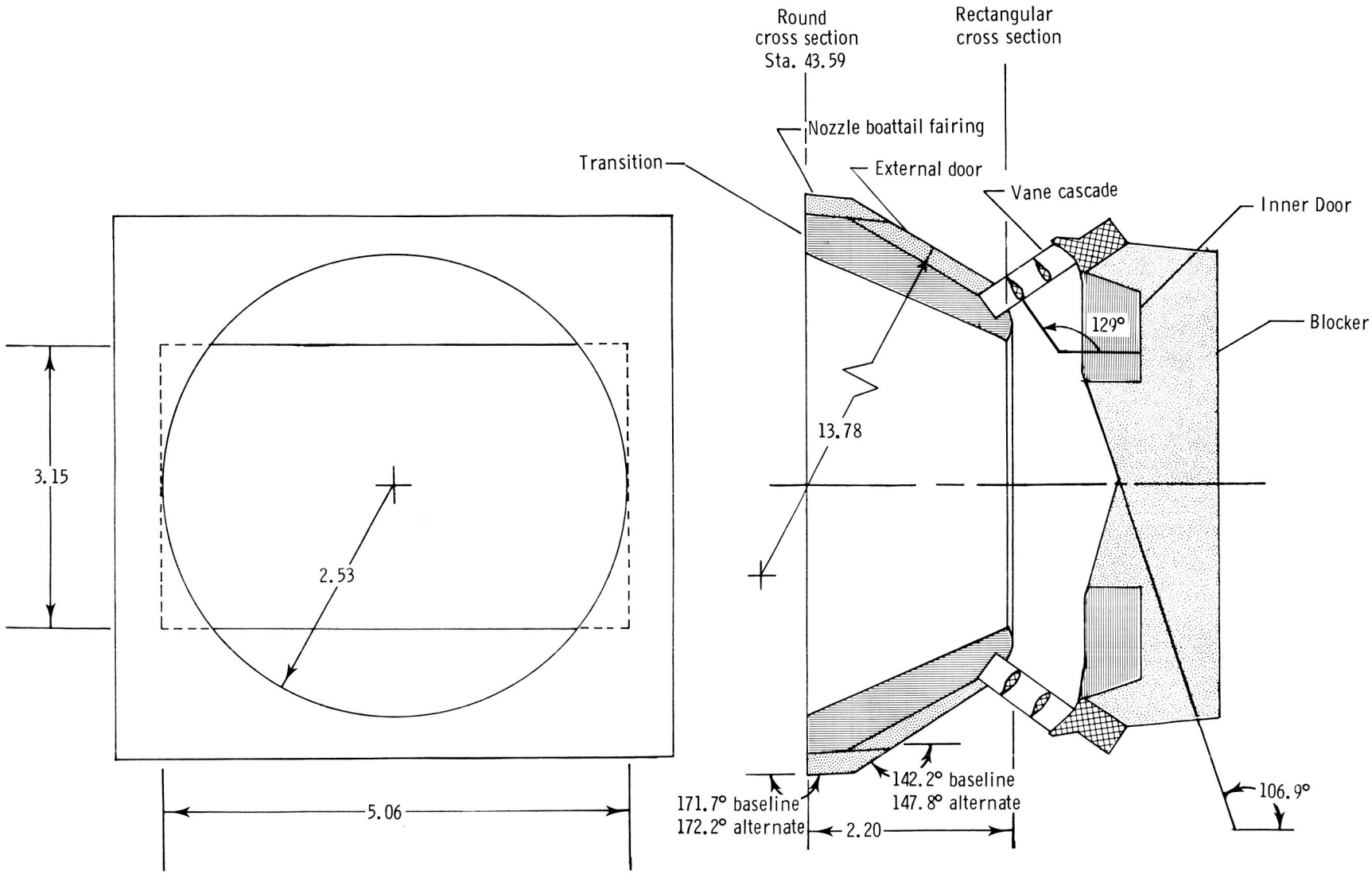

(a) Dual-port configuration.

Figure 4. Sketches of model hardware. Dimensions are in inches unless otherwise noted.

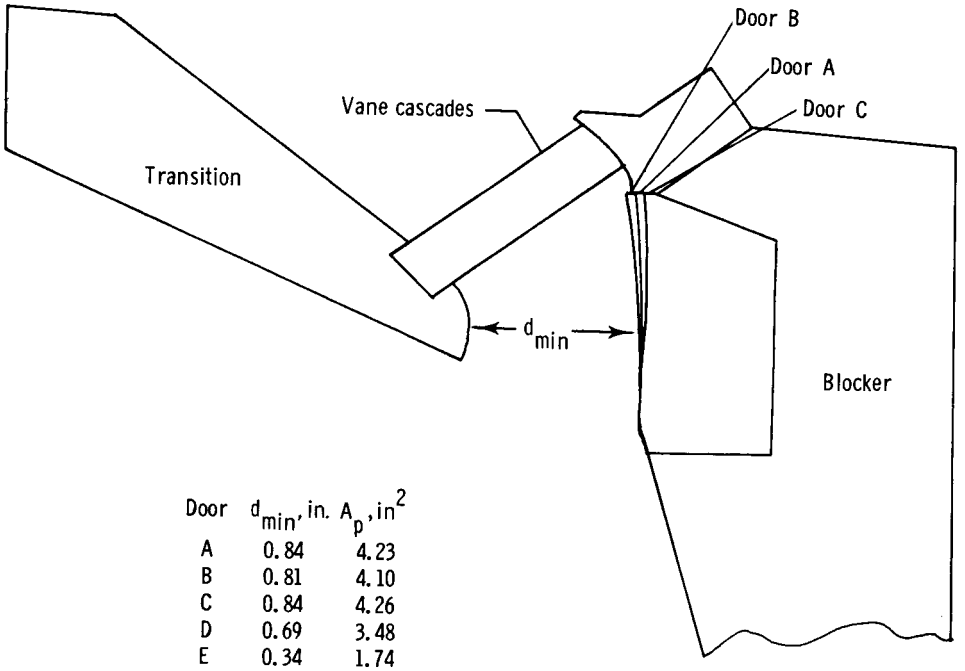

Door	d_{min}, in.	A_p, in^2
A	0.84	4.23
B	0.81	4.10
C	0.84	4.26
D	0.69	3.48
E	0.34	1.74

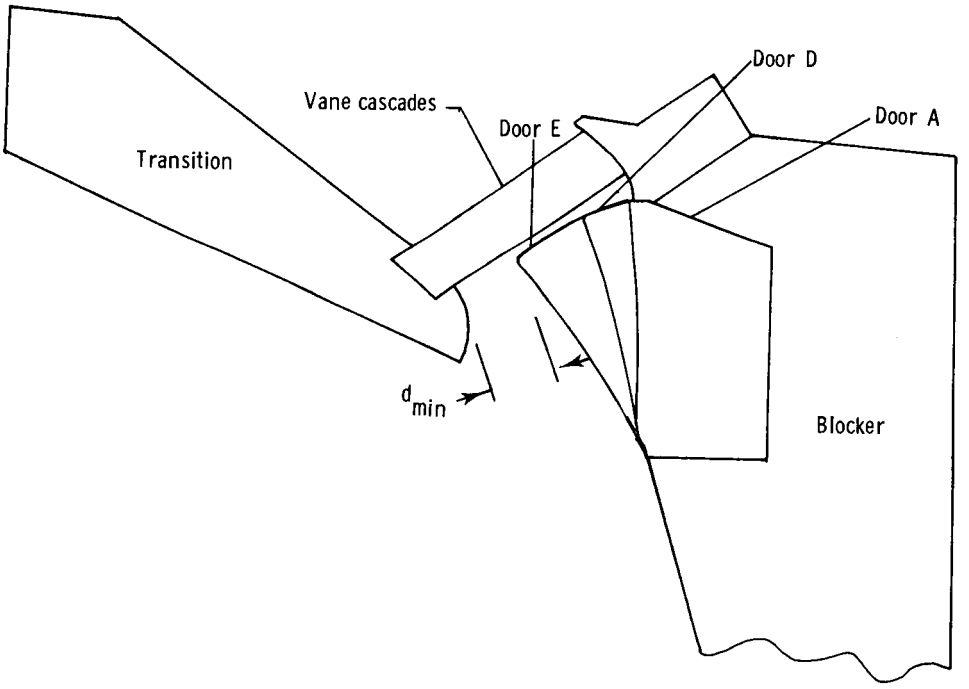

(b) Inner doors.

Figure 4. Continued.

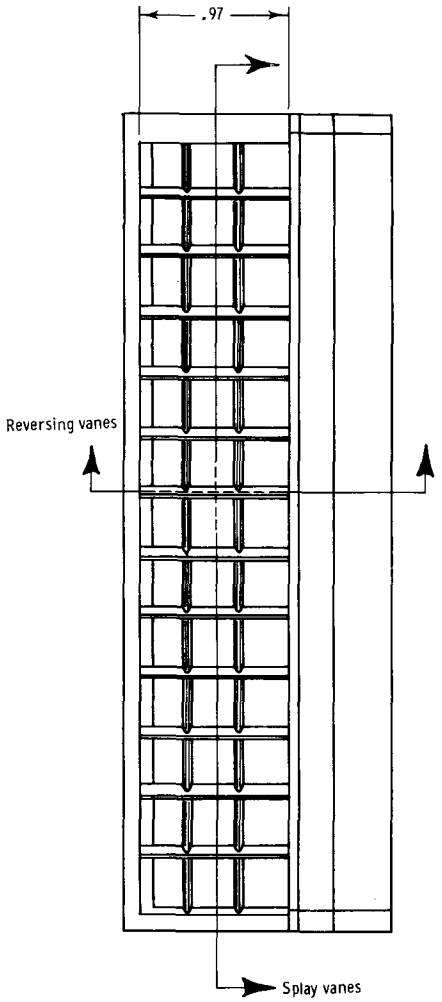

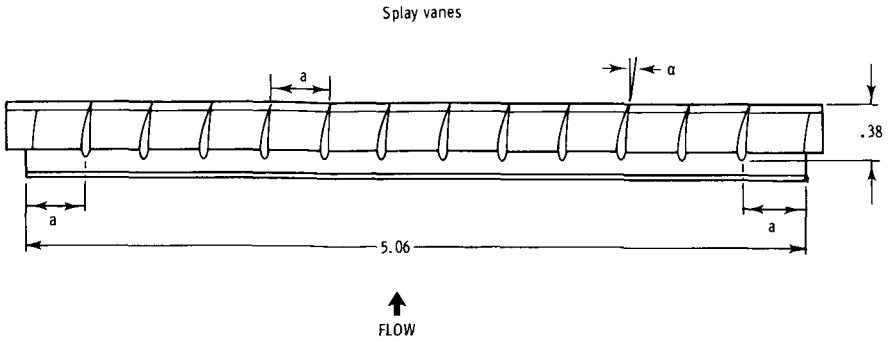

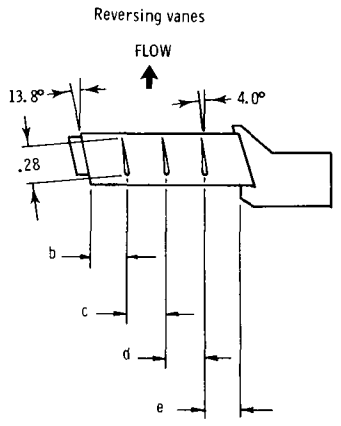

Vane Cascade	Number of reversing vanes	Number of splay vanes	α, deg	a	b	c	d	e	A_v, in^2
A1T	2	12	9	0.39	0.31	0.33	0.35		3.76
A1B	2	12	19	0.39	0.31	0.33	0.35		3.39
B1T	2	12	9	0.39	0.29	0.31	0.33		3.50
B1B	2	12	19	0.39	0.29	0.31	0.33		3.20
C1T	2	12	9	0.39	0.32	0.34	0.36		4.04
C1B	2	12	19	0.39	0.32	0.34	0.36		3.73
A3T	3	12	9	0.39	0.22	0.24	0.24	0.27	3.59
A2T	2	9	9	0.51	0.31	0.33	0.35		3.87
A2B	2	9	19	0.51	0.31	0.33	0.35		3.51

(c) Vane cascades.

Figure 4. Continued.

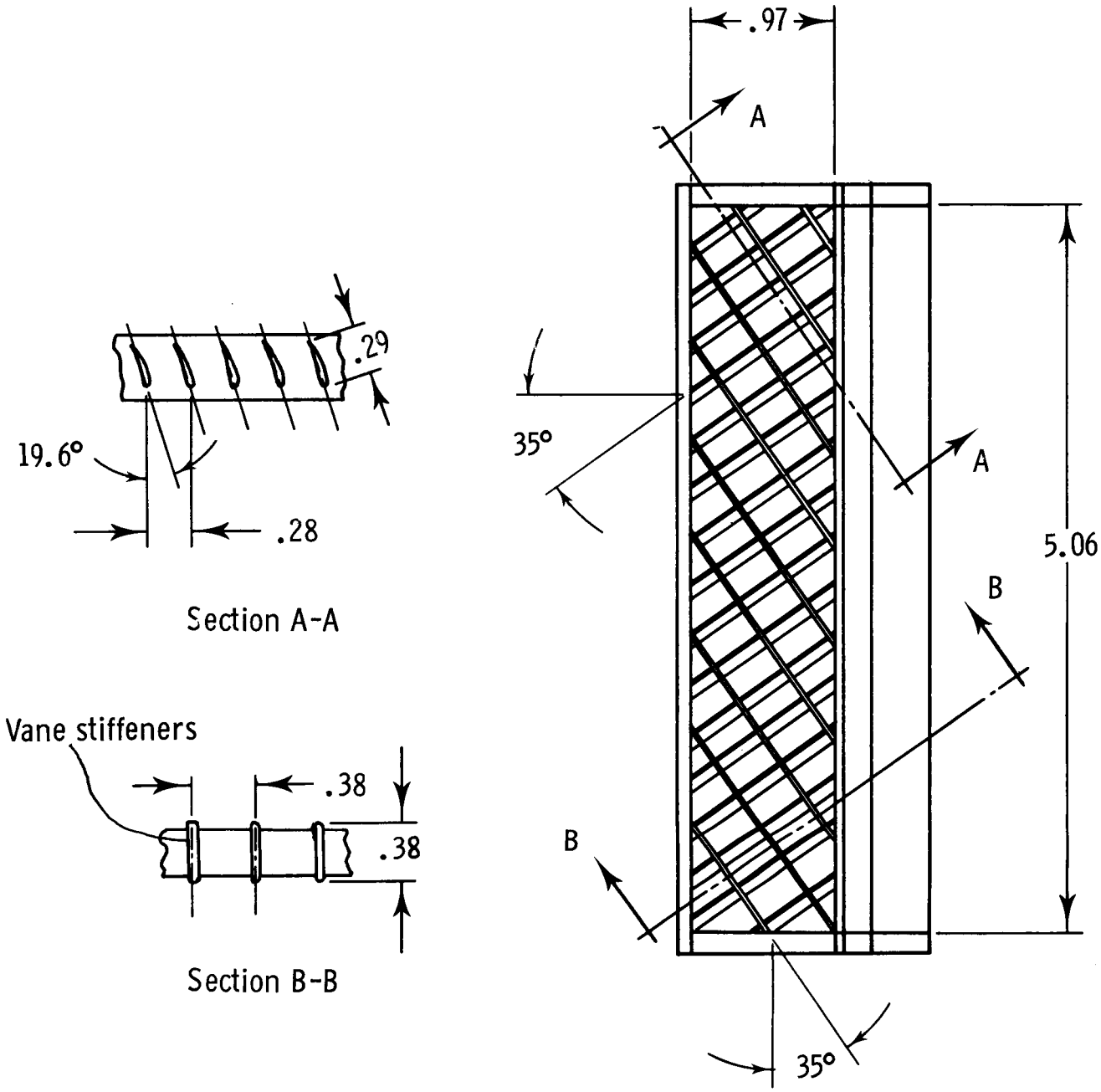

(d) Skewed vane cascade, A4B; $A_v = 3.21$ in^2.

Figure 4. Continued.

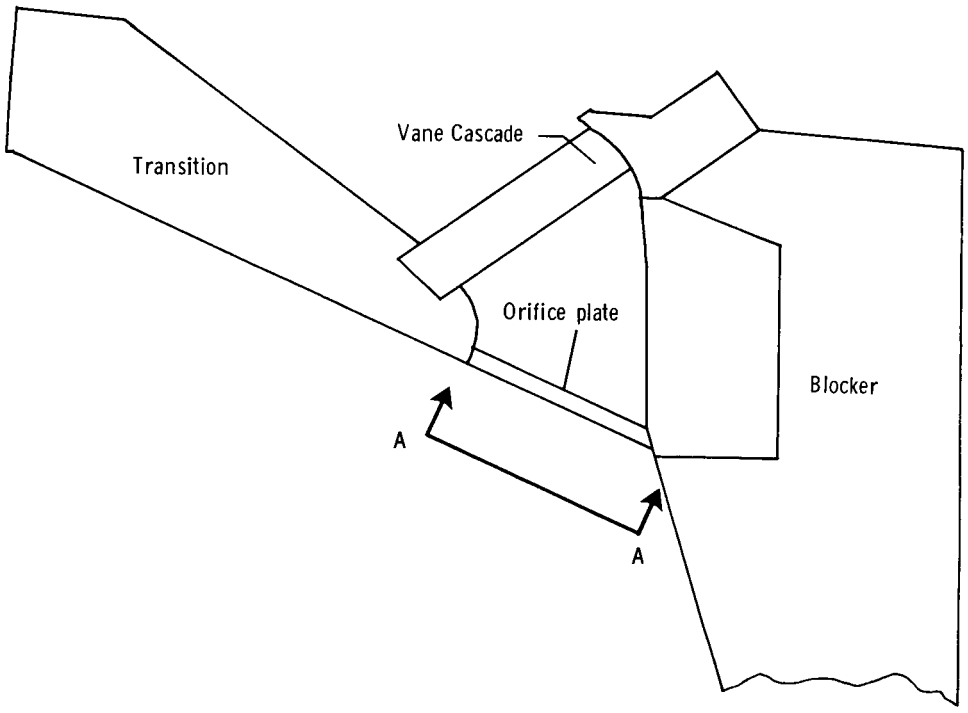

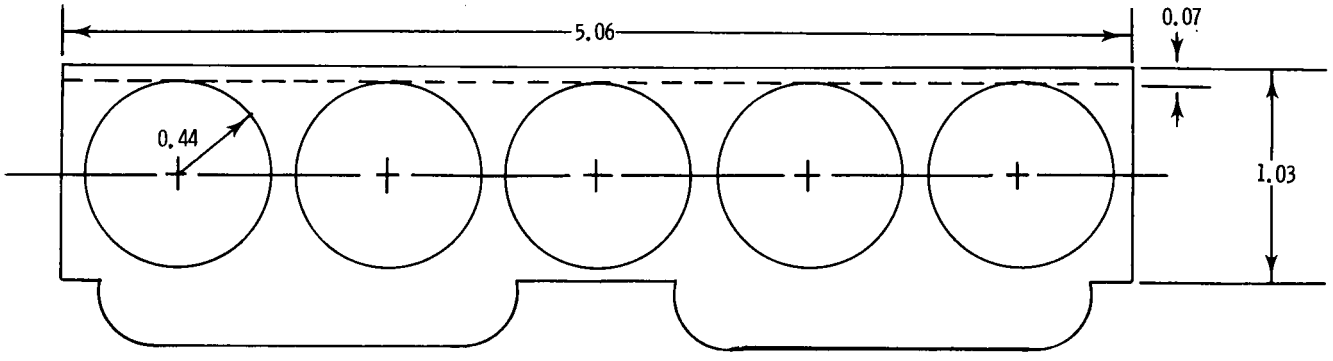

View A-A

(e) Orifice plate; $A_p = 3.04$ in^2.

Figure 4. Continued.

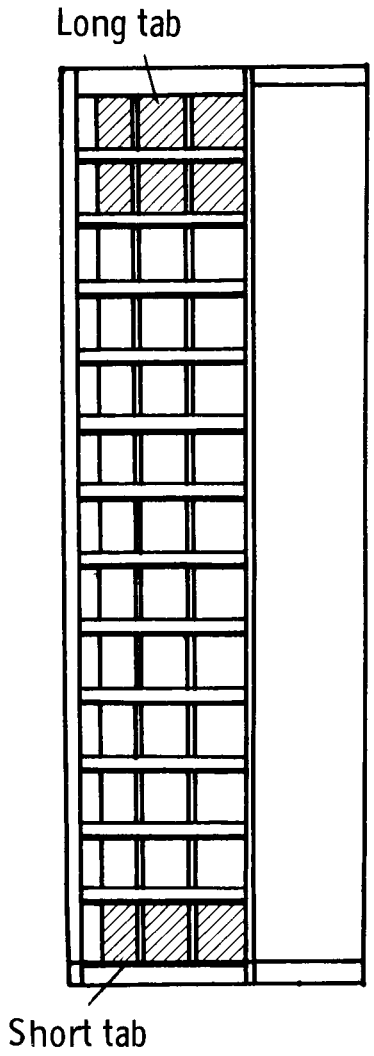

Configuration	A_V, in^2
Open	3.76
Short tab right	3.47
Short tab both	3.18
Long tab right	3.19
Long tab both	2.60

(f) Trim tabs.

Figure 4. Continued.

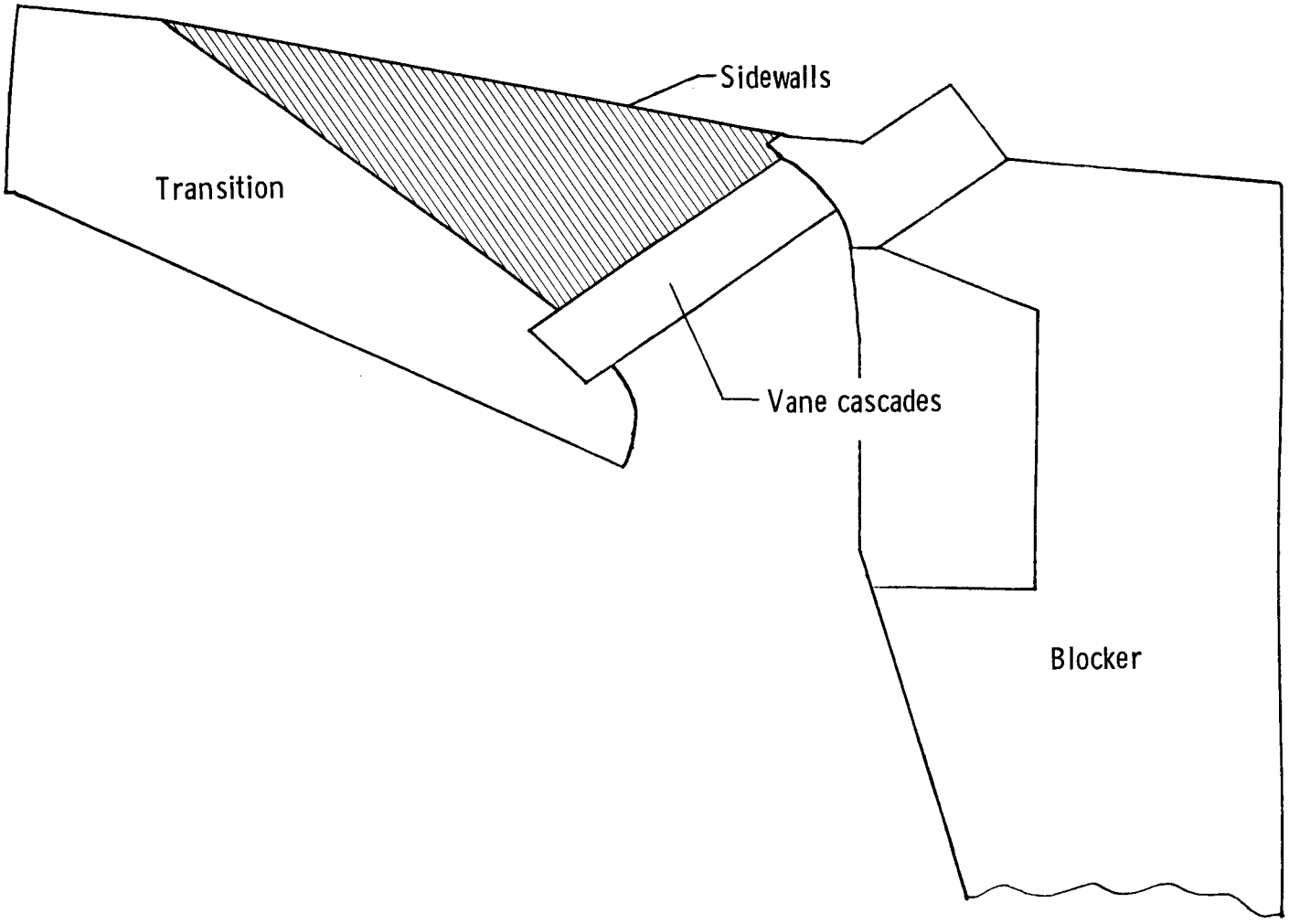

(g) Port sidewalls.

Figure 4. Continued.

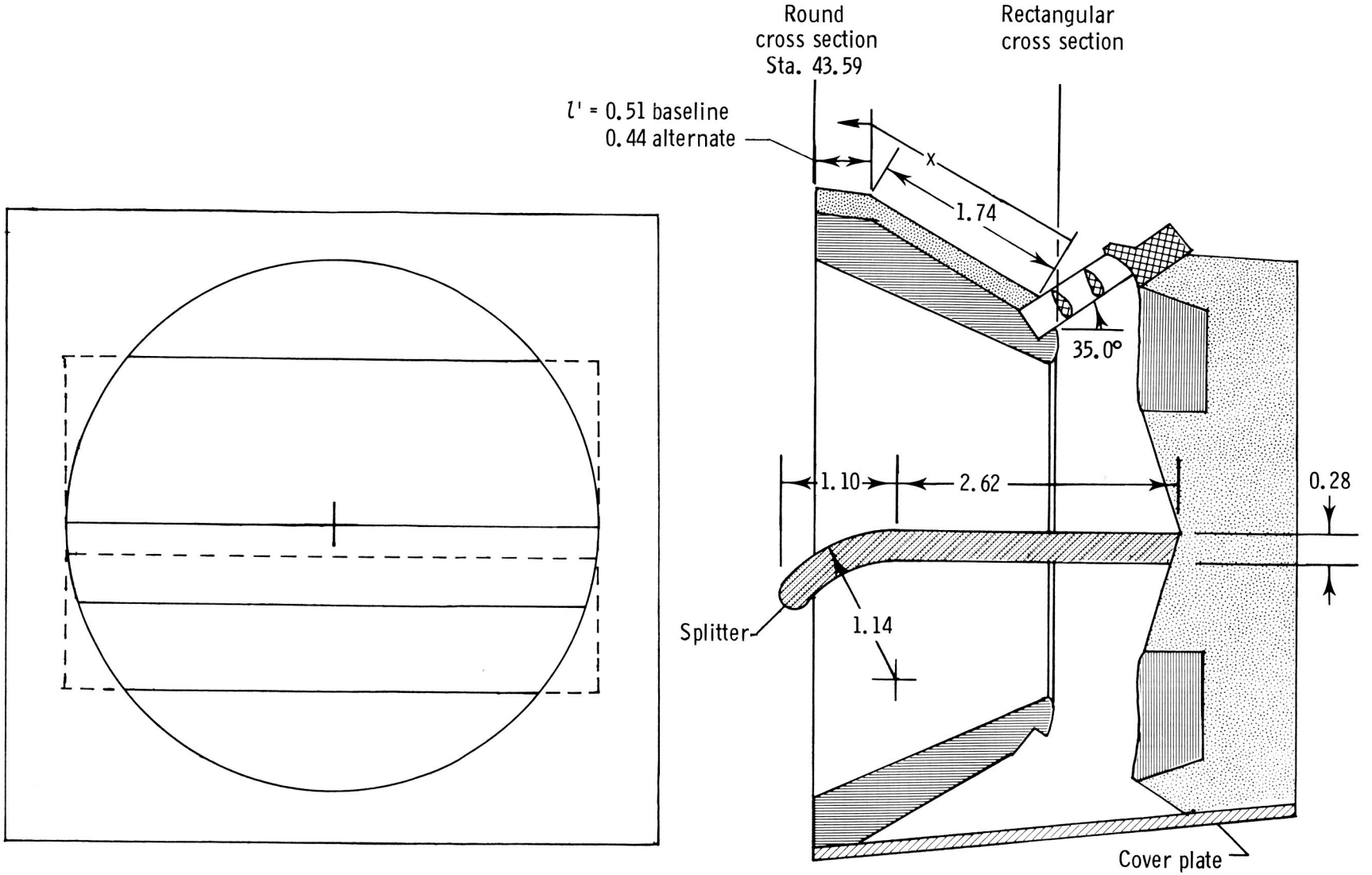

(h) Single-port configuration with splitter.

Figure 4. Concluded.

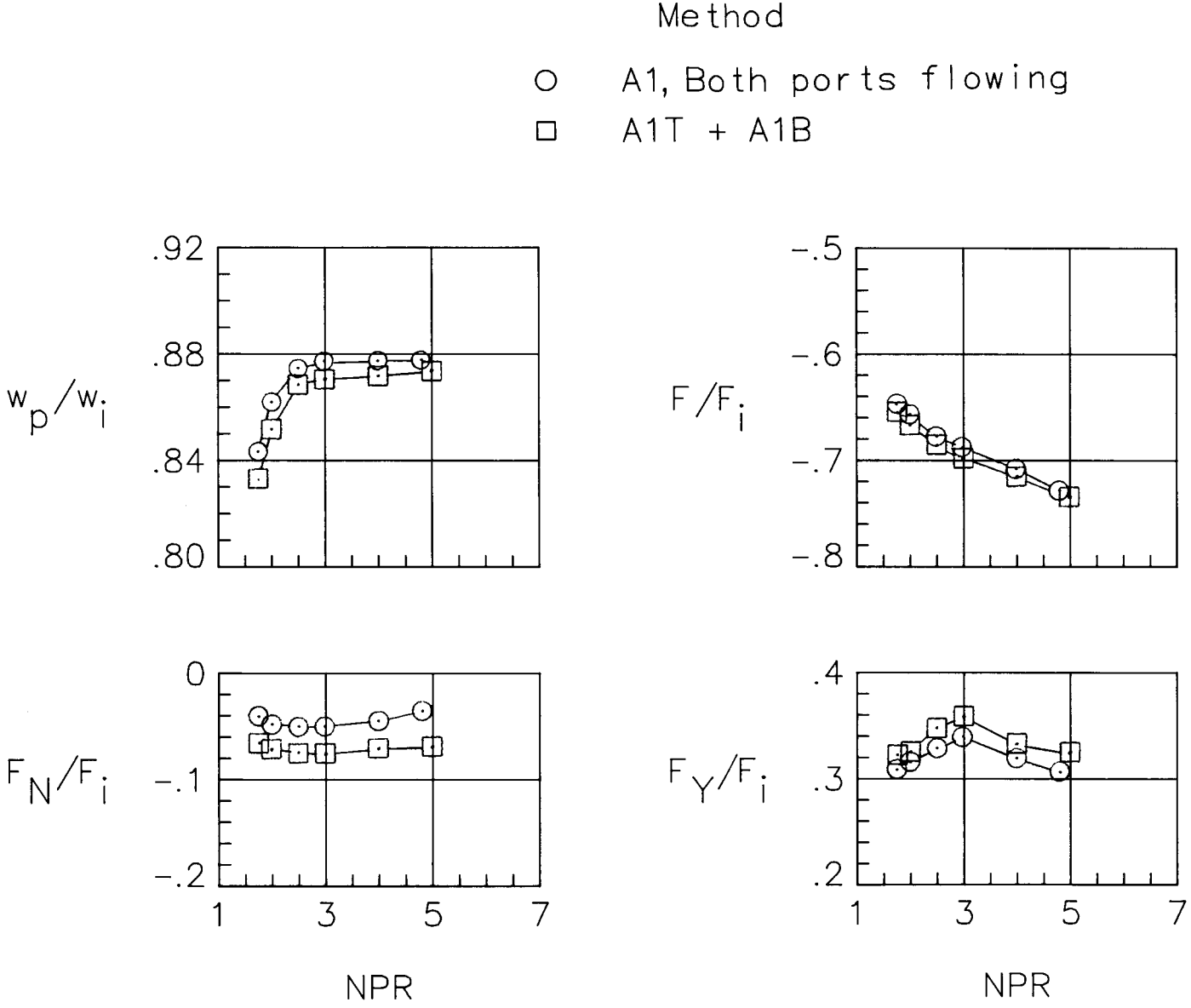

(a) Configuration A1.

Figure 5. Effect of splitter plate on basic performance.

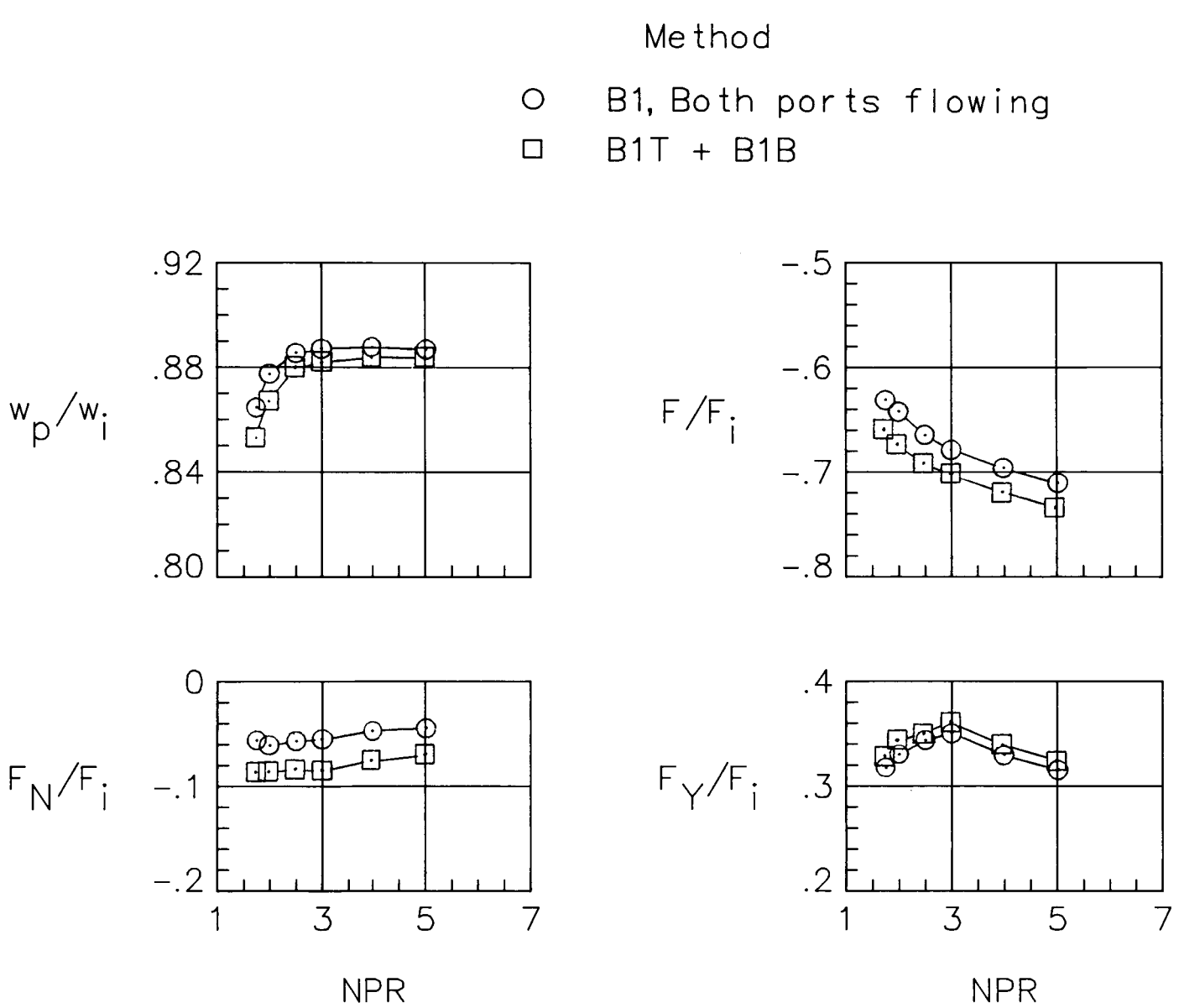

(b) Configuration B1.

Figure 5. Continued.

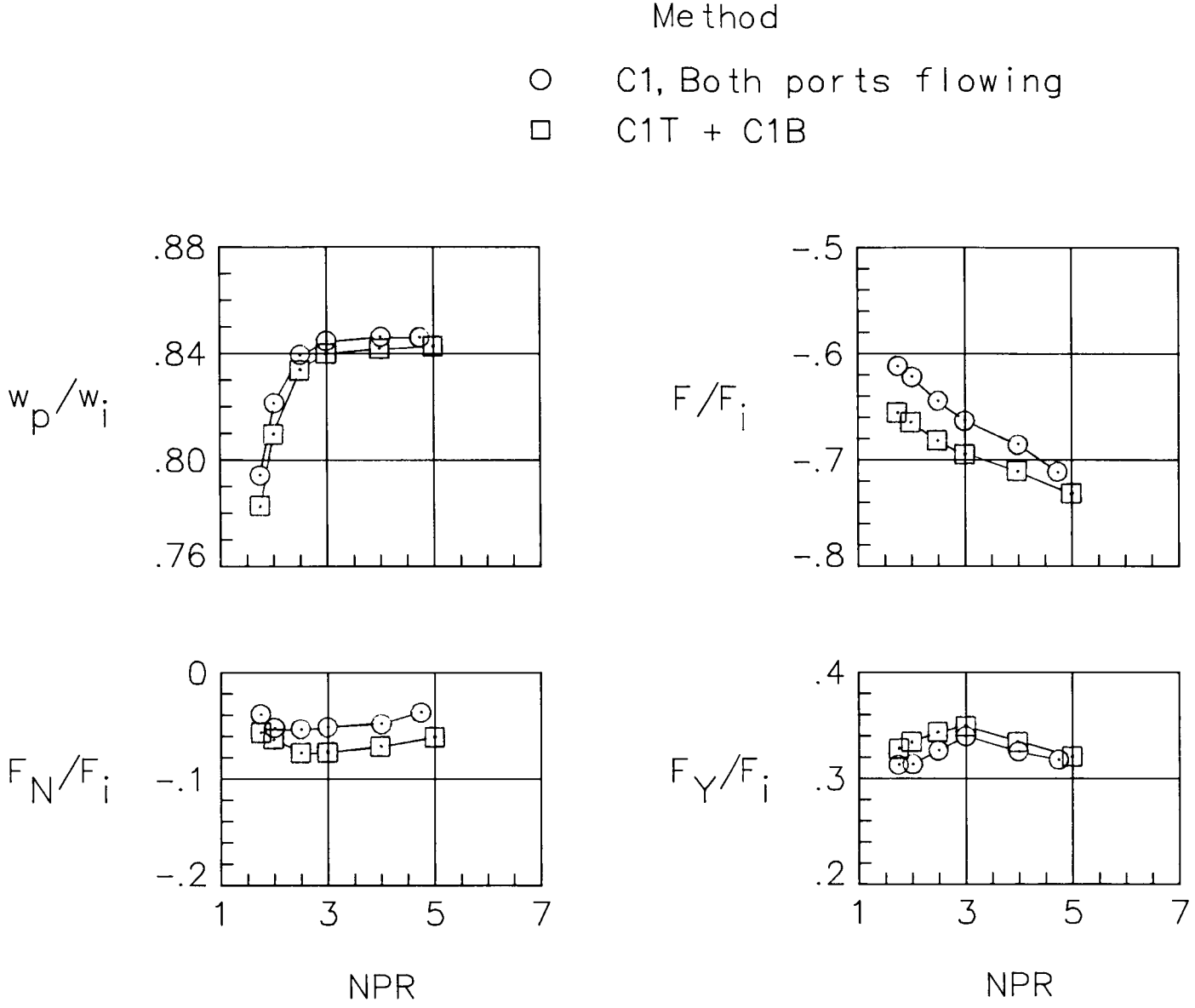

(c) Configuration C1.

Figure 5. Continued.

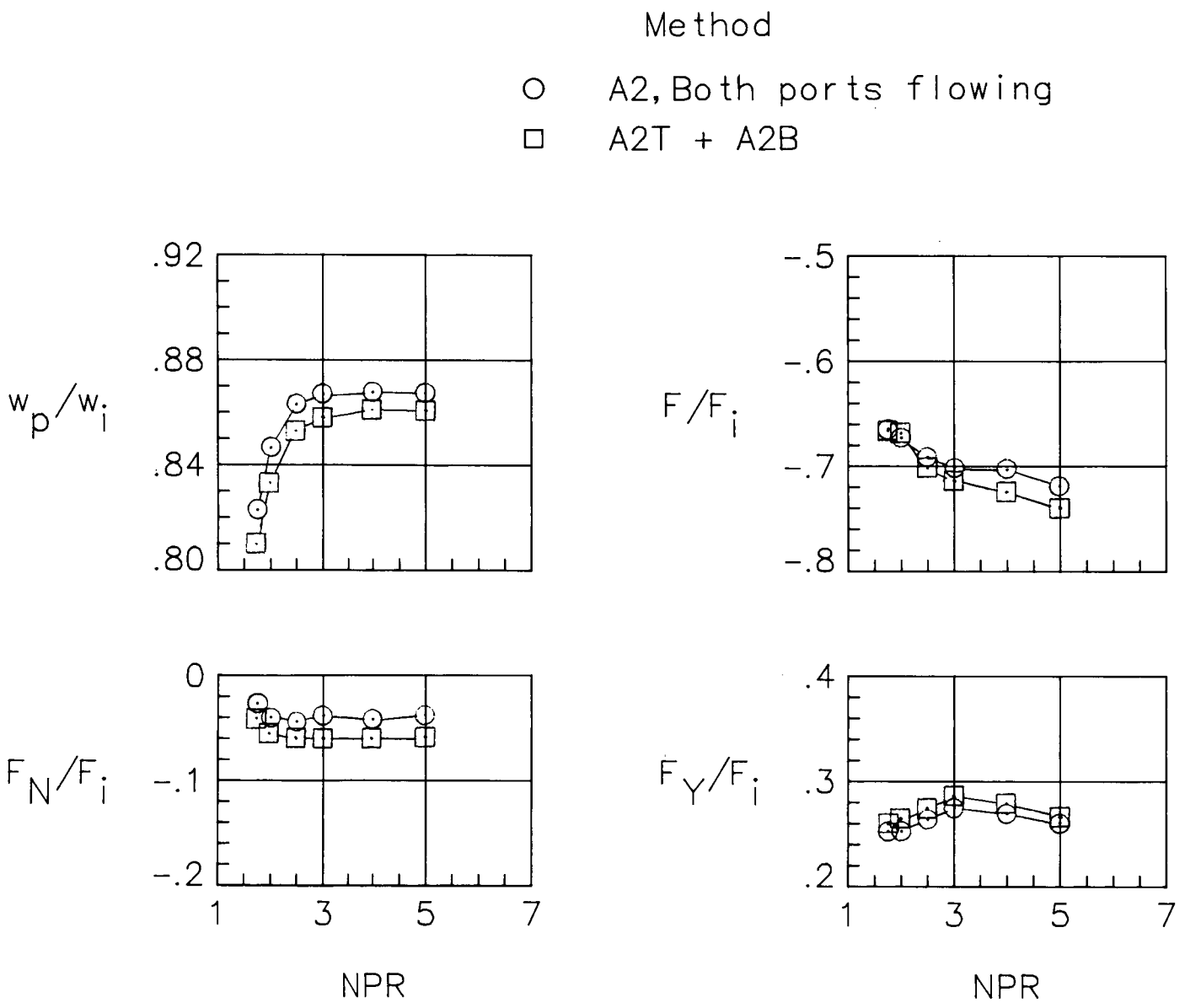

(d) Configuration A2.

Figure 5. Continued.

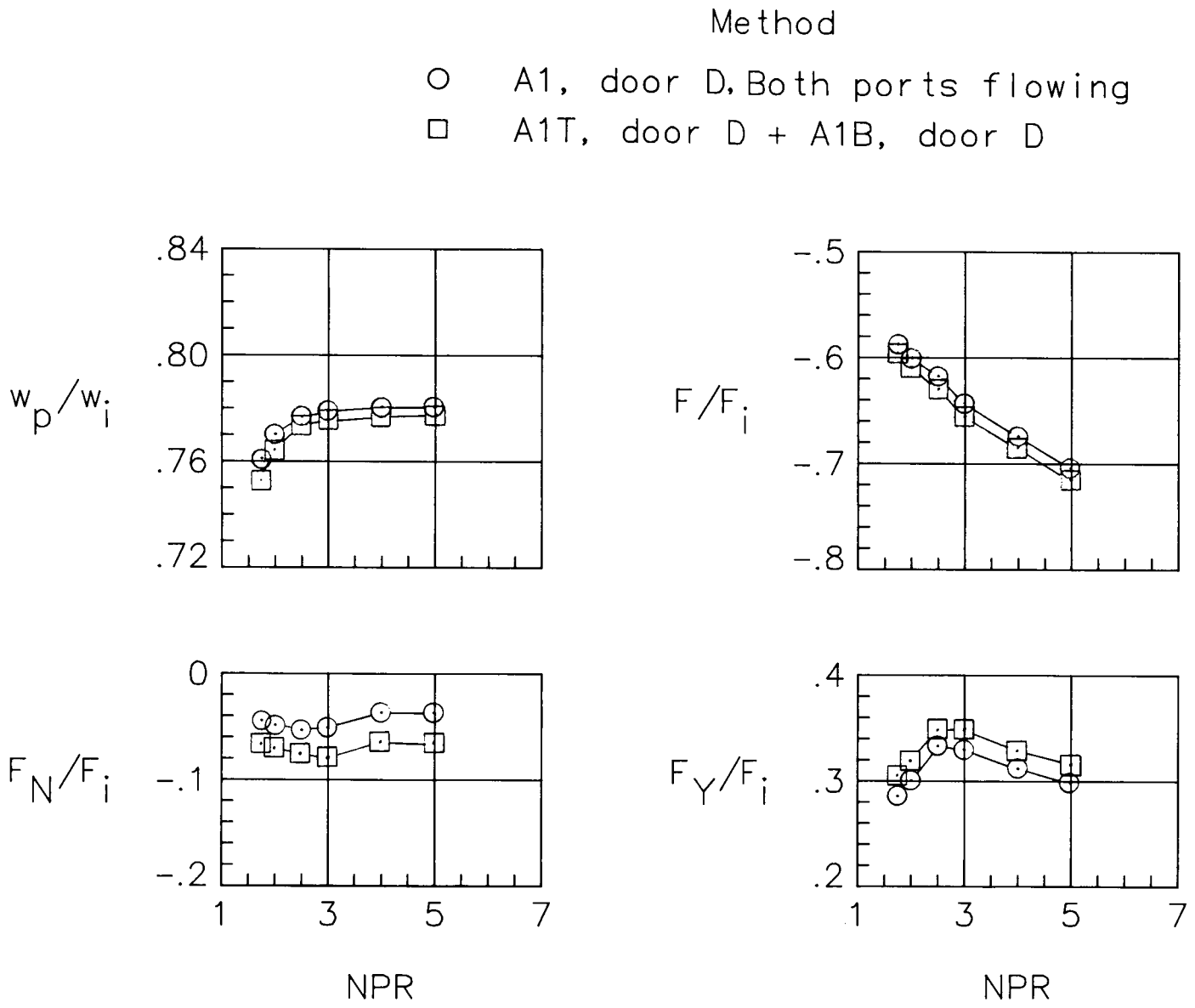

(e) Inner door D.

Figure 5. Continued.

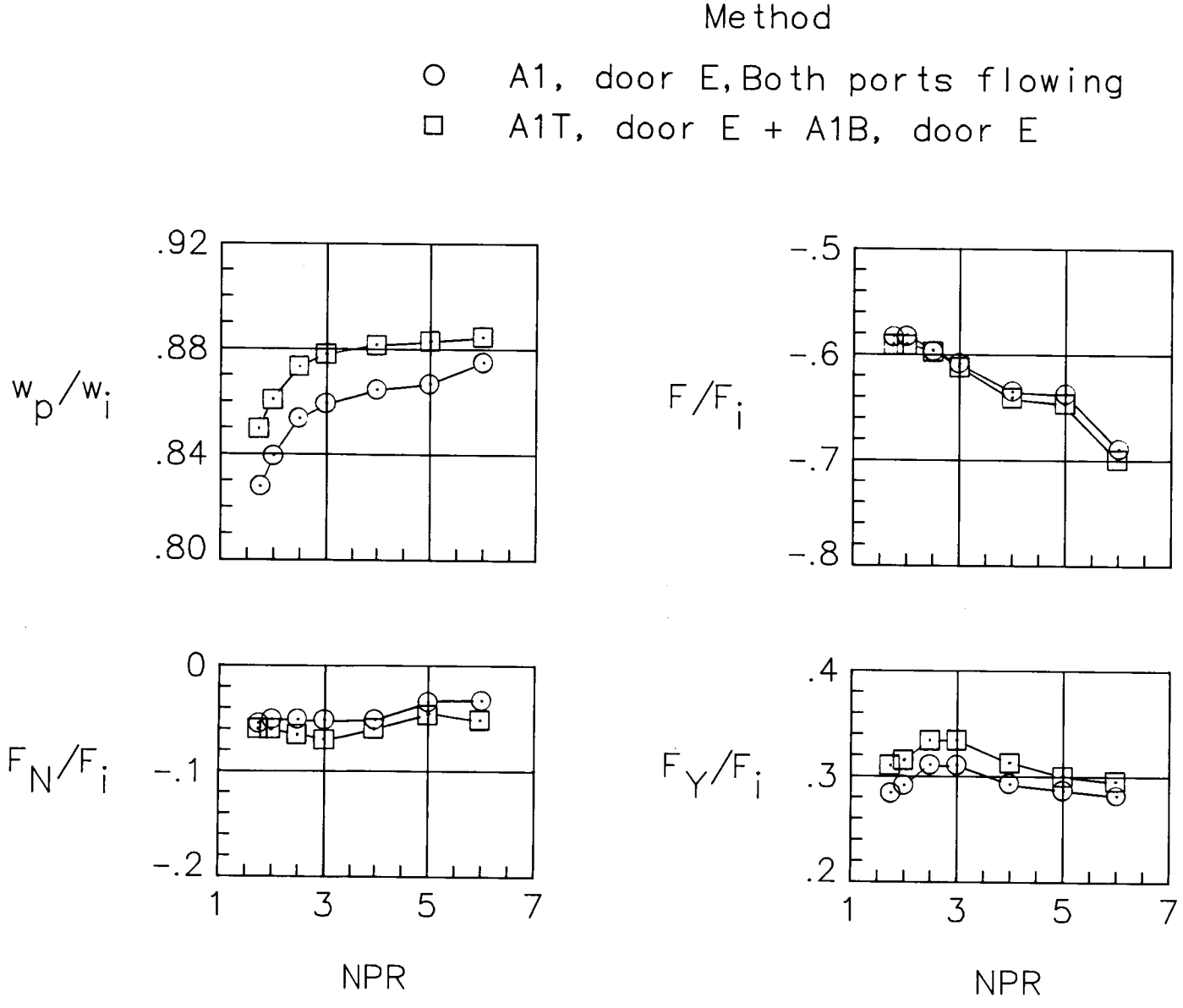

(f) Inner door E.

Figure 5. Concluded.

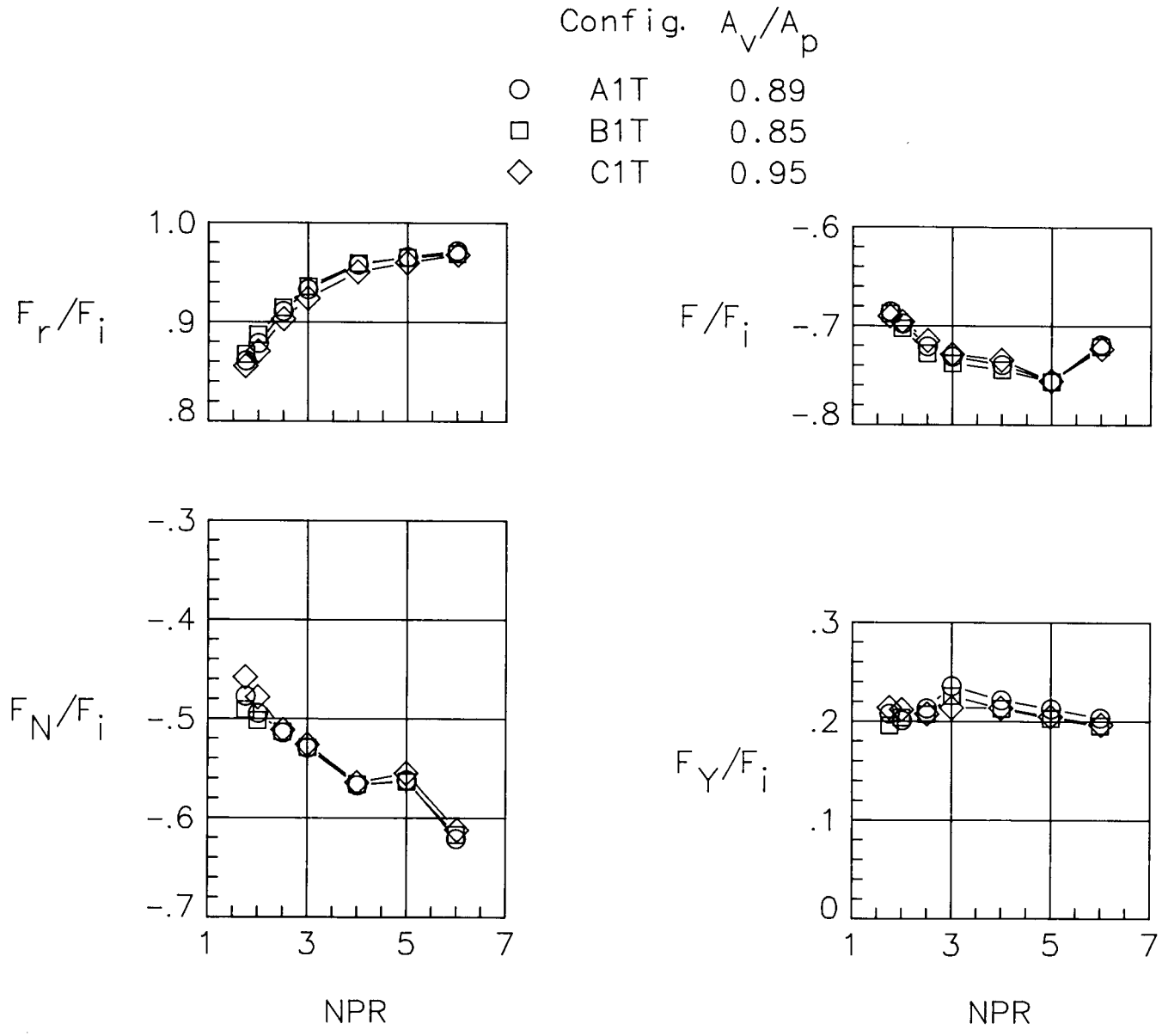

(a) Force data; top port.

Figure 6. Effect of port flow-path area on basic performance.

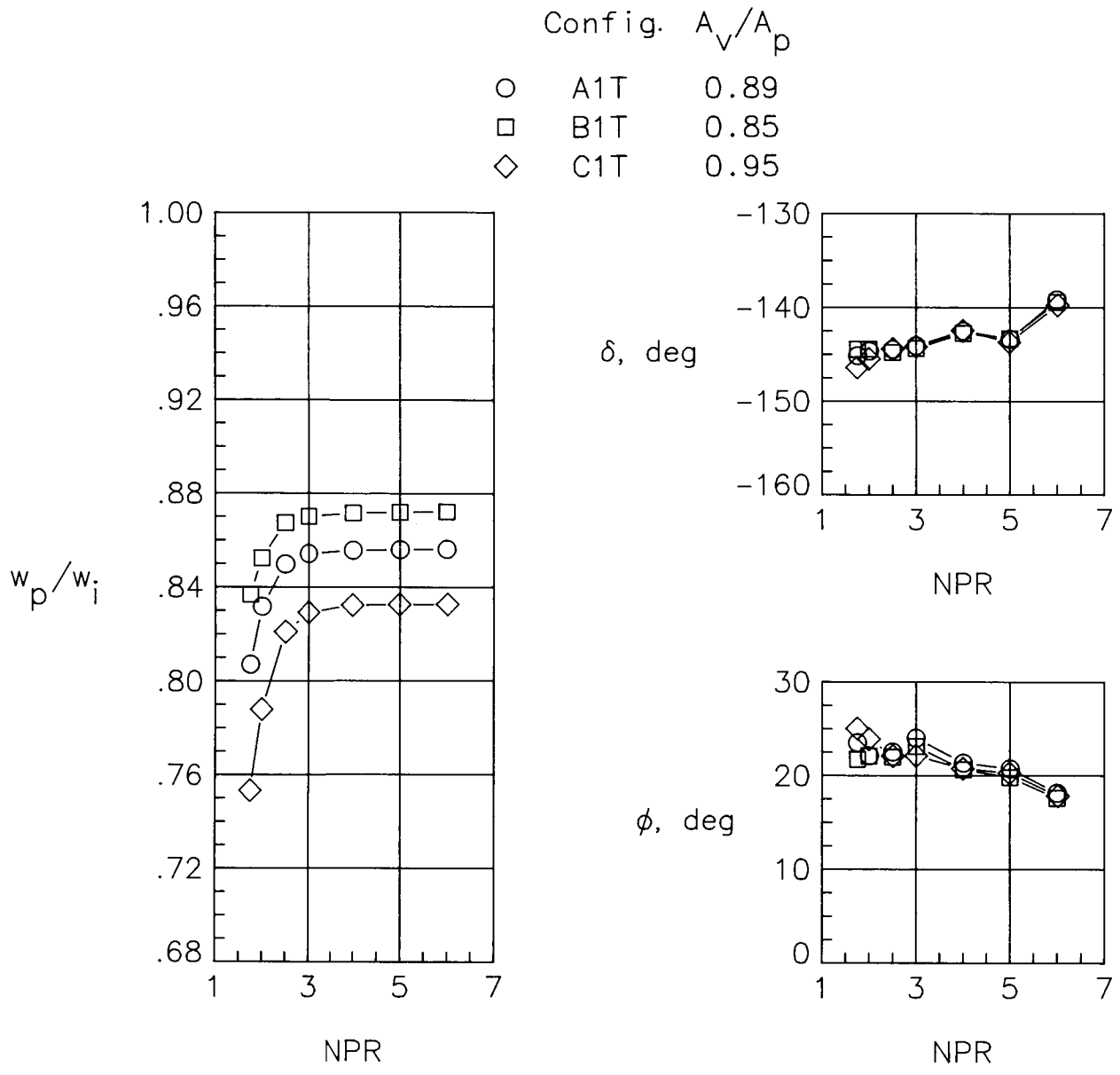

(b) Discharge coefficient and turning angles; top port.

Figure 6. Continued.

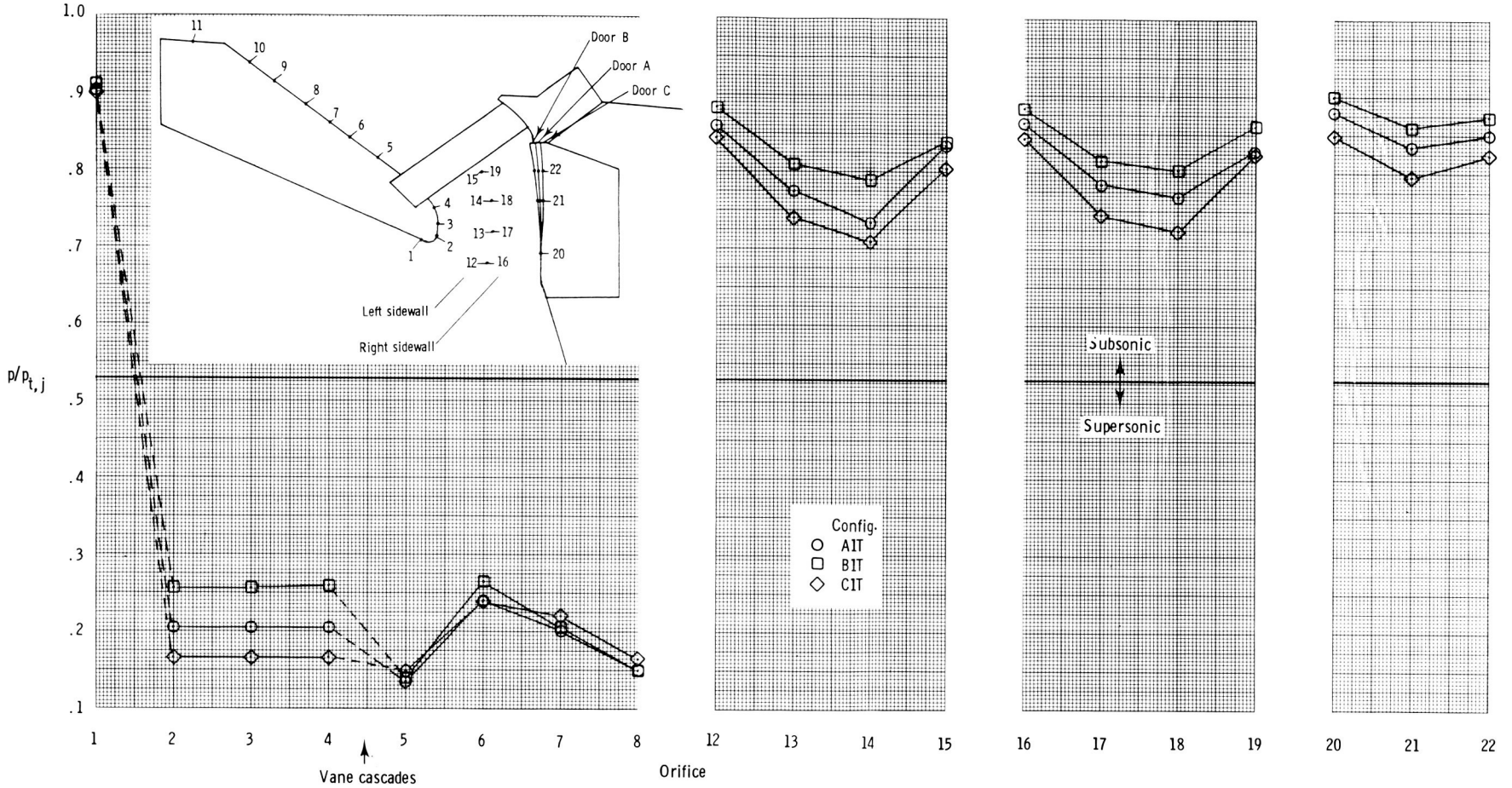

(c) Static pressures; top port; NPR = 5.0.

Figure 6. Continued.

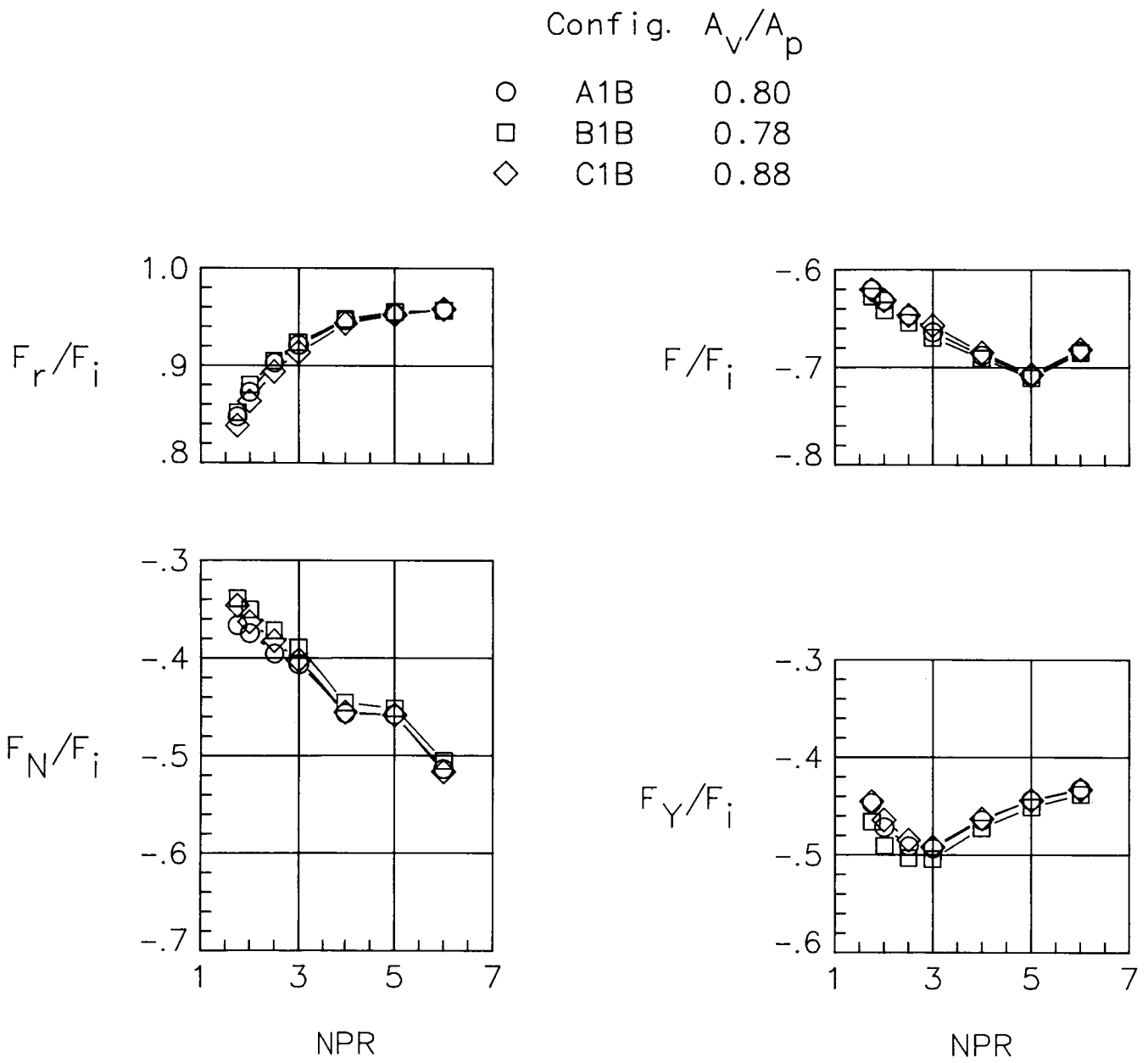

(d) Force data; bottom port.

Figure 6. Continued.

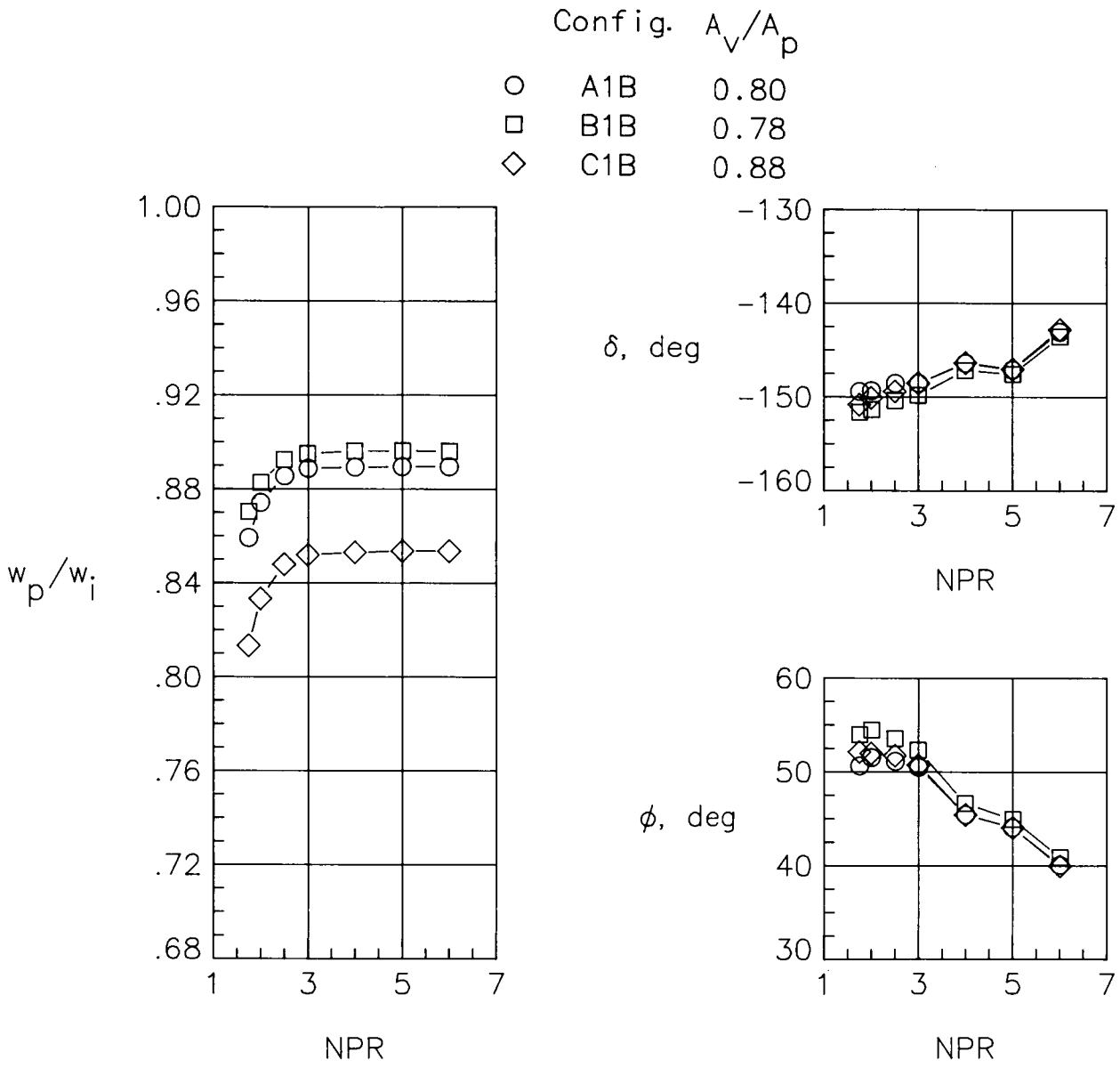

(e) Discharge coefficient and turning angles; bottom port.

Figure 6. Continued.

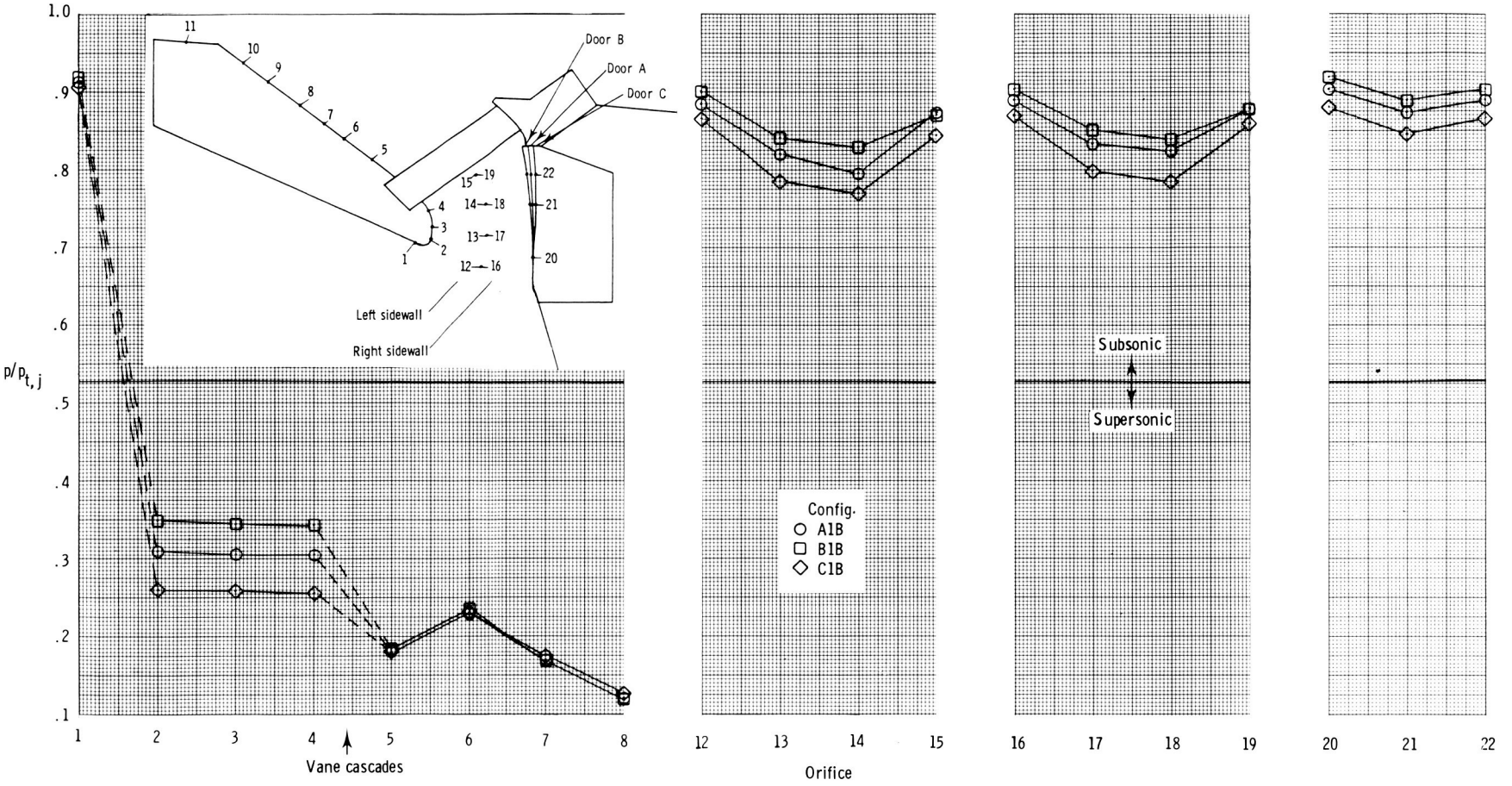

(f) Static pressures; bottom port; NPR = 5.0.

Figure 6. Concluded.

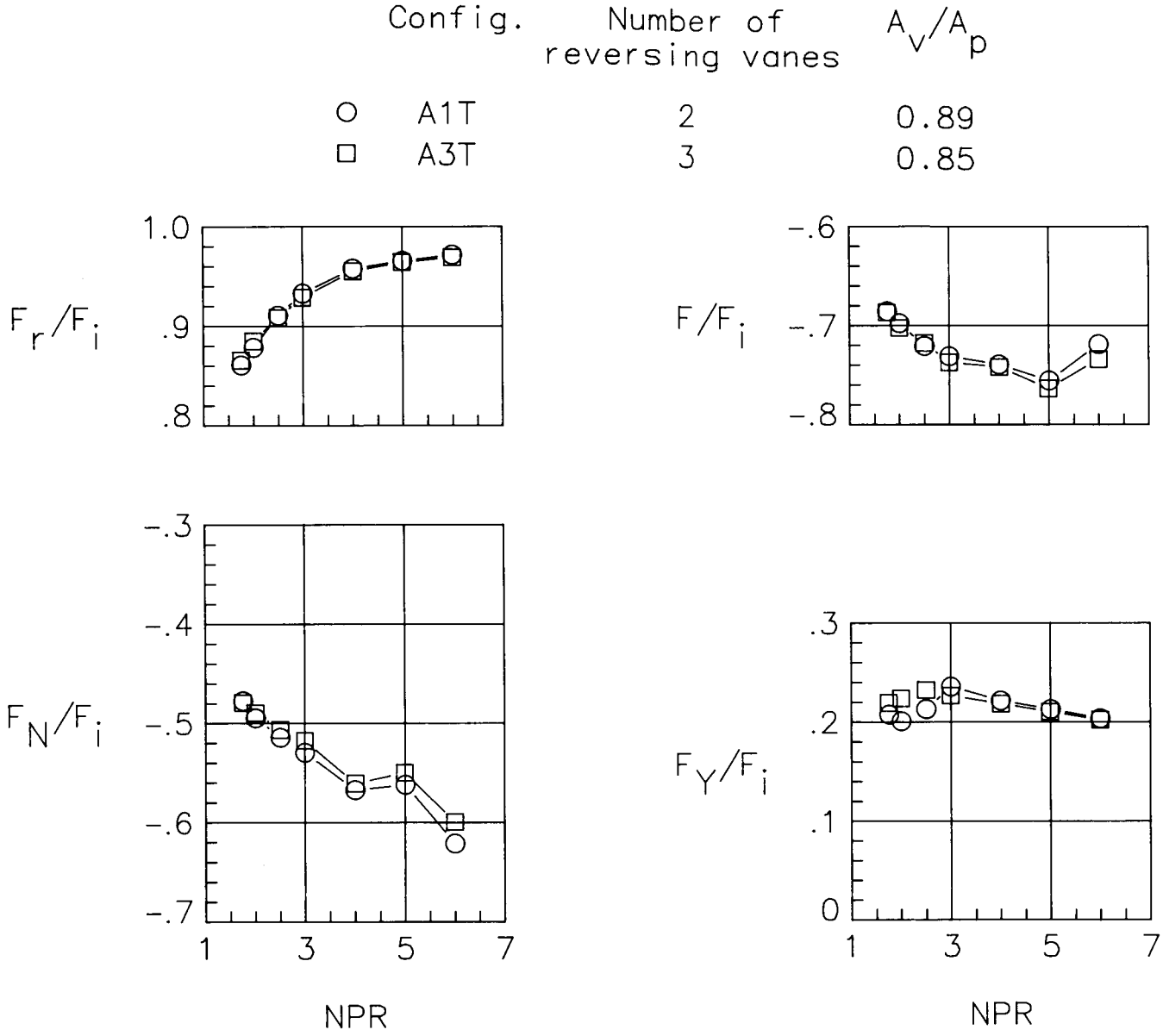

(a) Force data.

Figure 7. Effect of number of reversing vanes on basic performance.

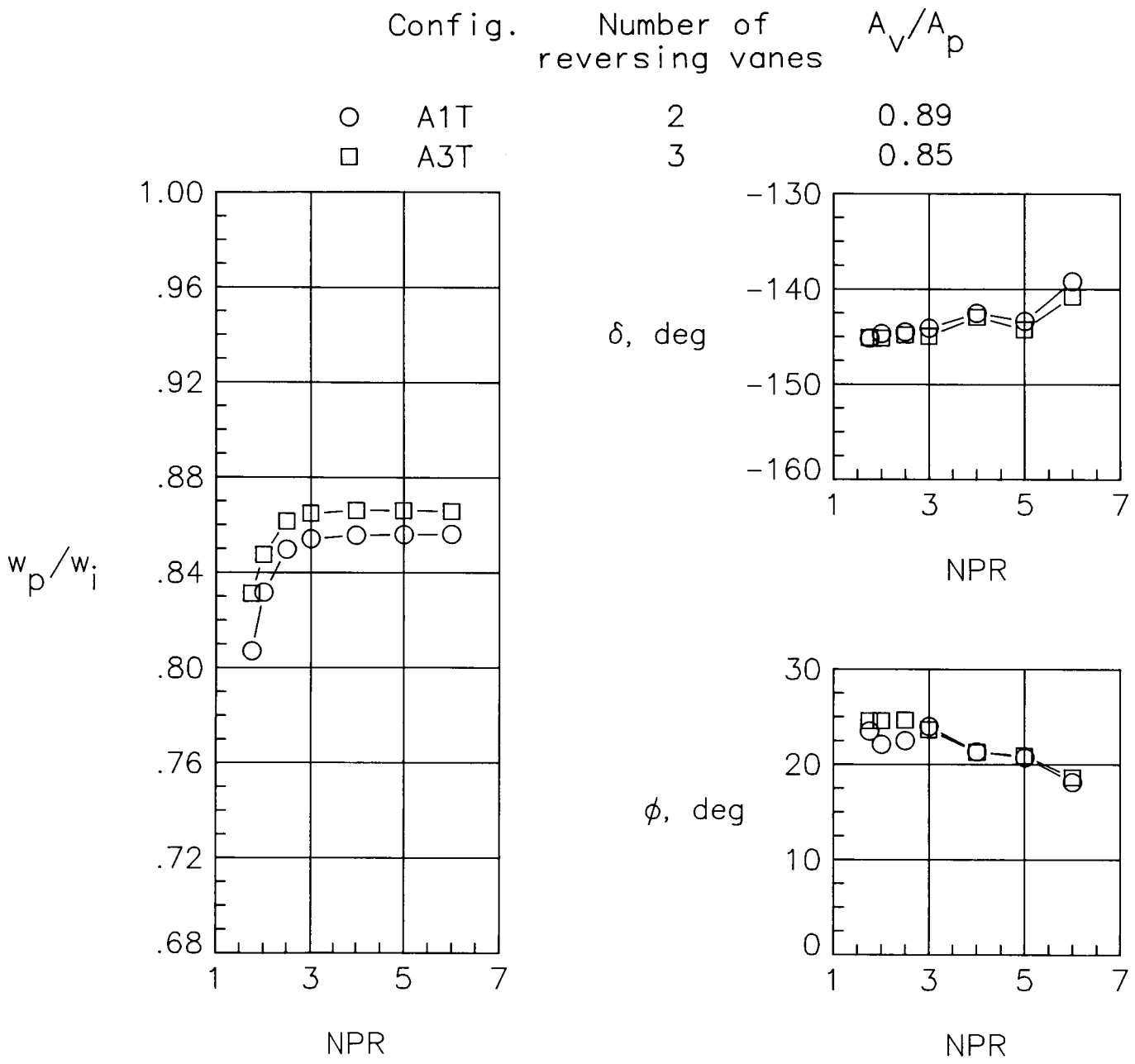

(b) Discharge coefficient and turning angles.

Figure 7. Continued.

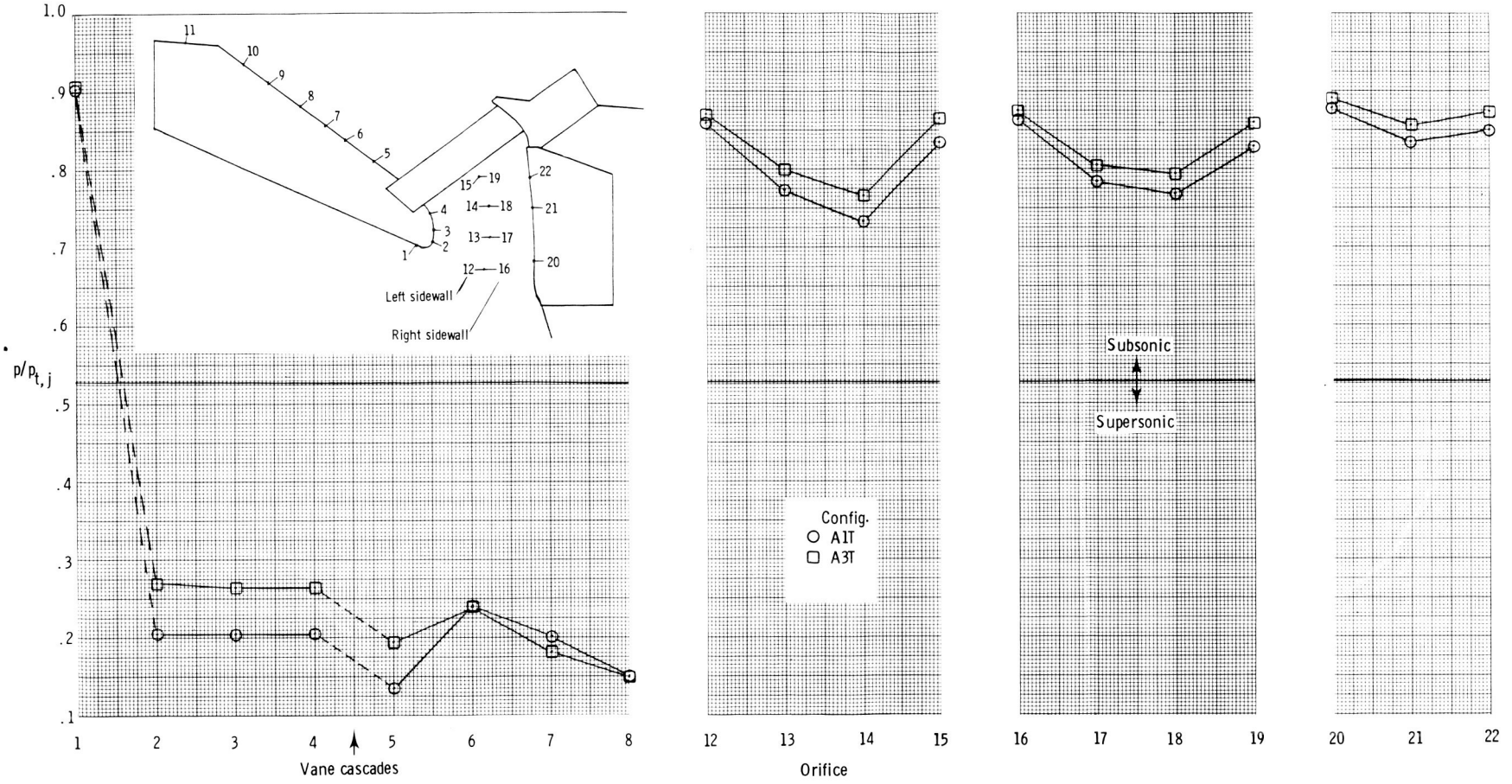

(c) Static pressures; NPR = 5.0.

Figure 7. Concluded.

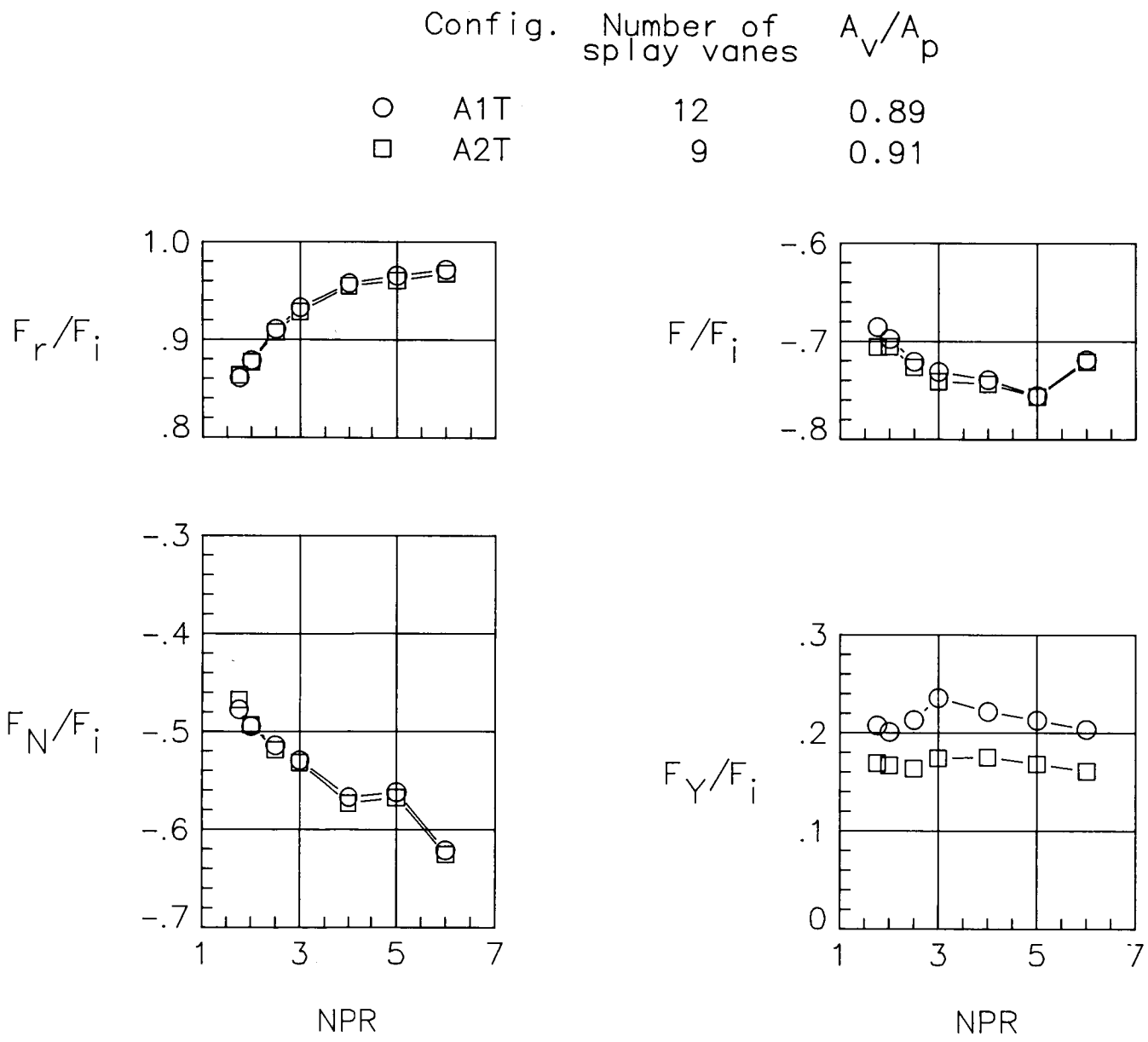

(a) Force data; top port.

Figure 8. Effect of number of splay vanes on basic performance.

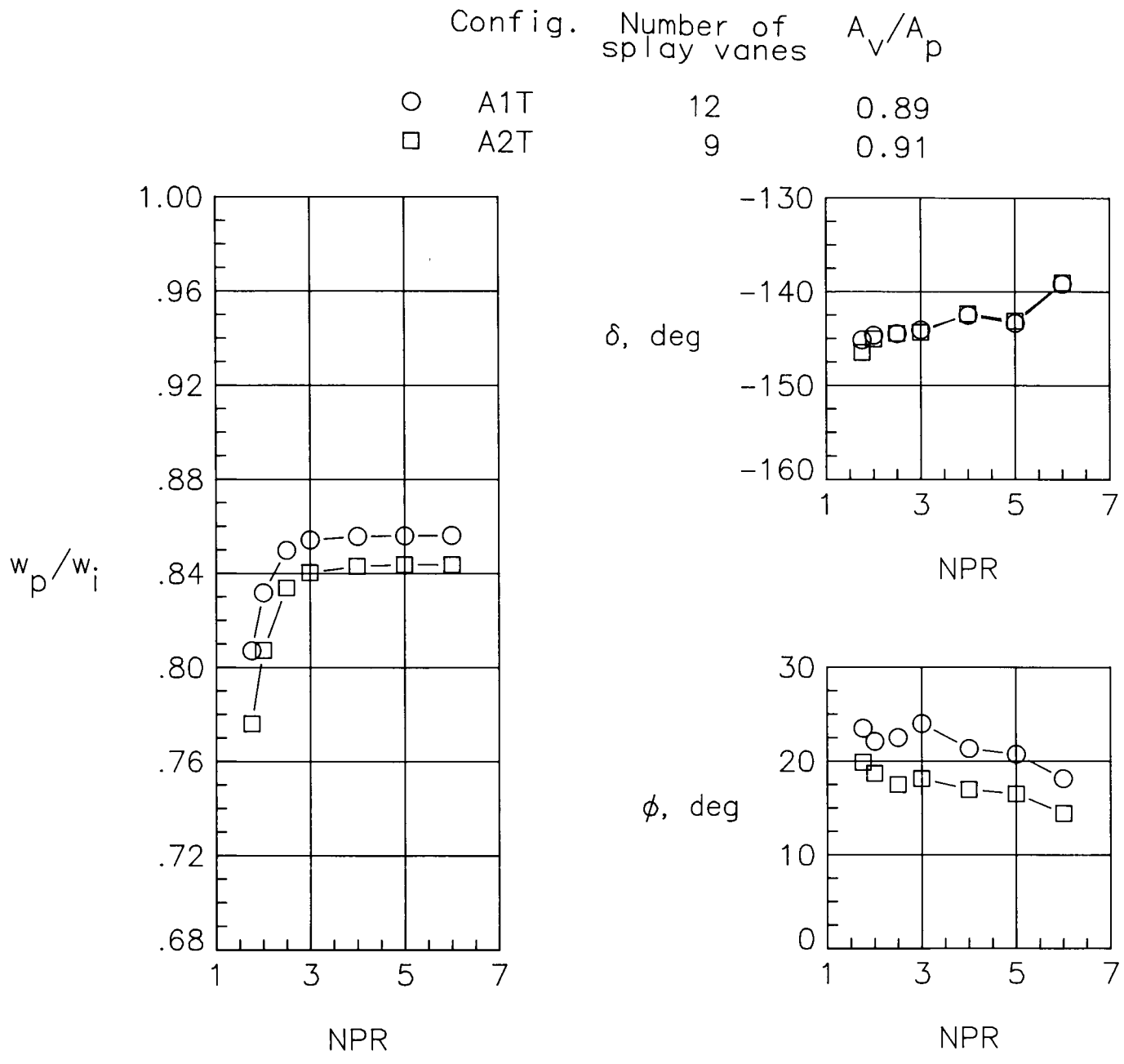

(b) Discharge coefficient and turning angles; top port.

Figure 8. Continued.

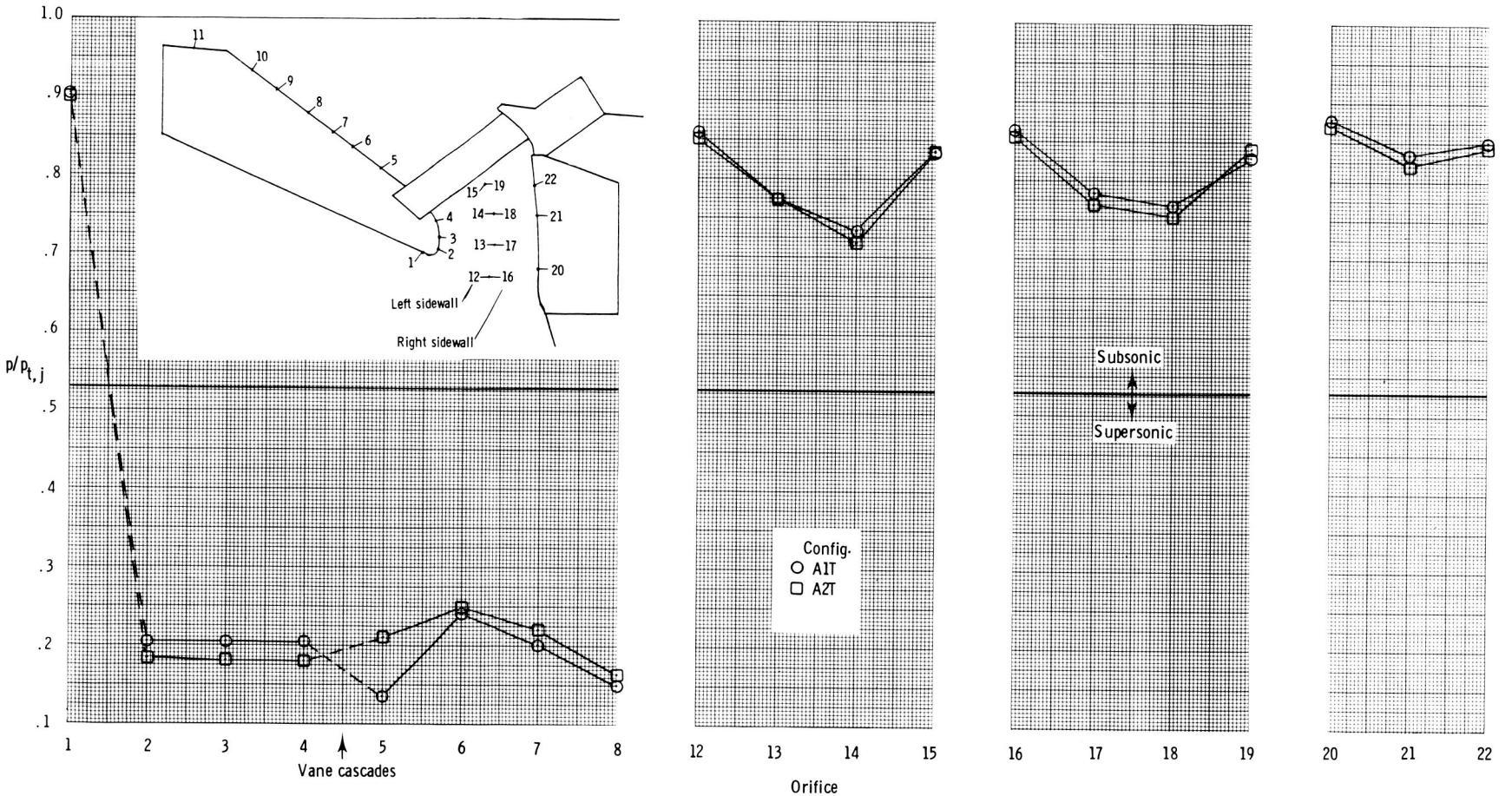

(c) Static pressures; top port; NPR = 5.0.

Figure 8. Continued.

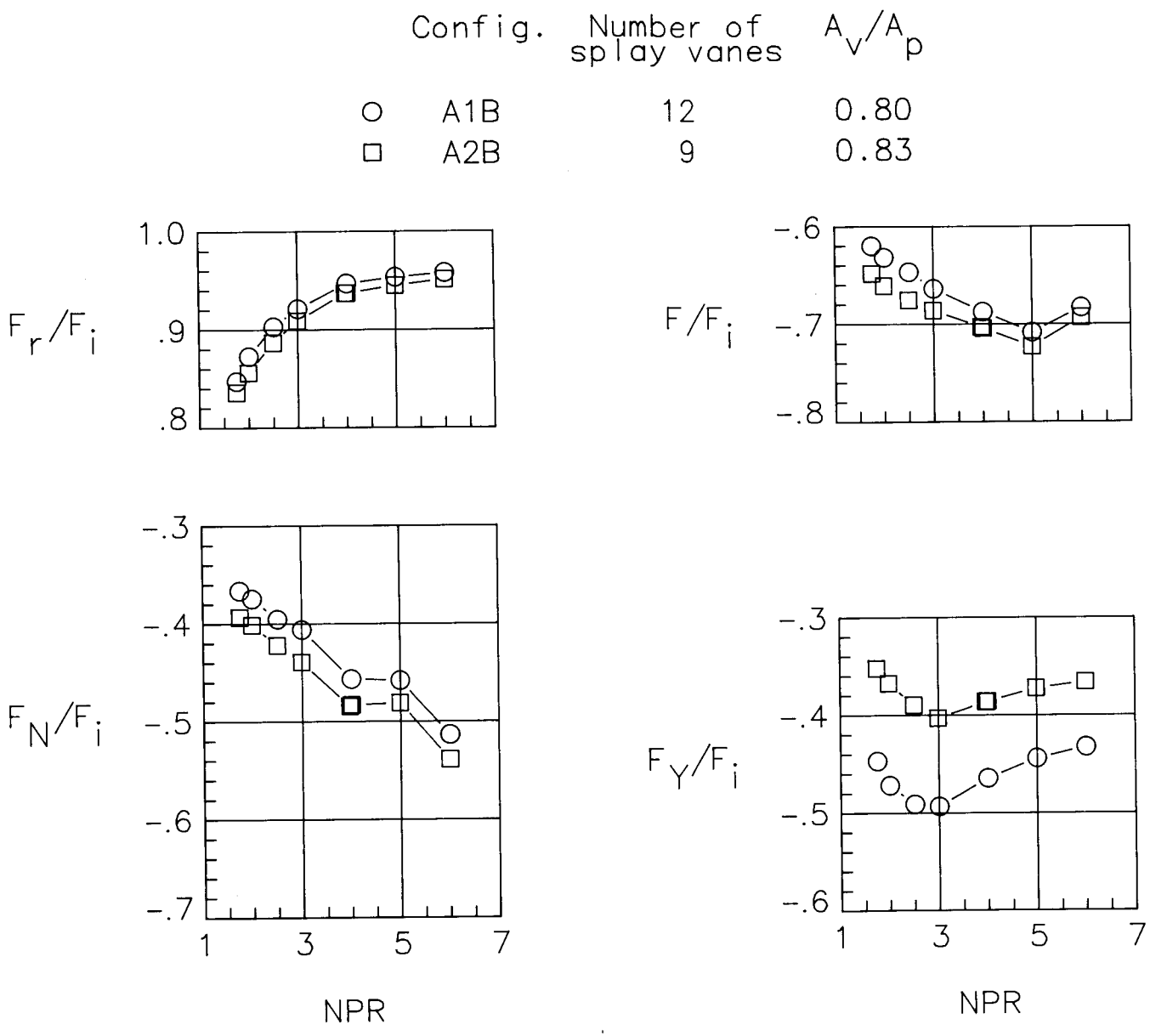

(d) Force data; bottom port.

Figure 8. Continued.

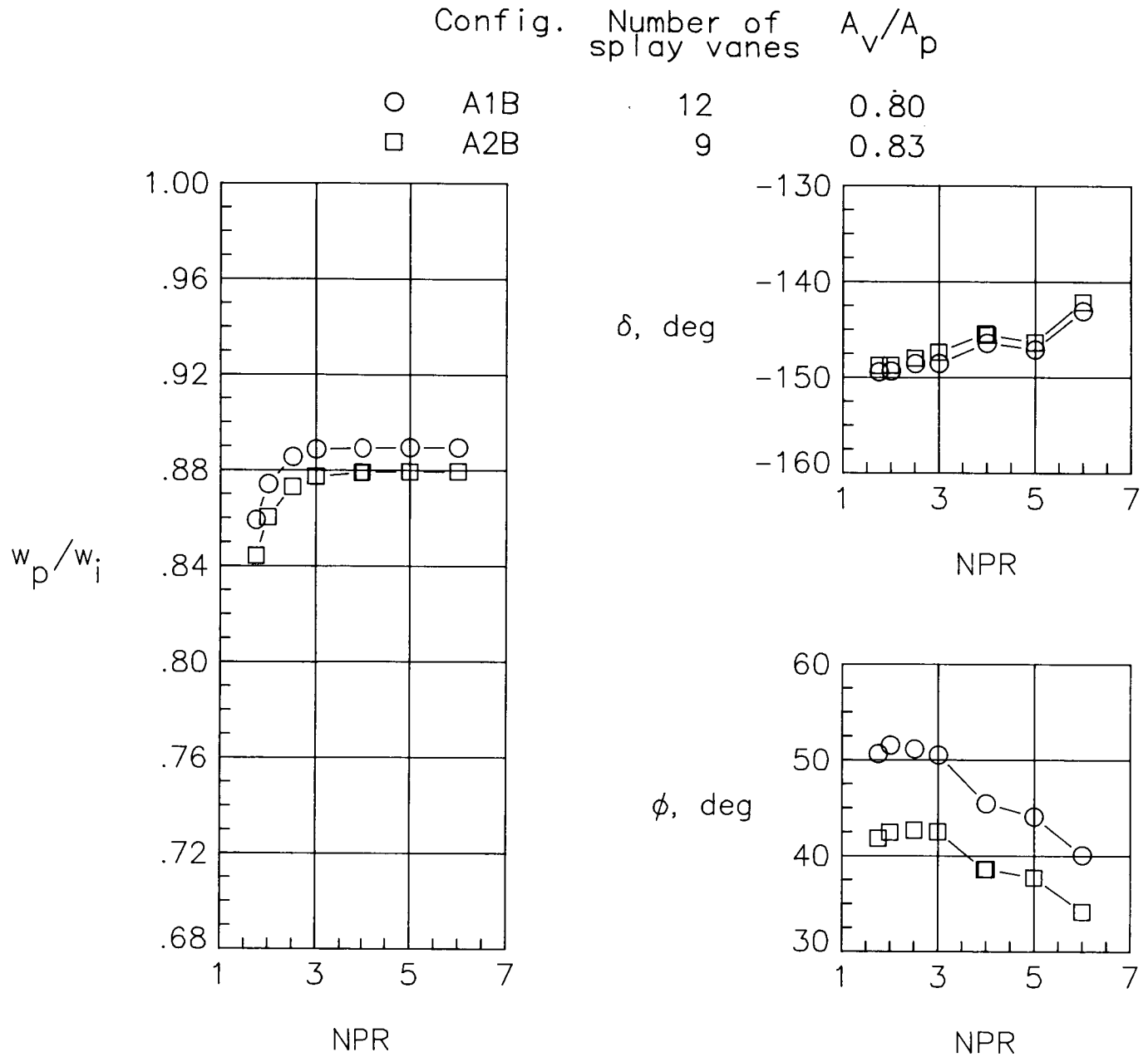

(e) Discharge coefficient and turning angles; bottom port.

Figure 8. Continued.

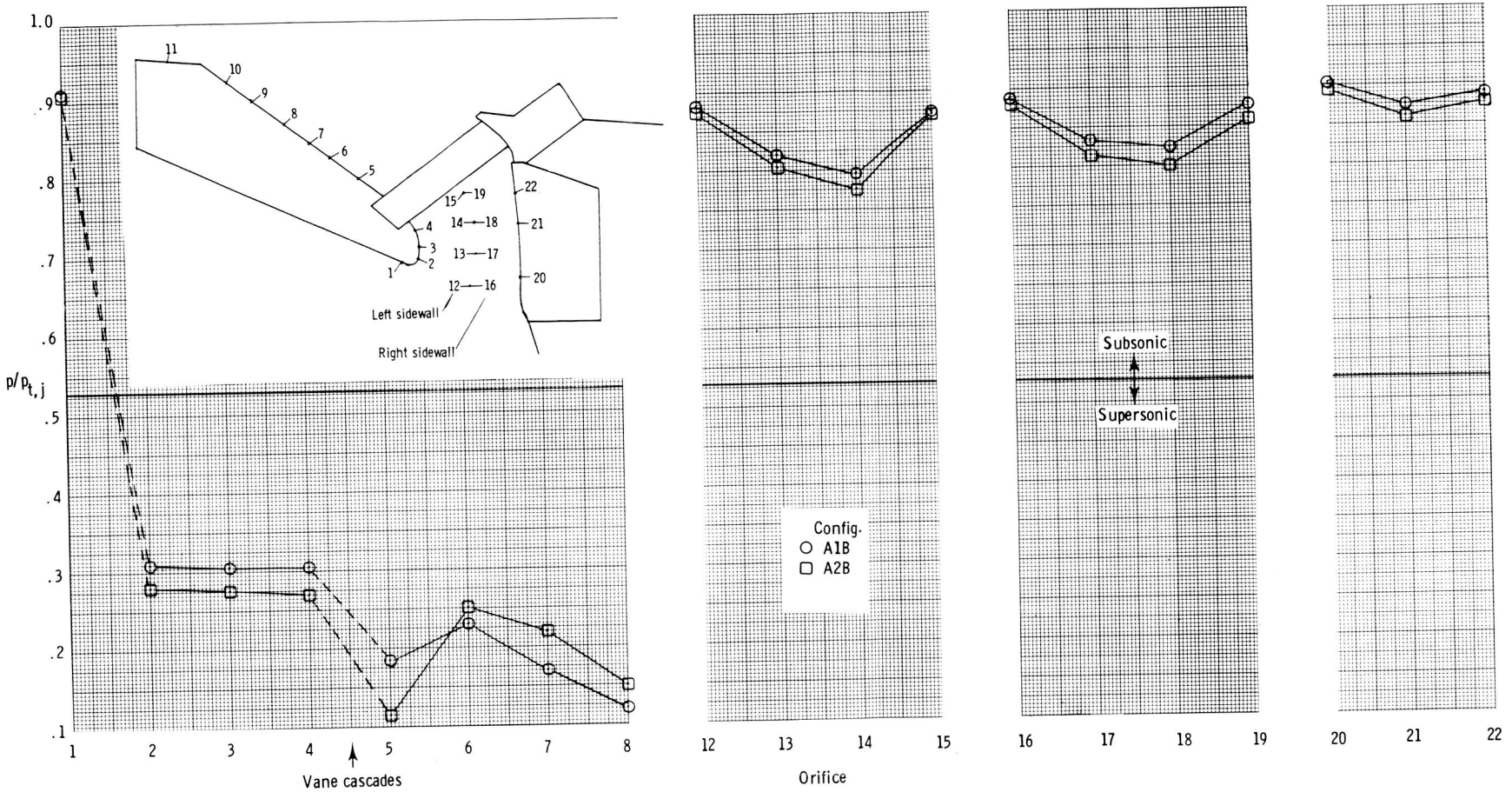

(f) Static pressures; bottom port; NPR = 5.0.

Figure 8. Concluded.

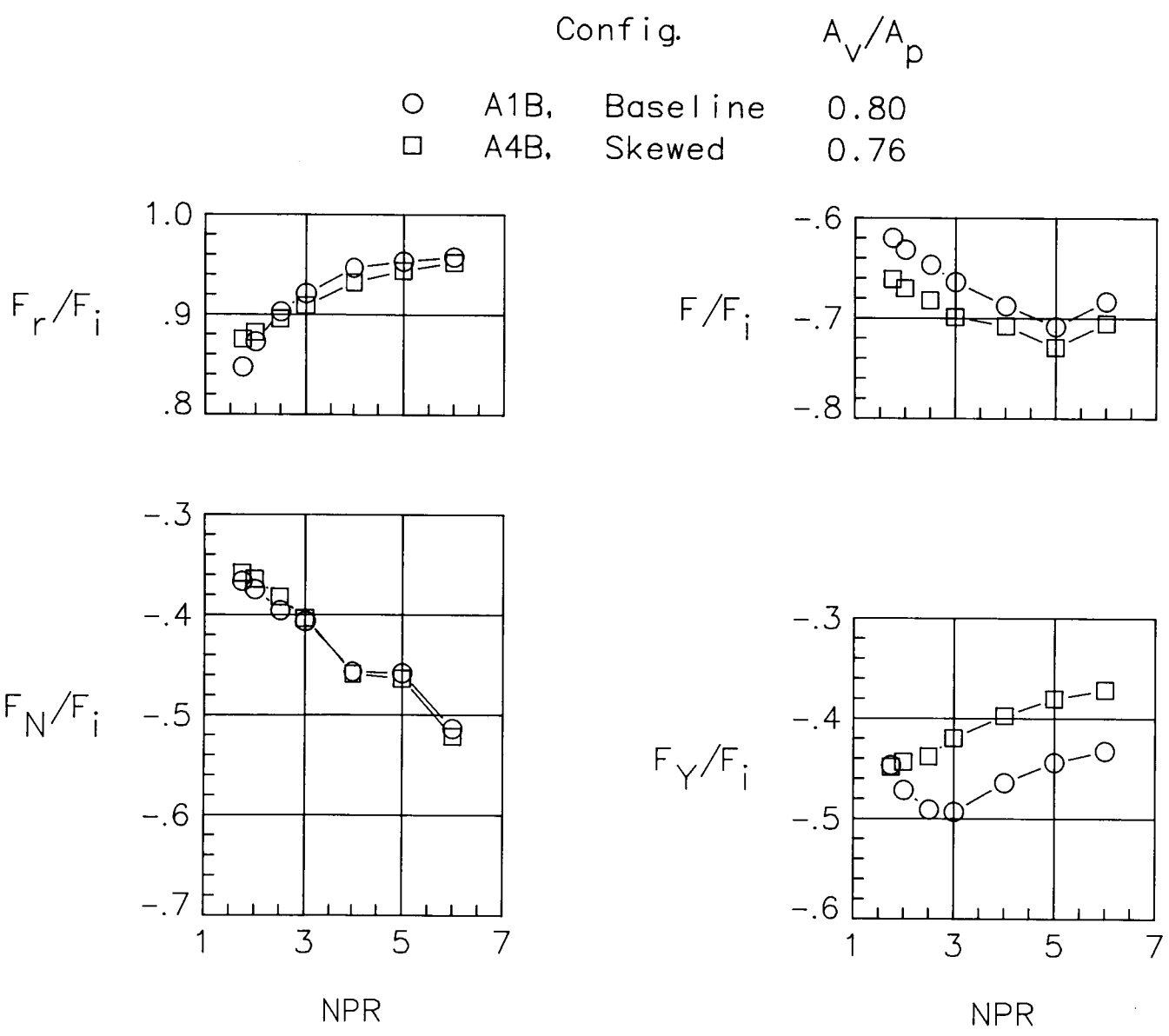

(a) Force data.

Figure 9. Effect of skewed vane cascade on basic performance.

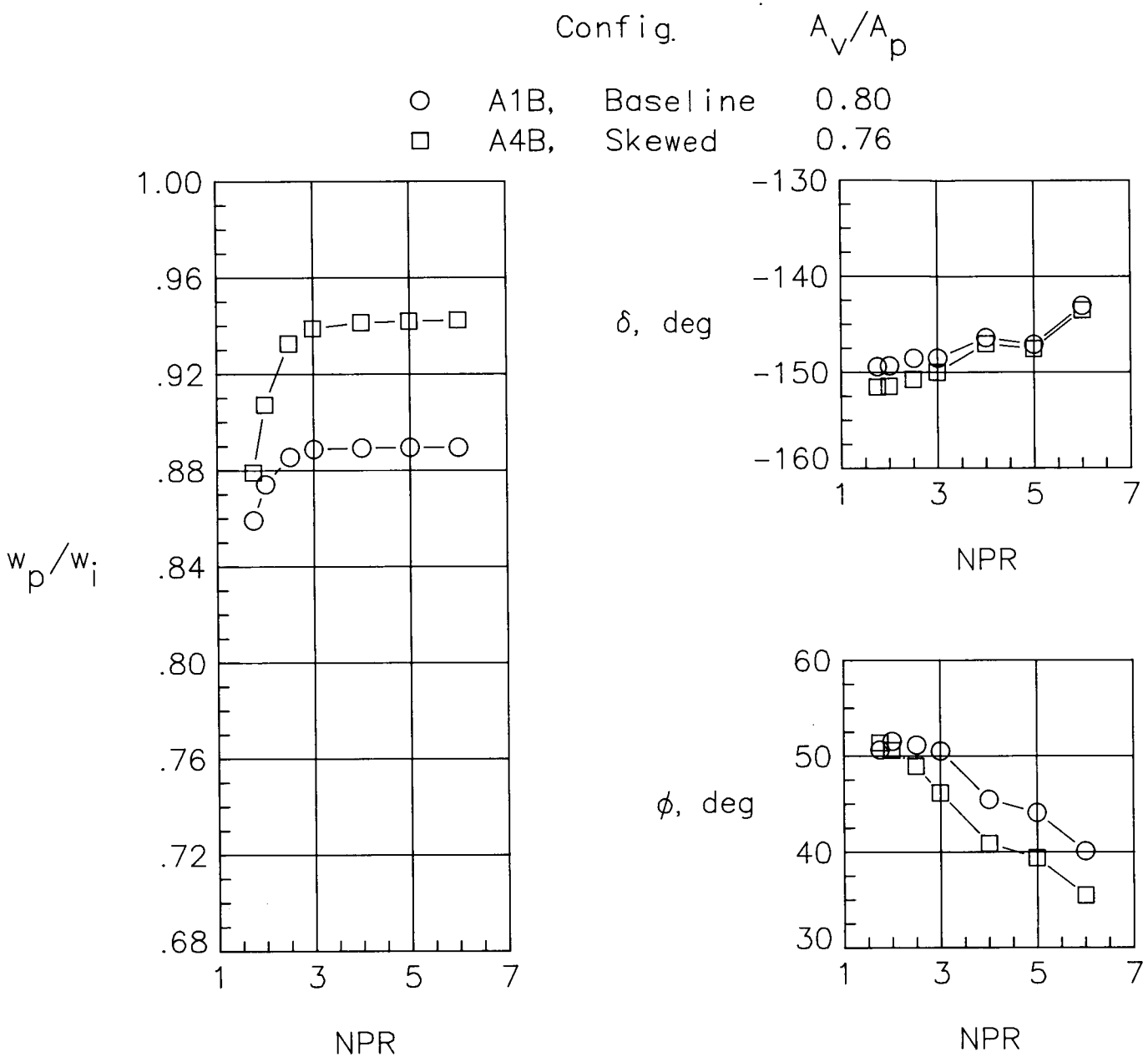

(b) Discharge coefficient and turning angles.

Figure 9. Continued.

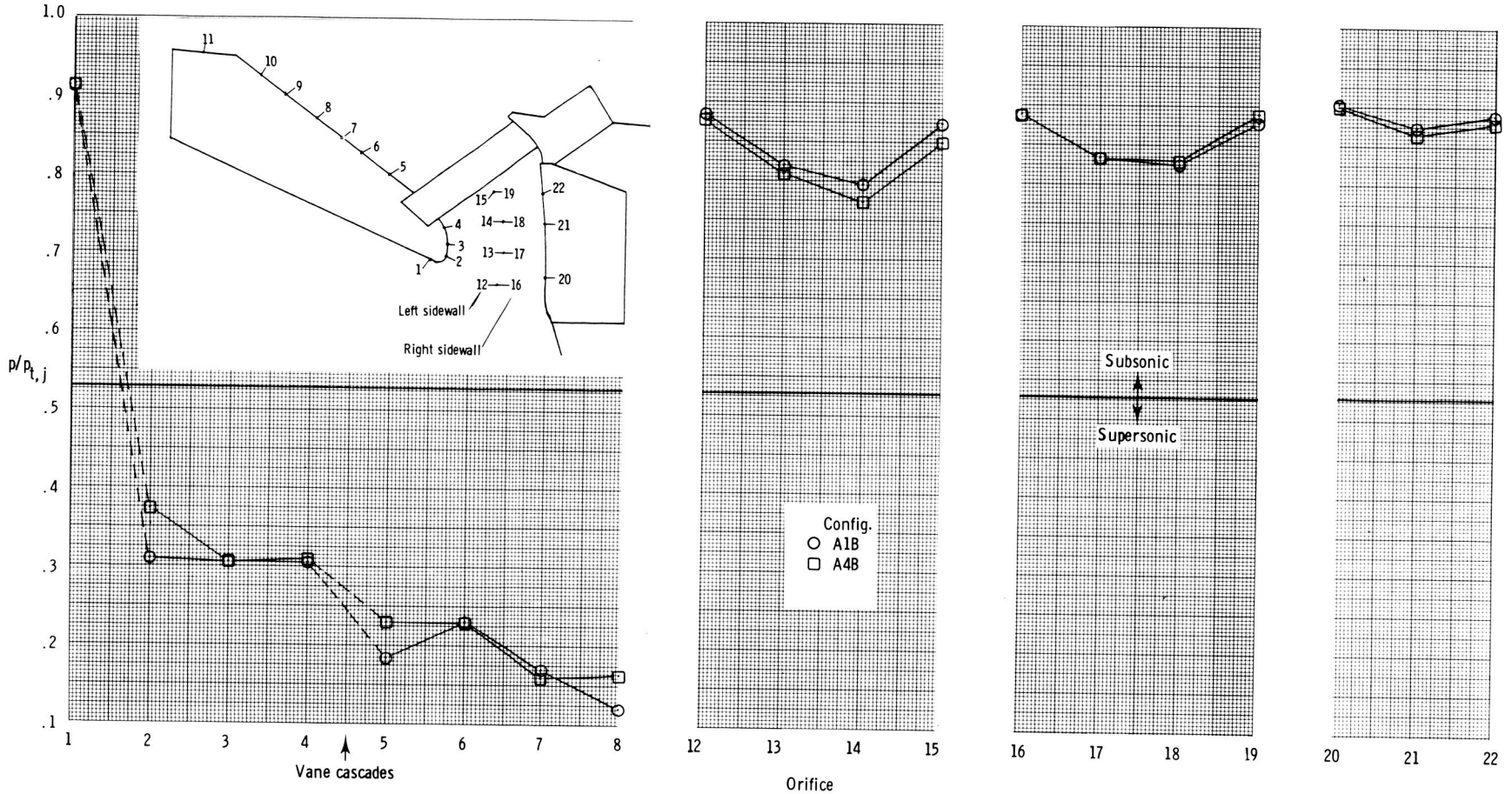

(c) Static pressures; NPR = 5.0.

Figure 9. Concluded.

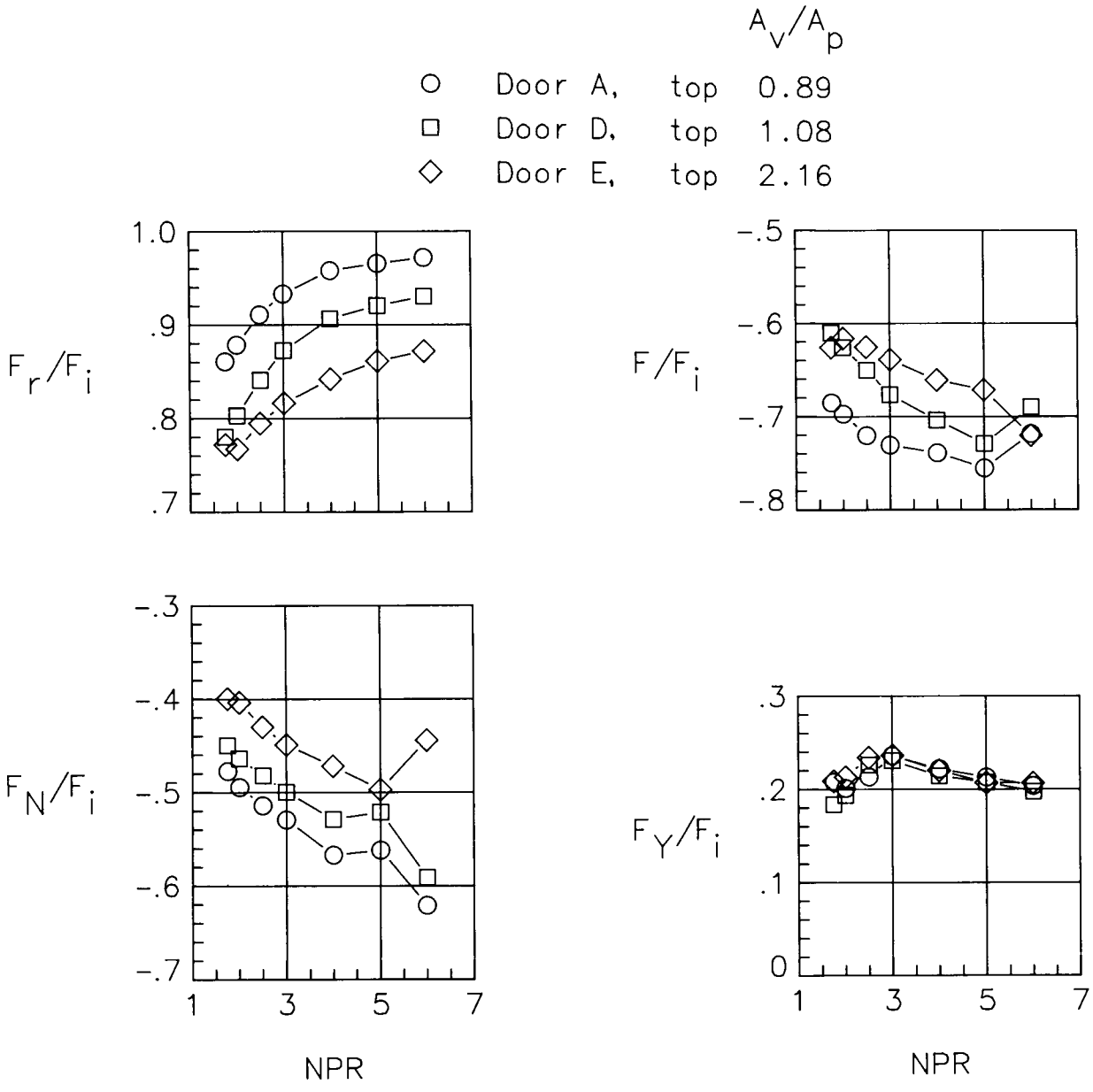

(a) Force data; top port.

Figure 10. Effect of inner door position on basic performance with vane cascades A1.

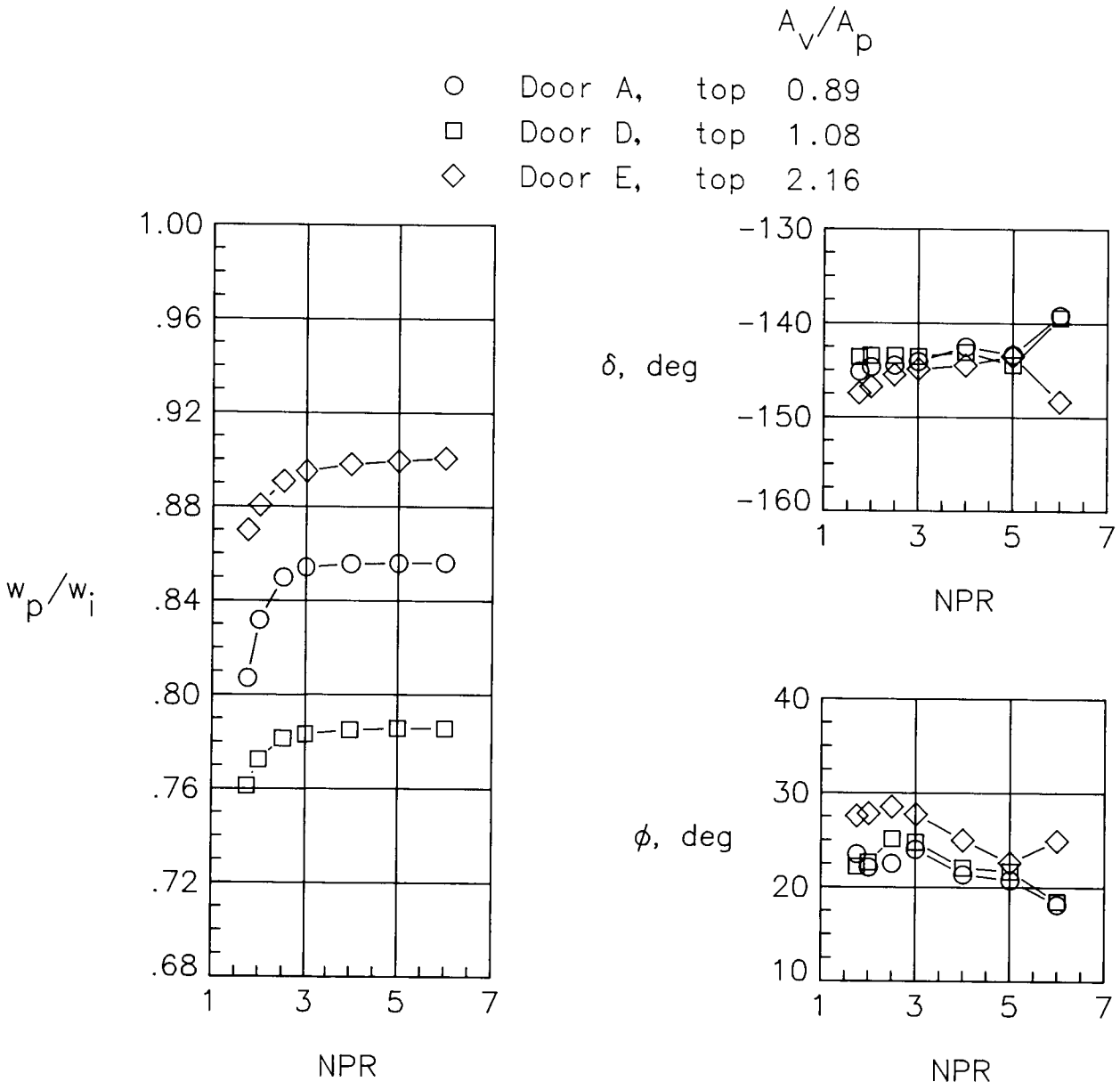

(b) Discharge coefficient and turning angles; top port.

Figure 10. Continued.

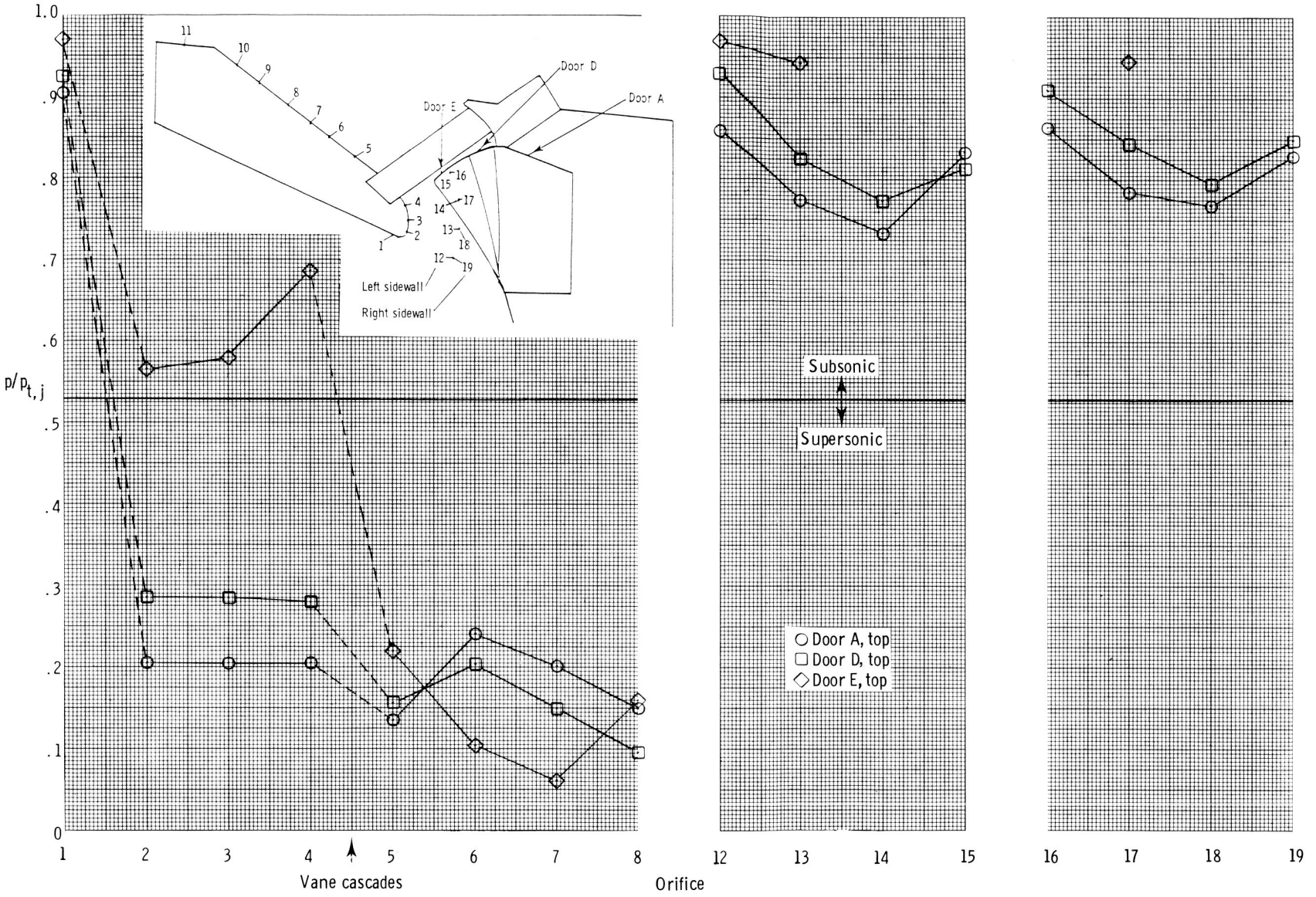

(c) Static pressures; top port; NPR = 5.0.

Figure 10. Continued.

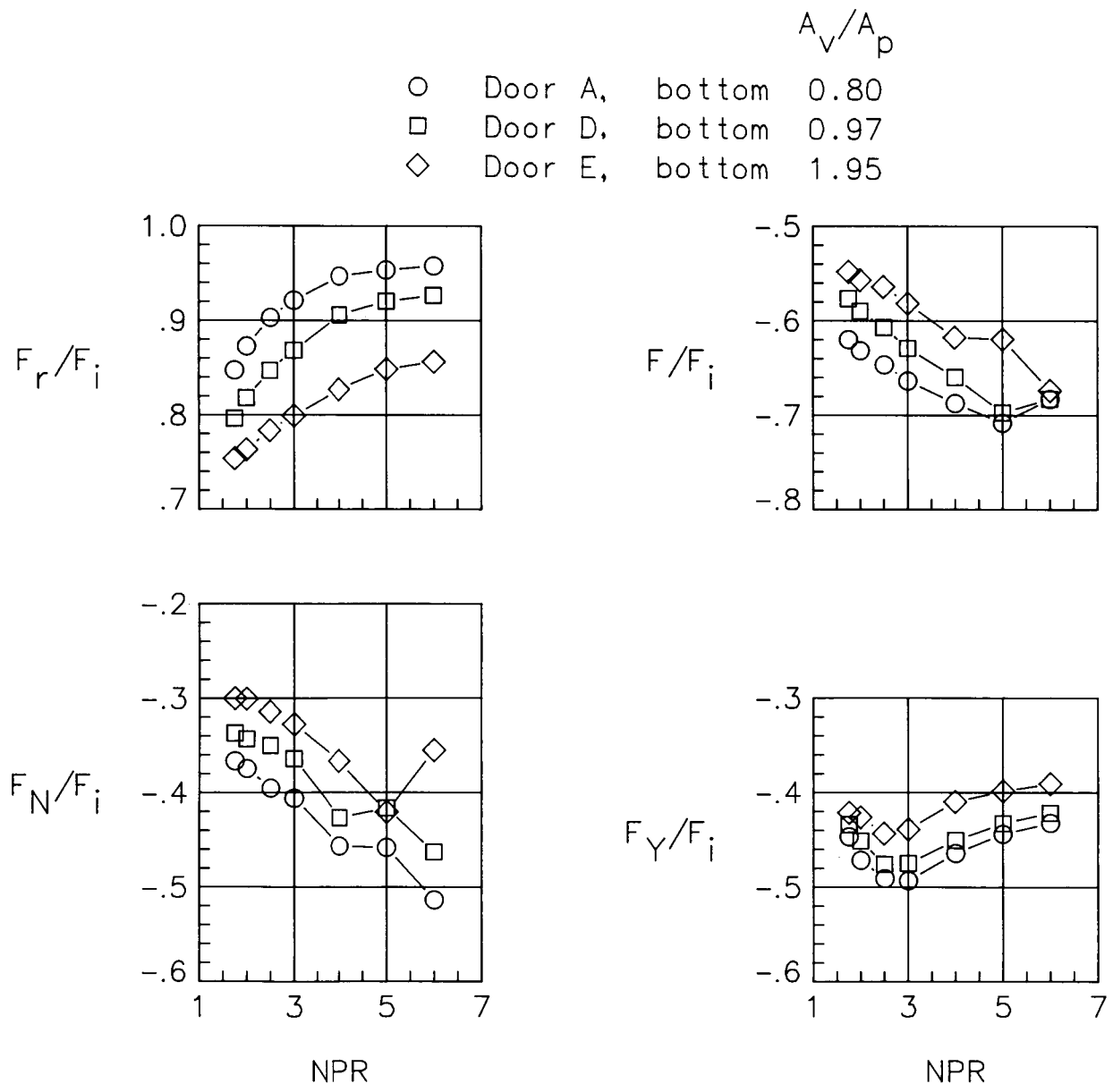

(d) Force data; bottom port.

Figure 10. Continued.

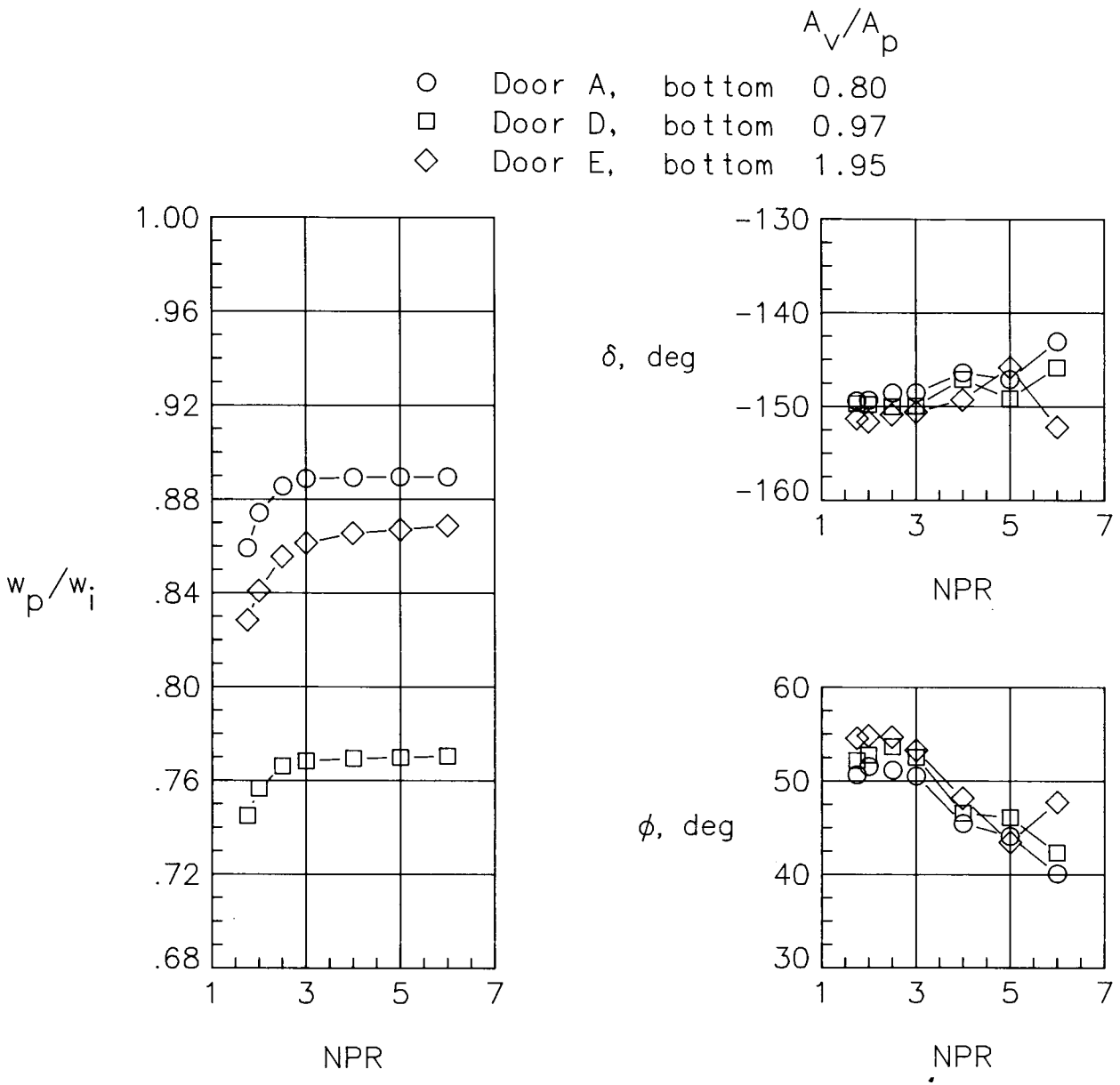

(e) Discharge coefficient and turning angles; bottom port.

Figure 10. Continued.

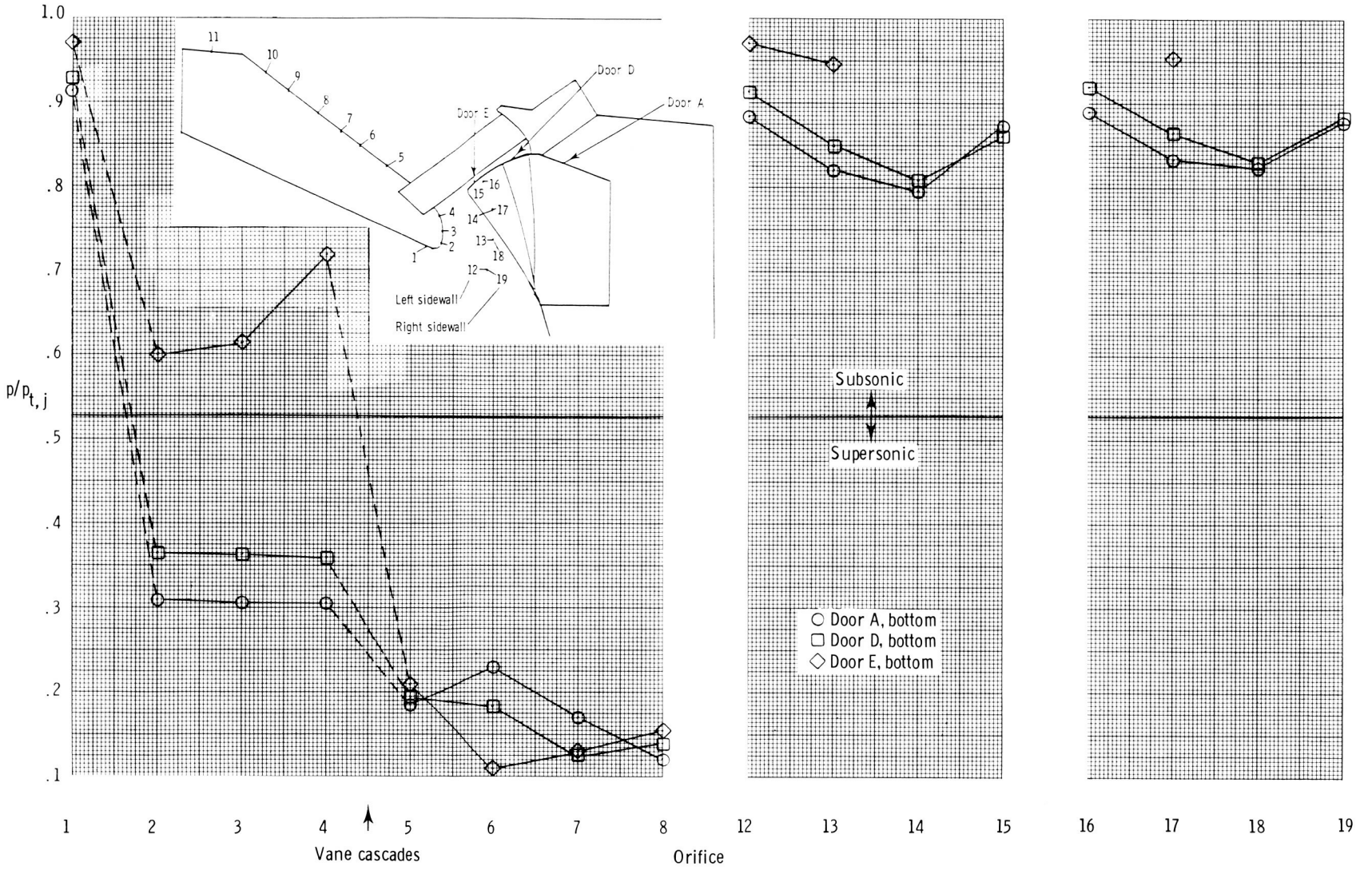

(f) Static pressures; bottom port; NPR = 5.0.

Figure 10. Concluded.

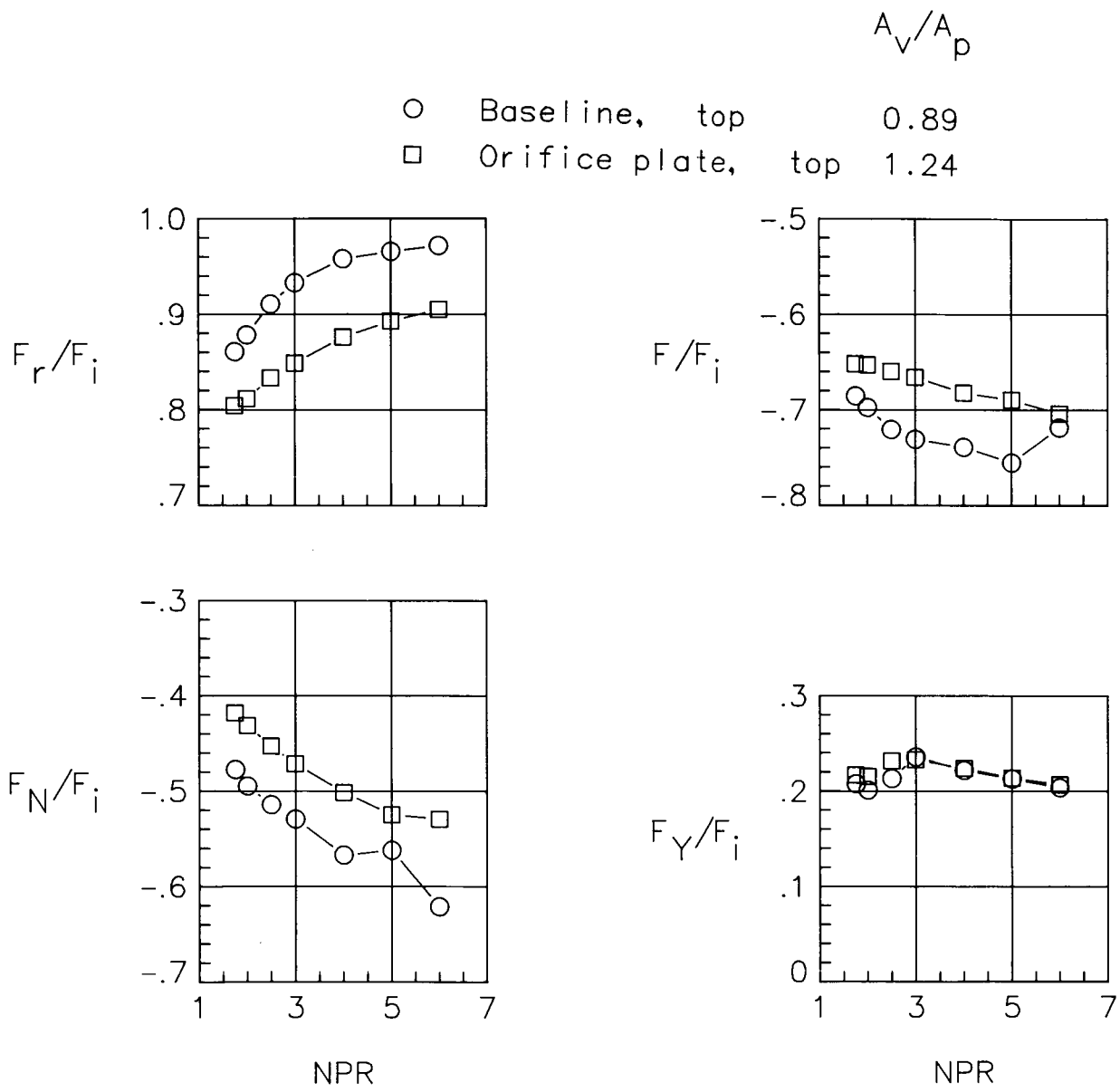

(a) Force data; top port.

Figure 11. Effect of orifice plate on basic performance with vane cascades A1.

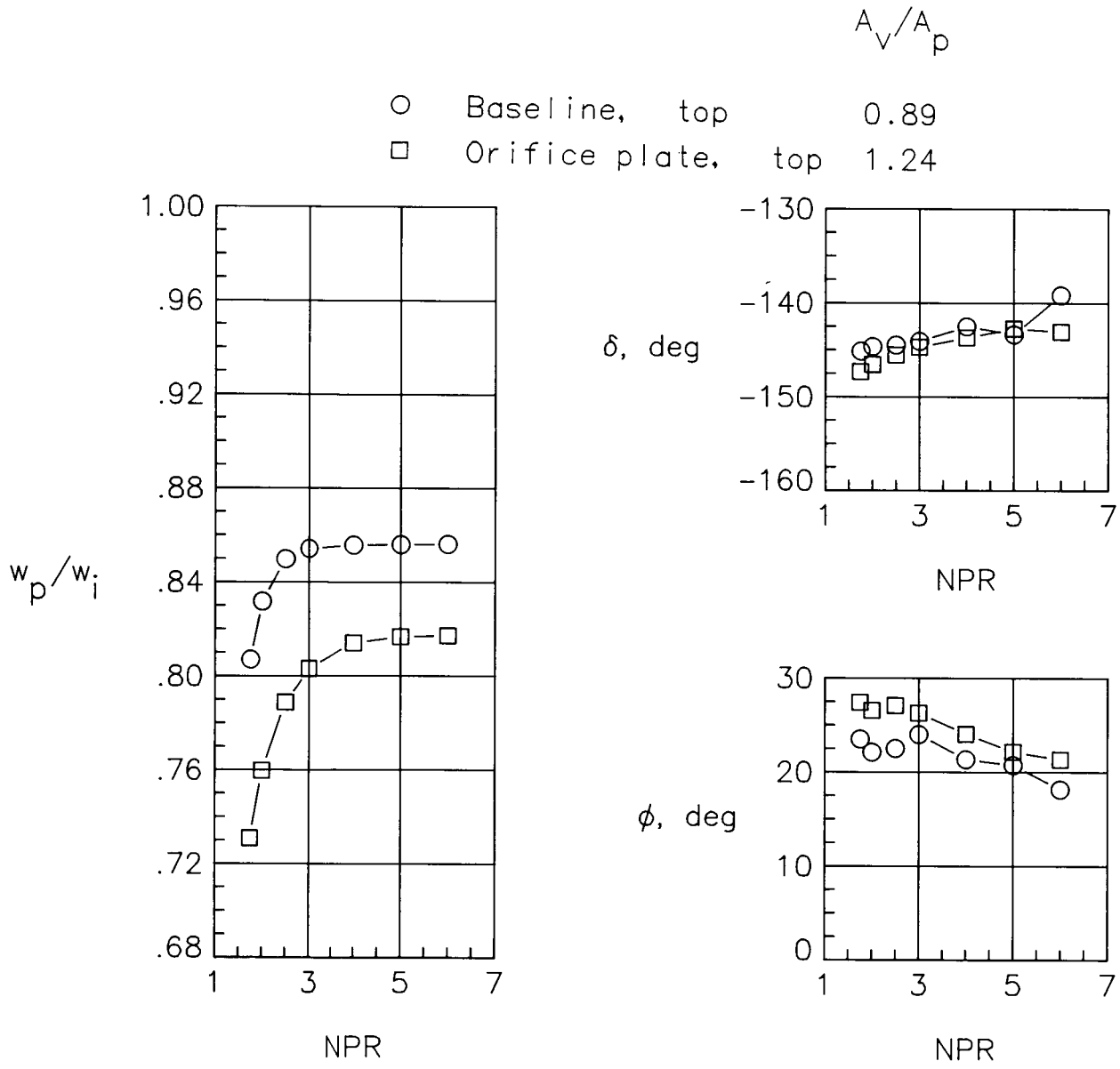

(b) Discharge coefficient and turning angles; top port.

Figure 11. Continued.

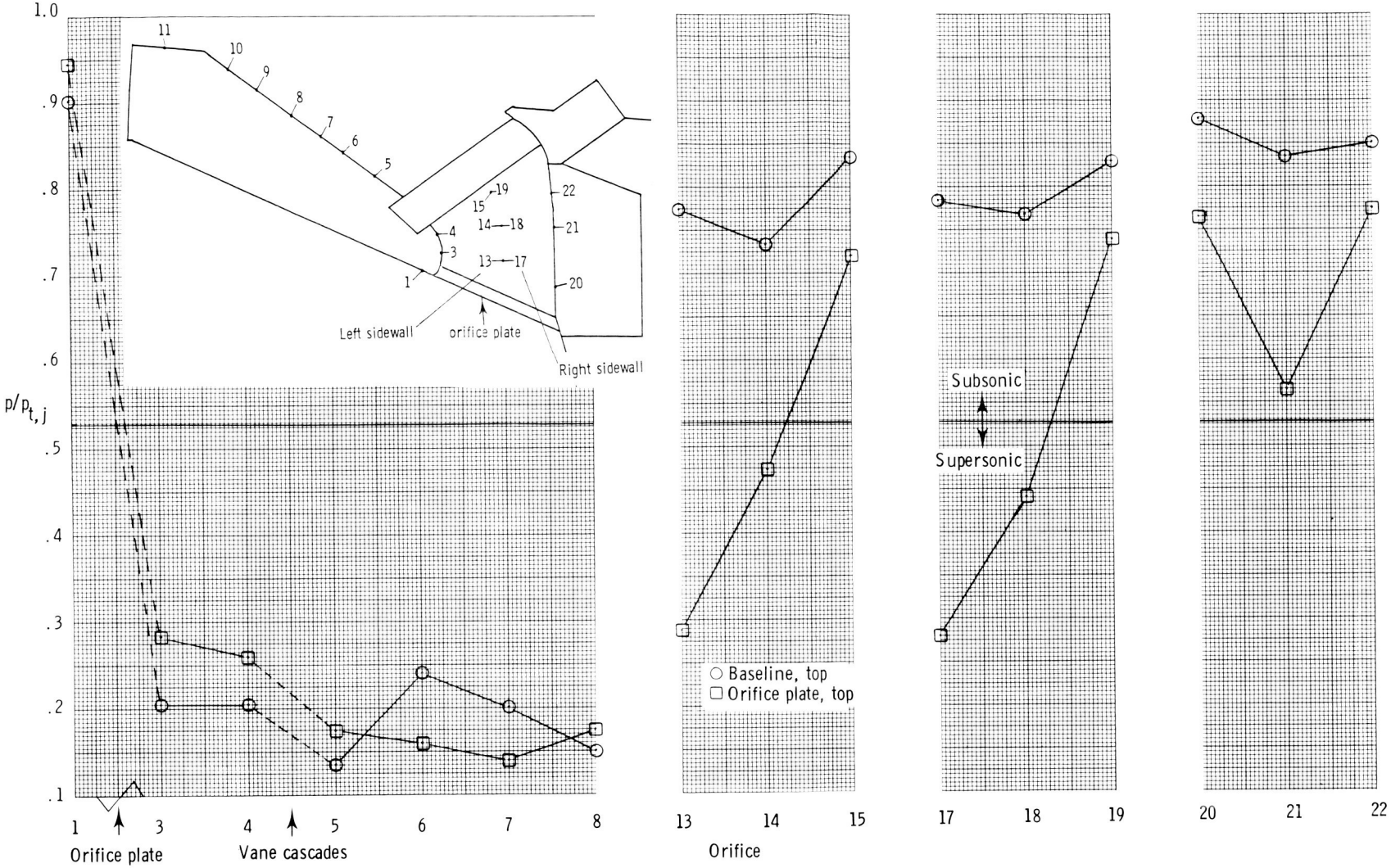

(c) Static pressures; top port; NPR = 5.0.

Figure 11. Continued.

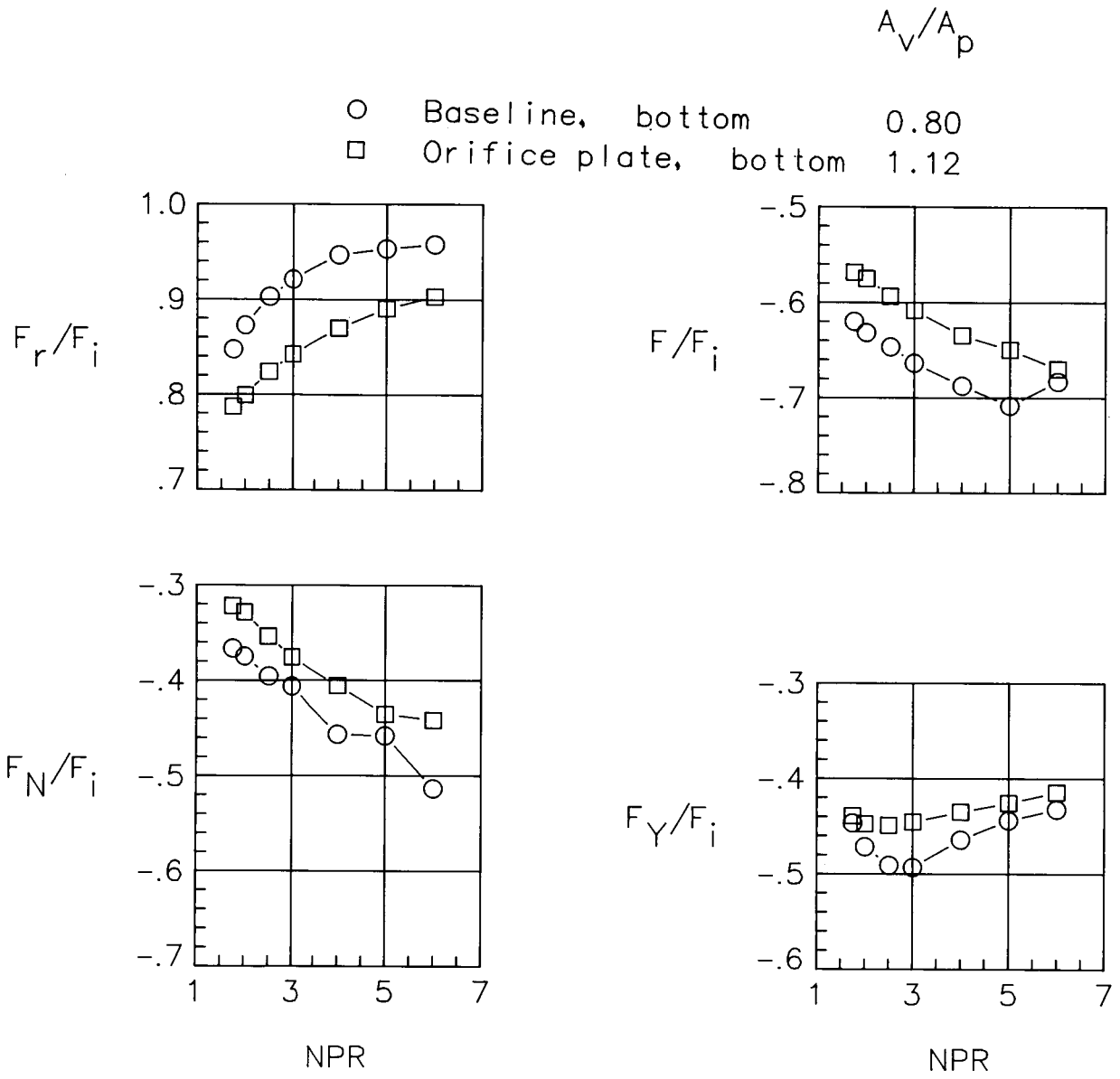

(d) Force data; bottom port.

Figure 11. Continued.

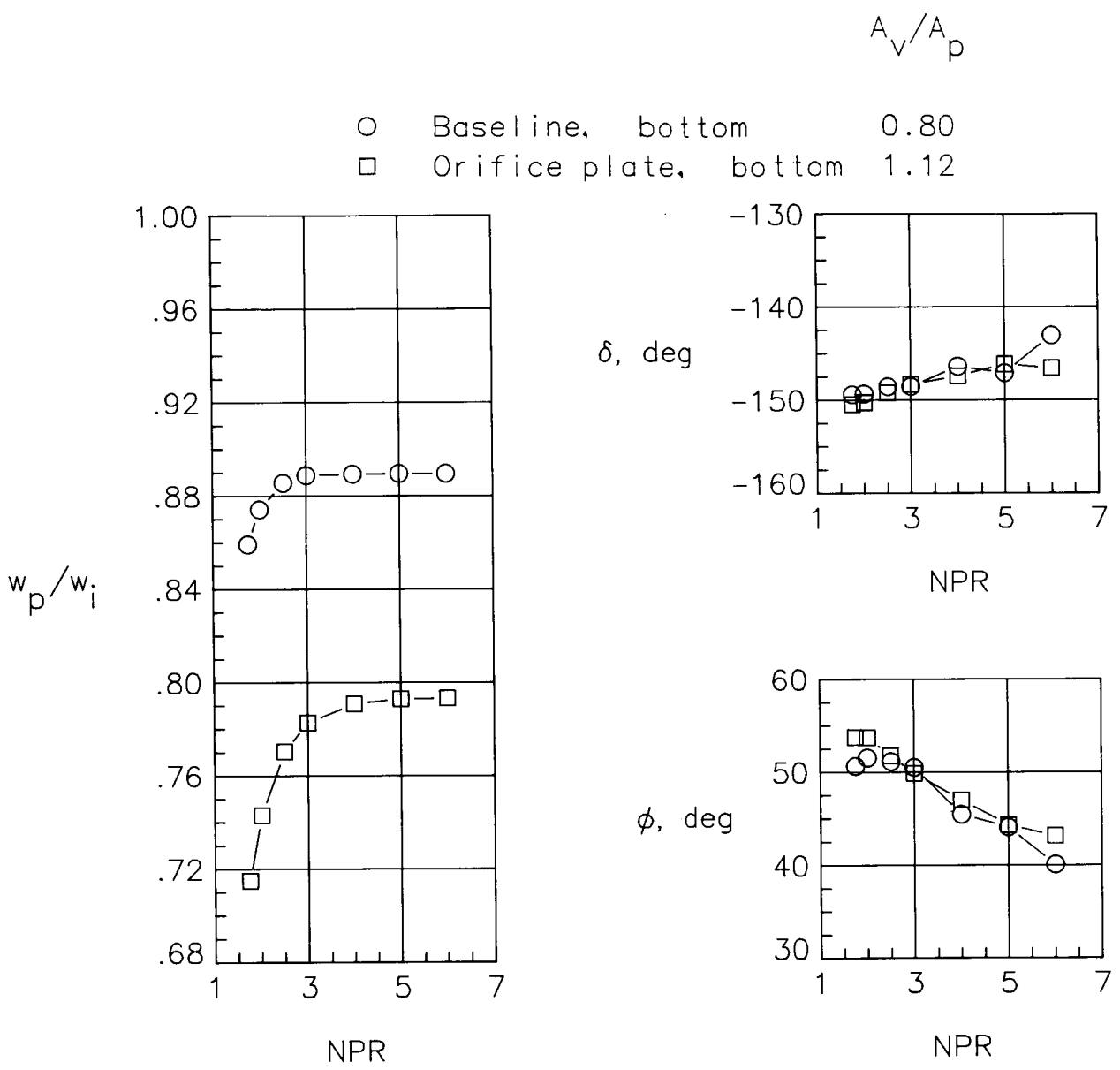

(e) Discharge coefficient and turning angles; bottom port.

Figure 11. Continued.

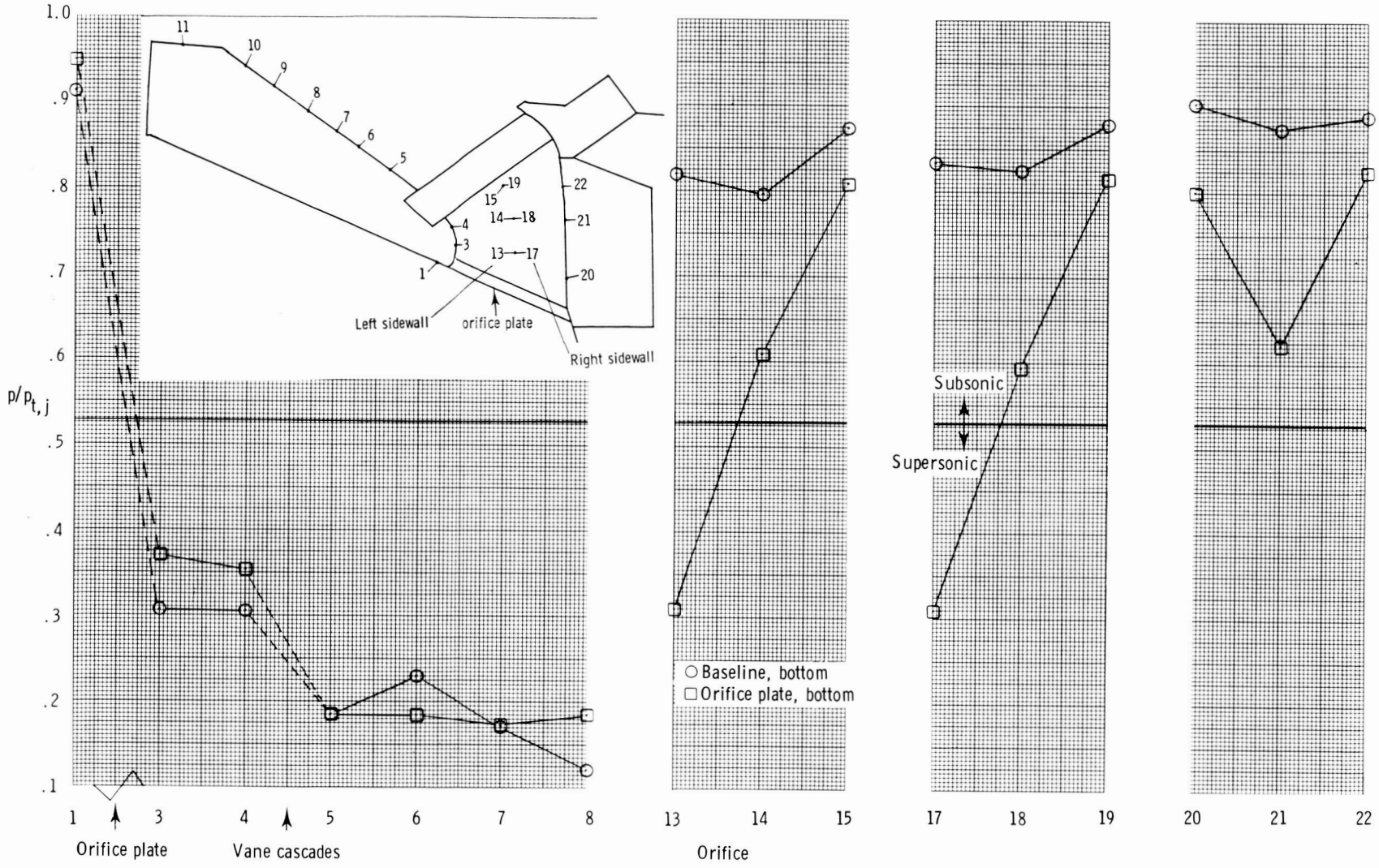

(f) Static pressures, bottom port, NPR = 5.0.

Figure 11. Concluded.

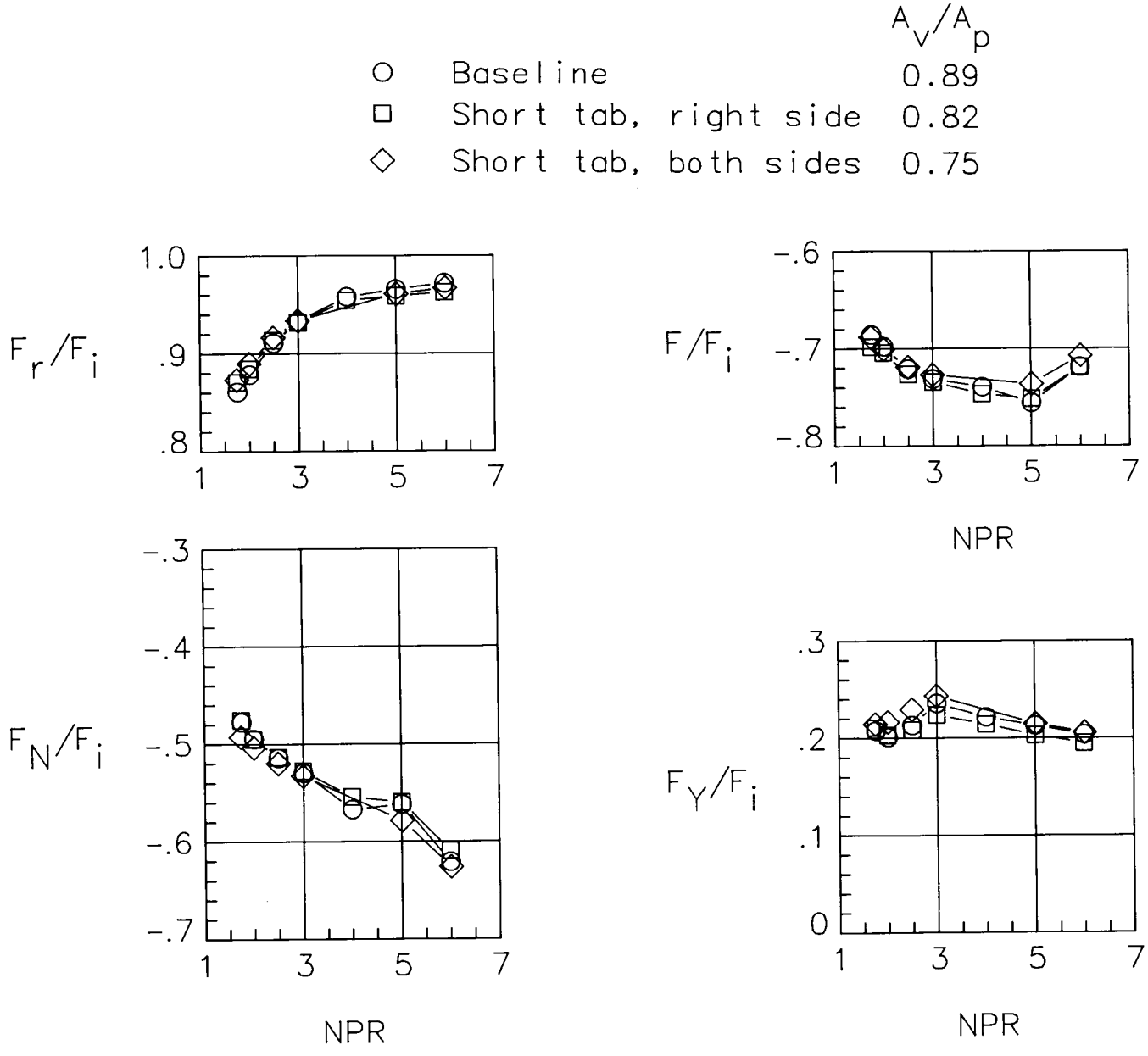

(a) Force data; top port.

Figure 12. Effect of trim tabs on basic performance with vane cascade A1T.

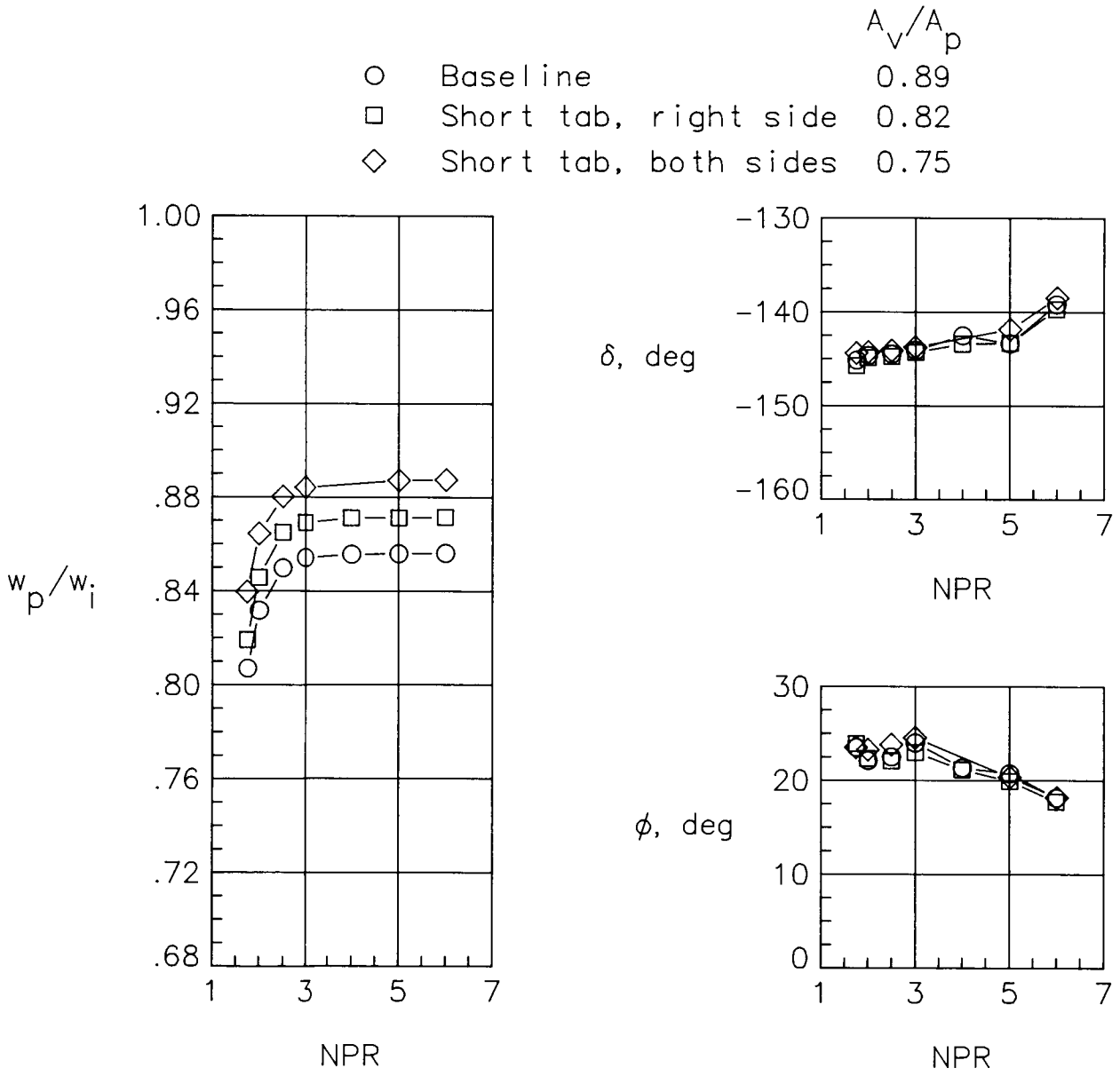

(b) Discharge coefficient and turning angles; top port.

Figure 12. Continued.

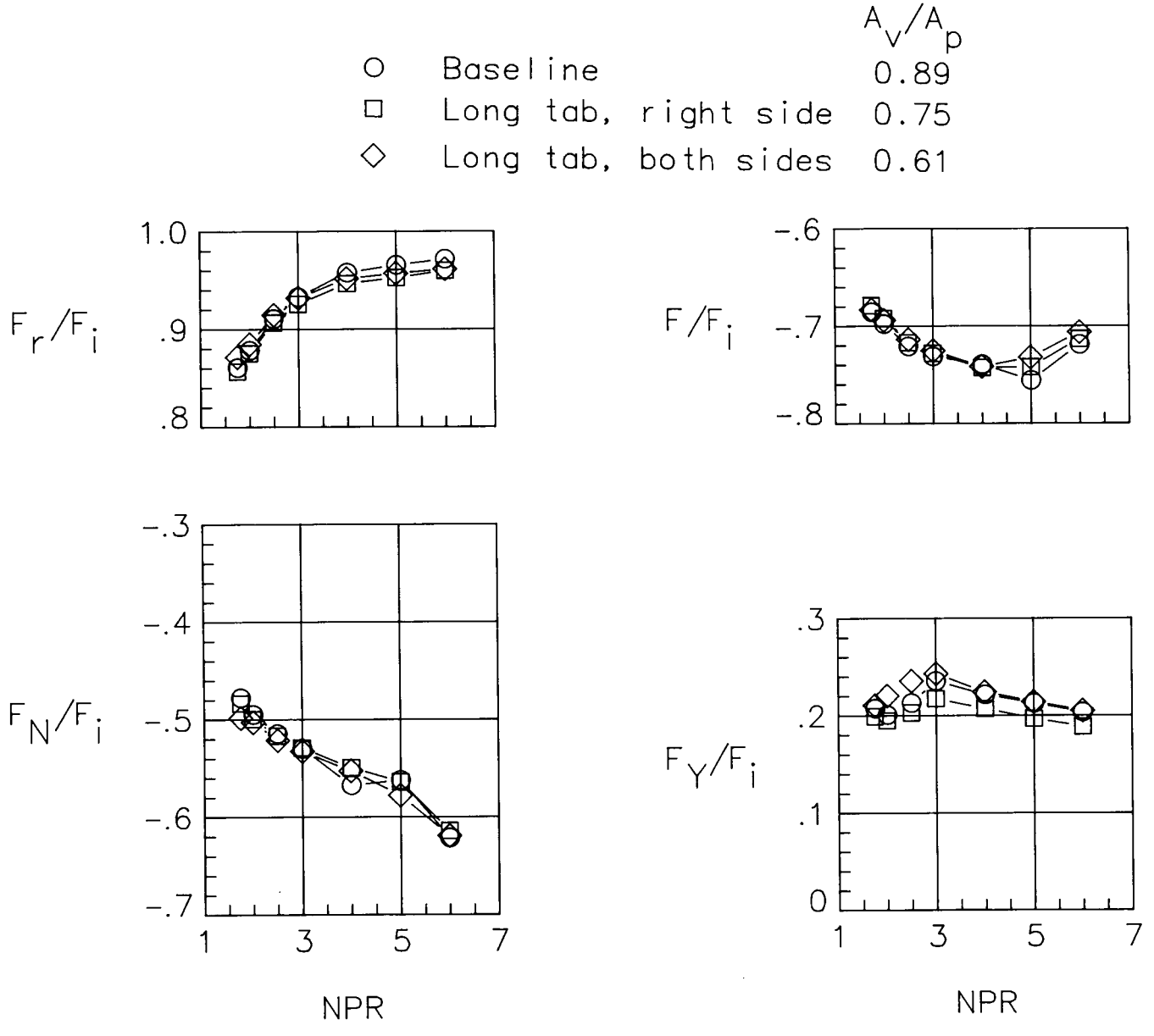

(c) Force data; top port.

Figure 12. Continued.

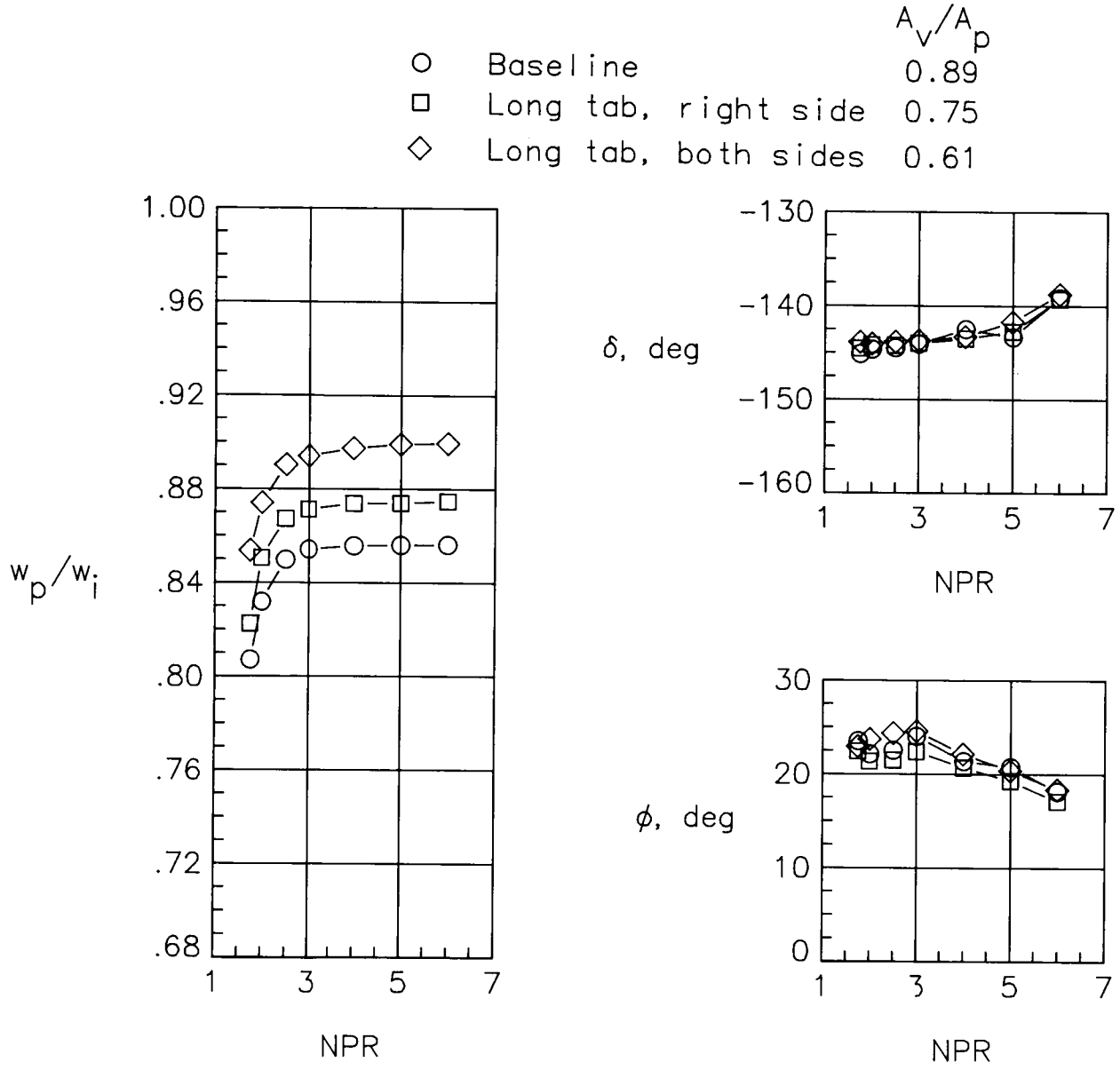

(d) Discharge coefficient and turning angles; top port.

Figure 12. Continued.

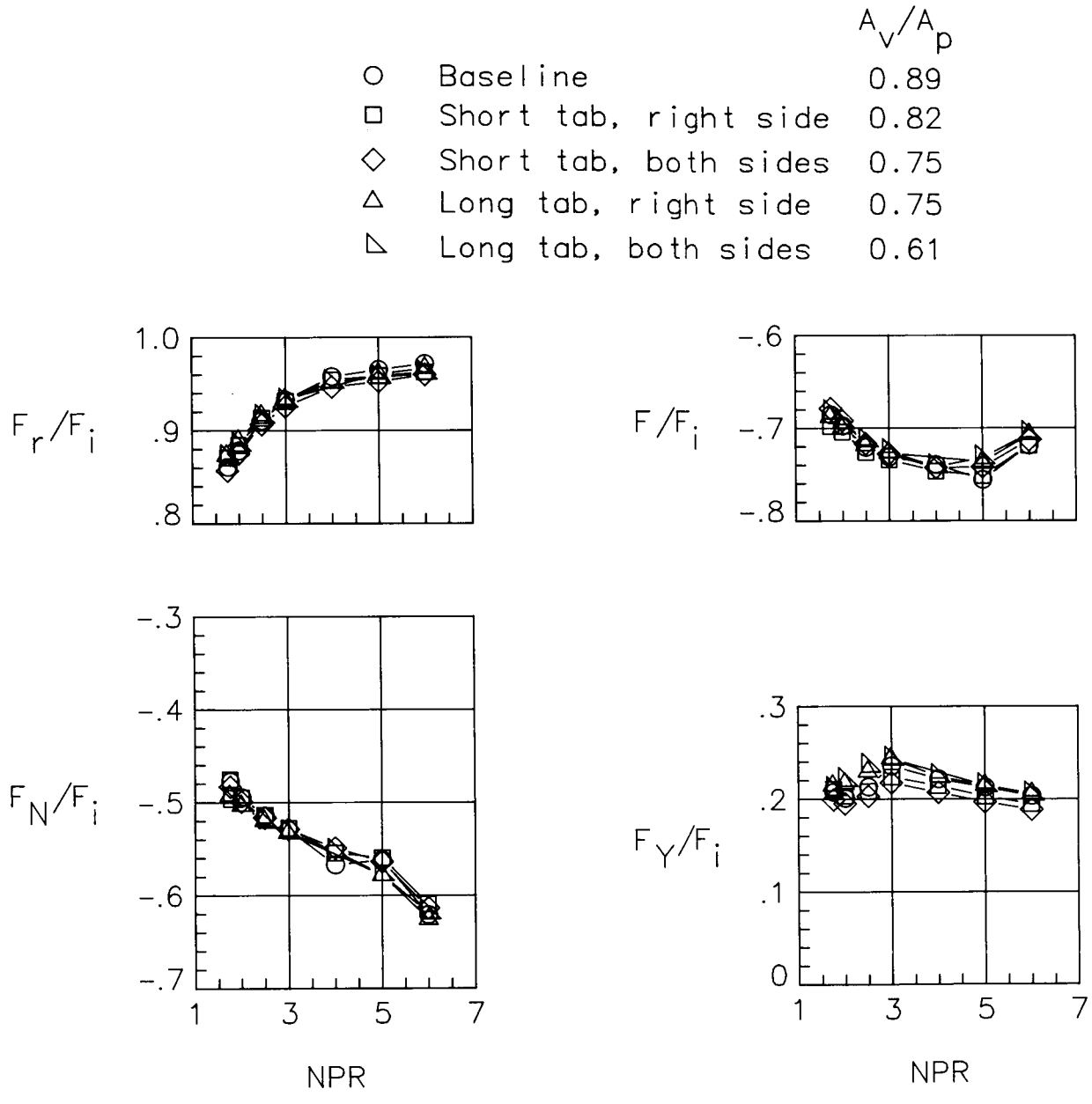

(e) Force data; top port.

Figure 12. Continued.

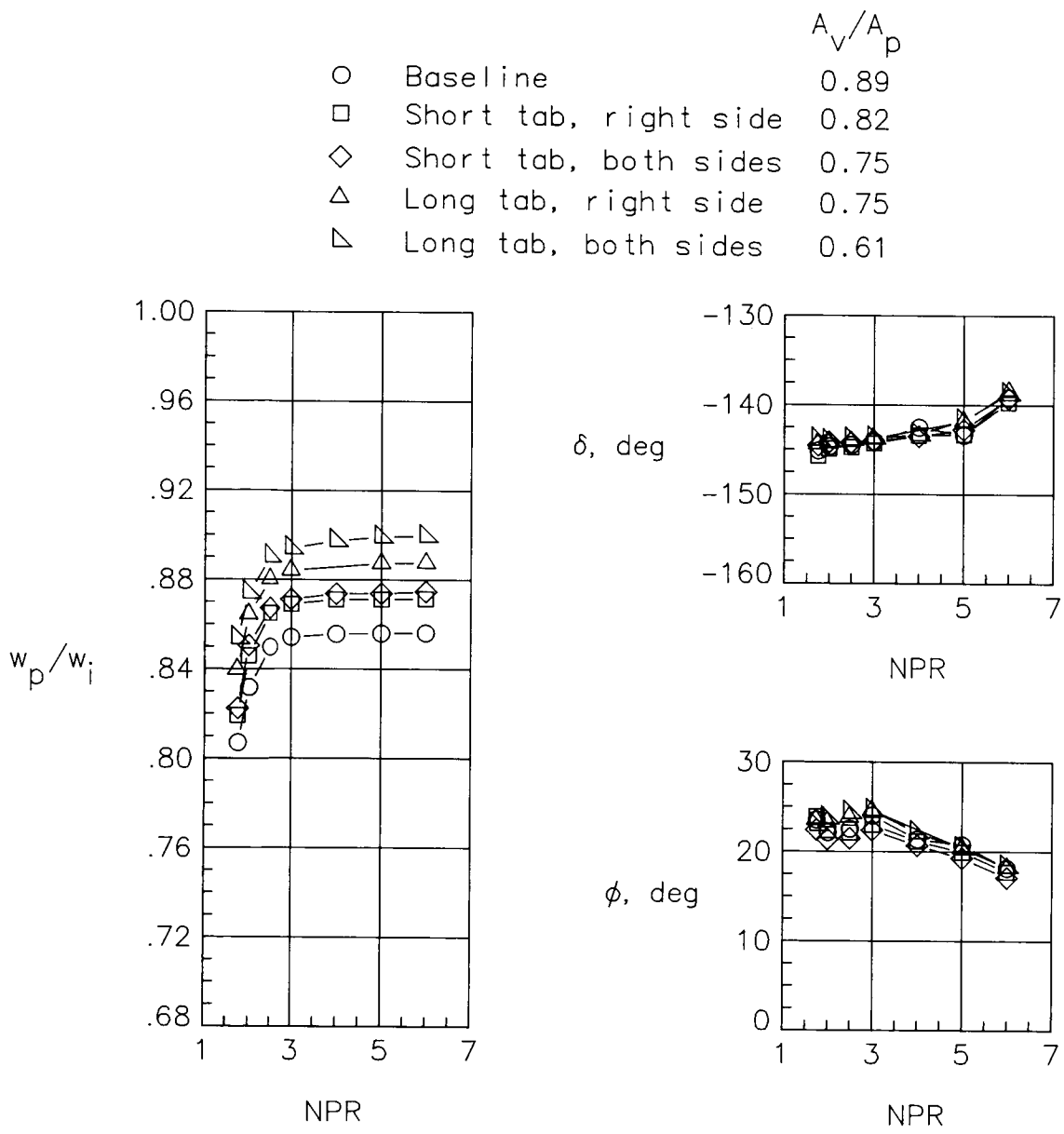

(f) Discharge coefficient and turning angles; top port.

Figure 12. Continued.

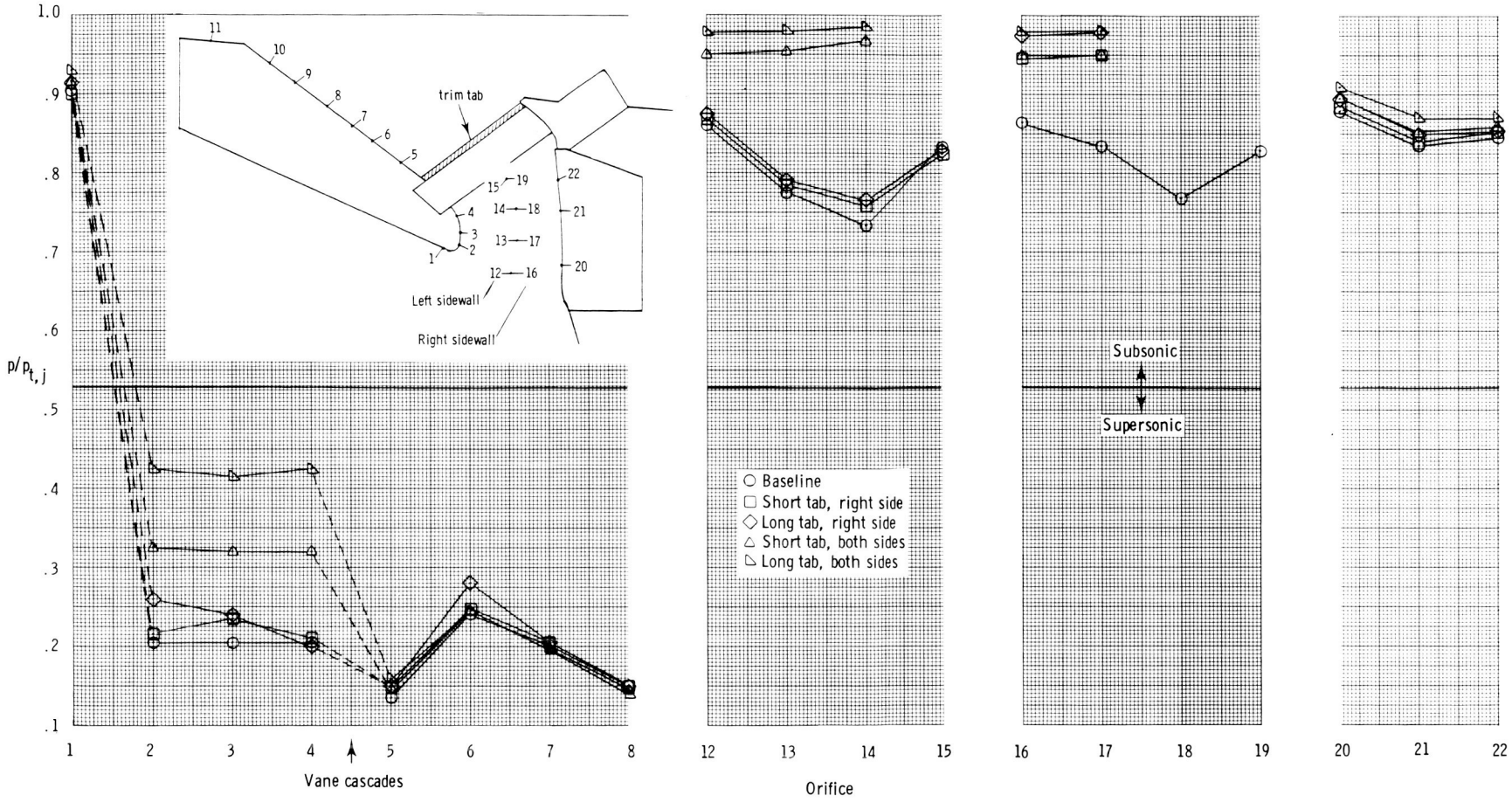

(g) Static pressures; NPR = 5.0.

Figure 12. Concluded.

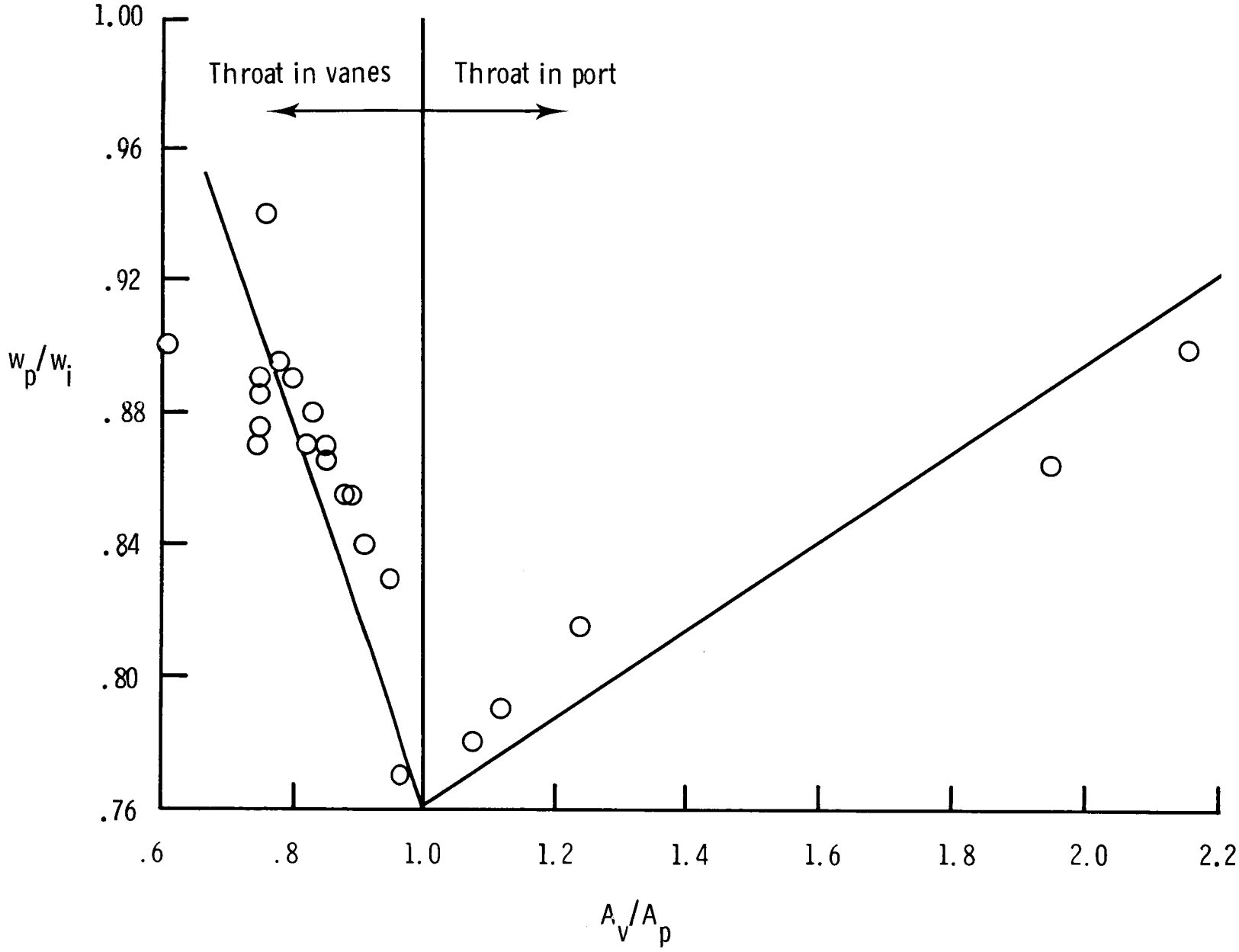

Figure 13. Effect of ratio of vane area to port area on discharge coefficient.

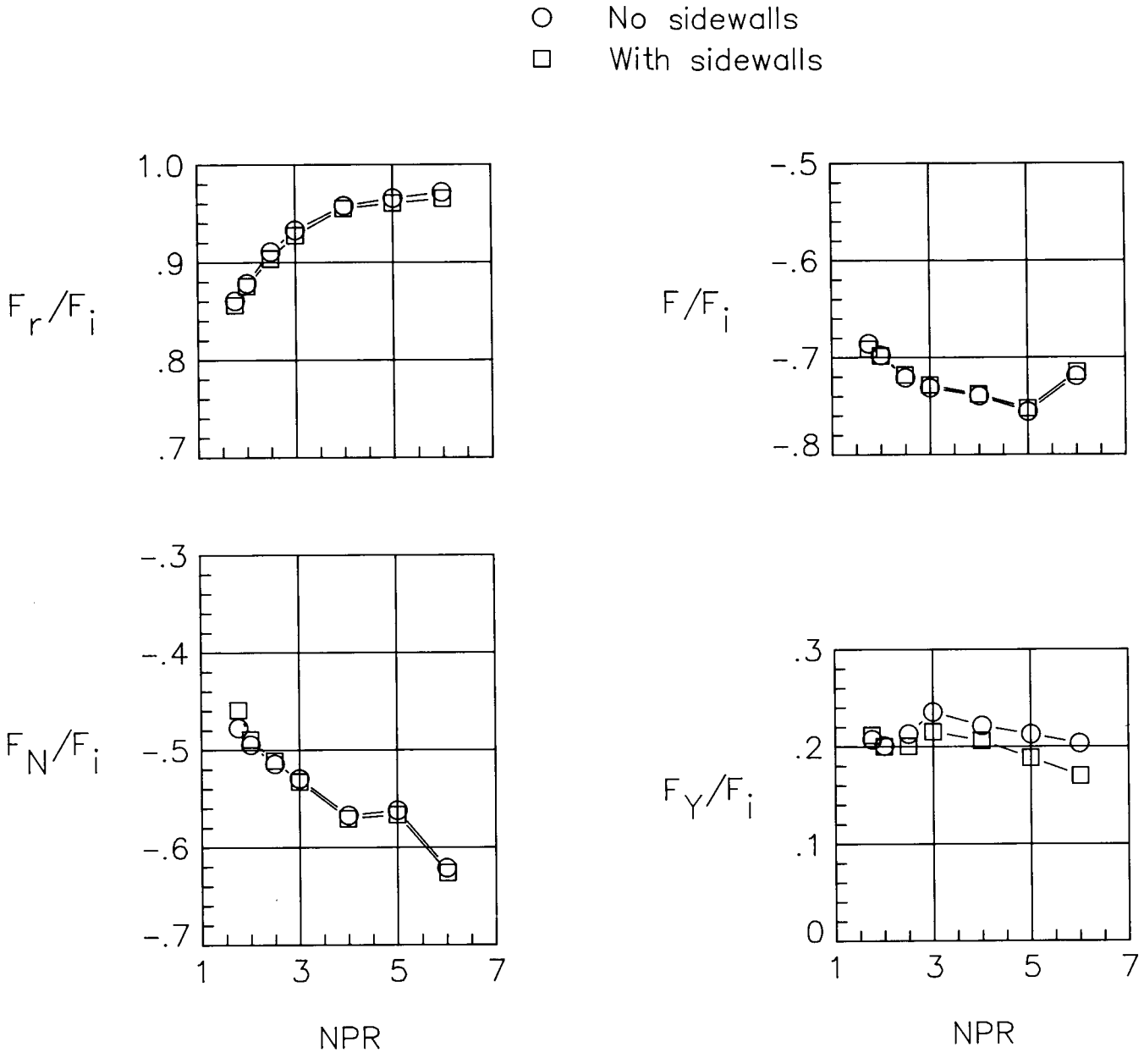

(a) Force data; top port.

Figure 14. Effect of sidewalls on basic performance with vane cascade A1.

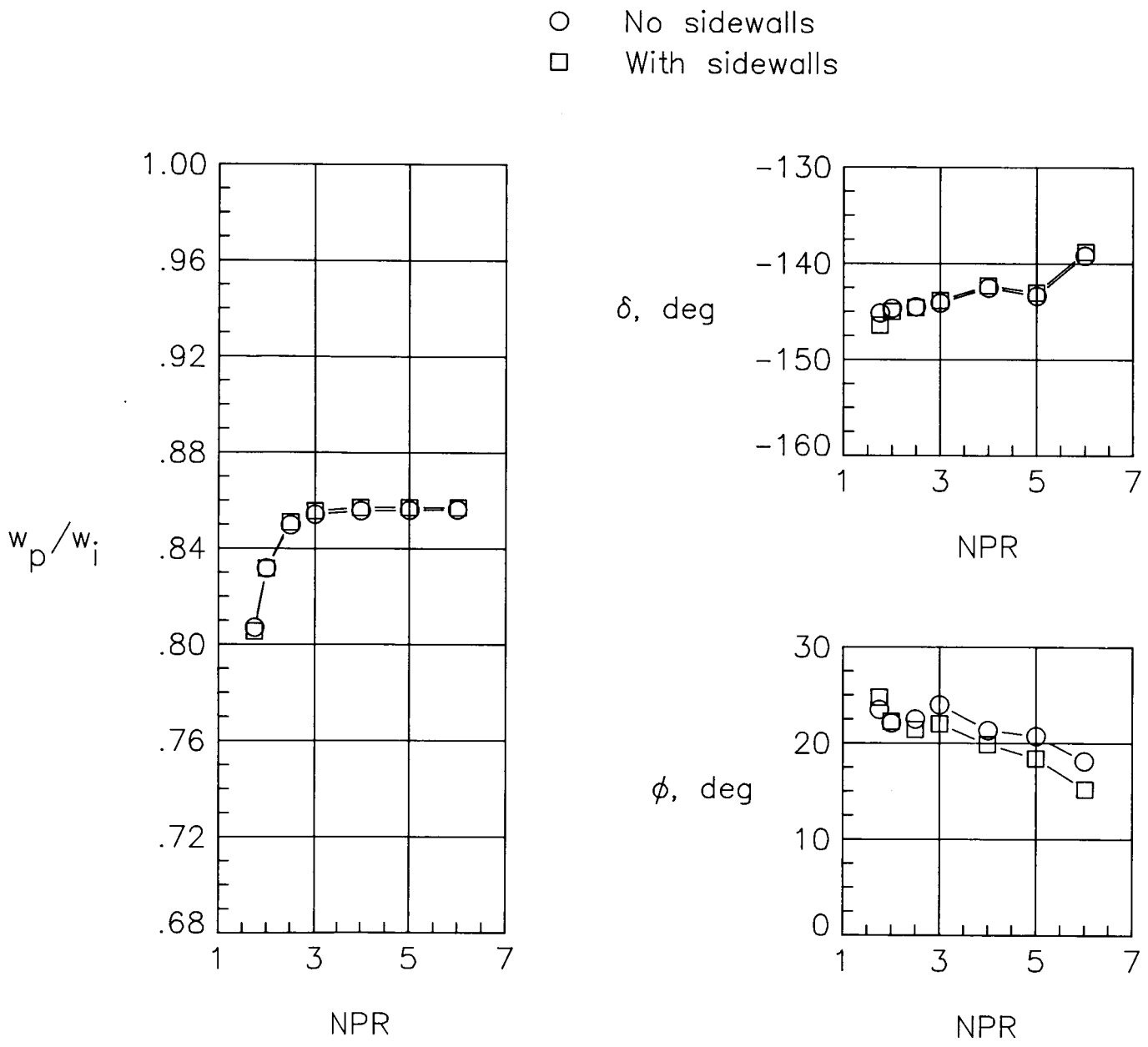

(b) Discharge coefficient and turning angles; top port.

Figure 14. Continued.

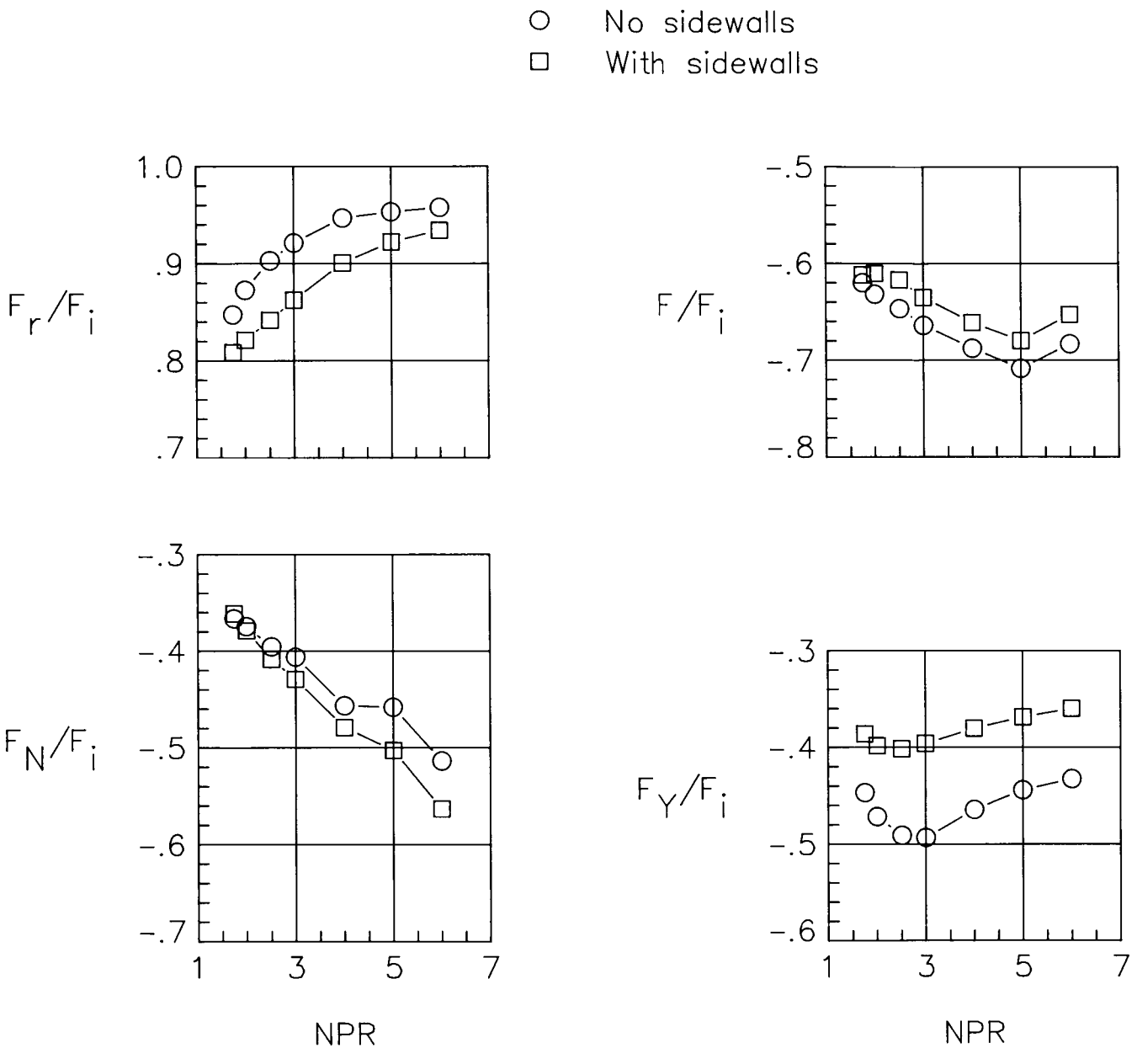

(c) Force data; bottom port.

Figure 14. Continued.

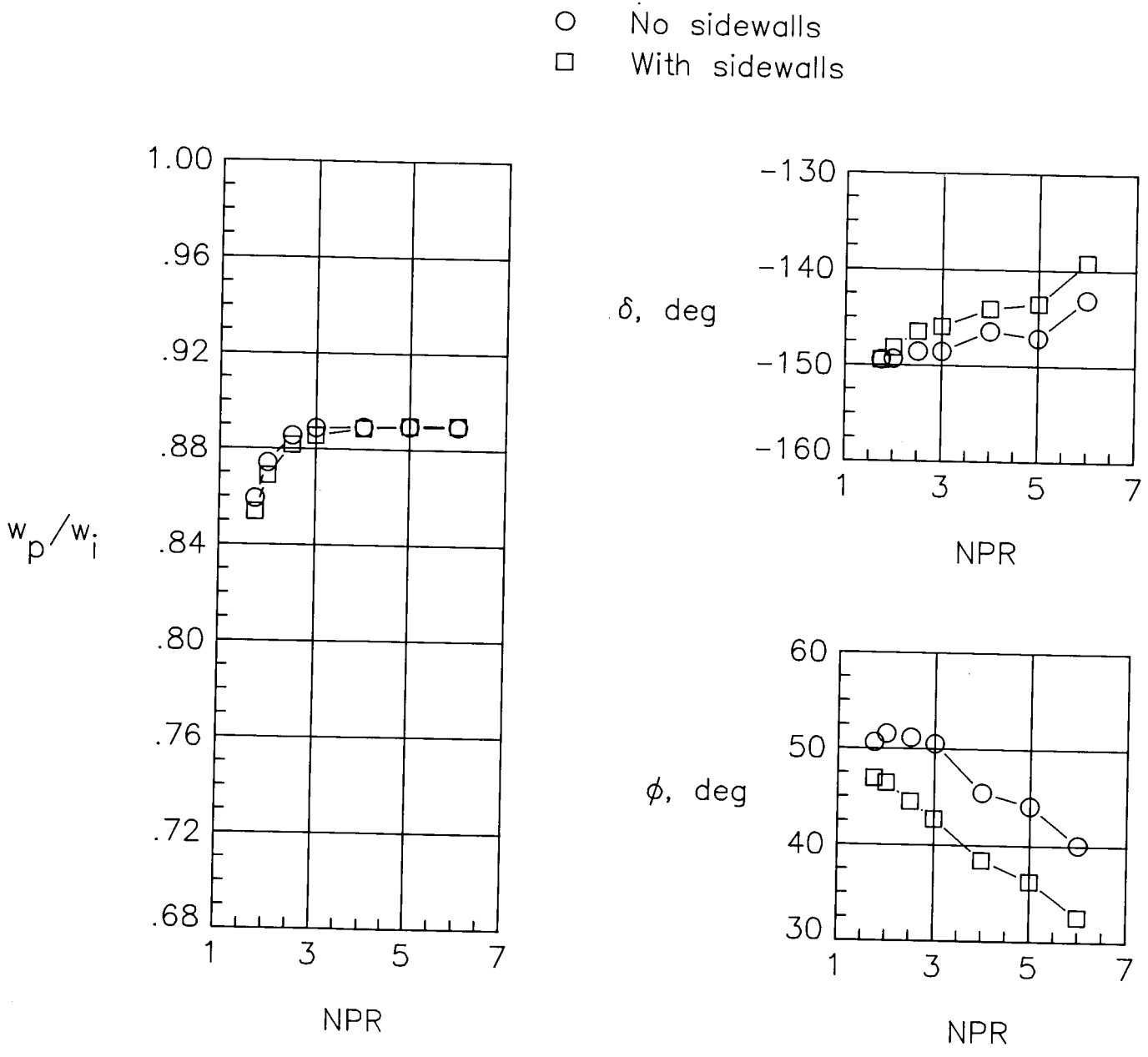

(d) Discharge coefficient and turning angles; bottom port.

Figure 14. Concluded.

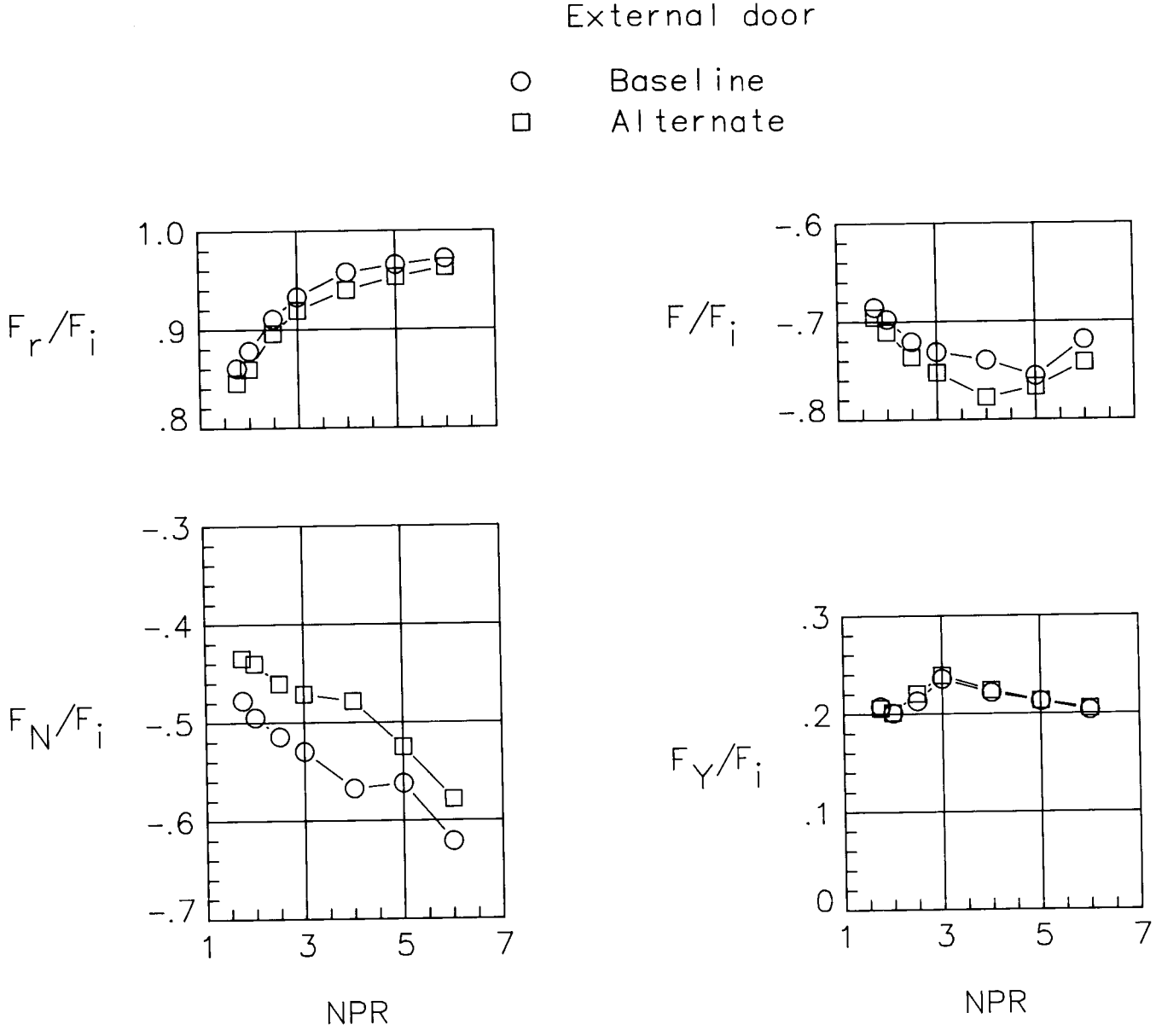

(a) Force data; top port.

Figure 15. Effect of outer door position on basic performance and vane cascade A1.

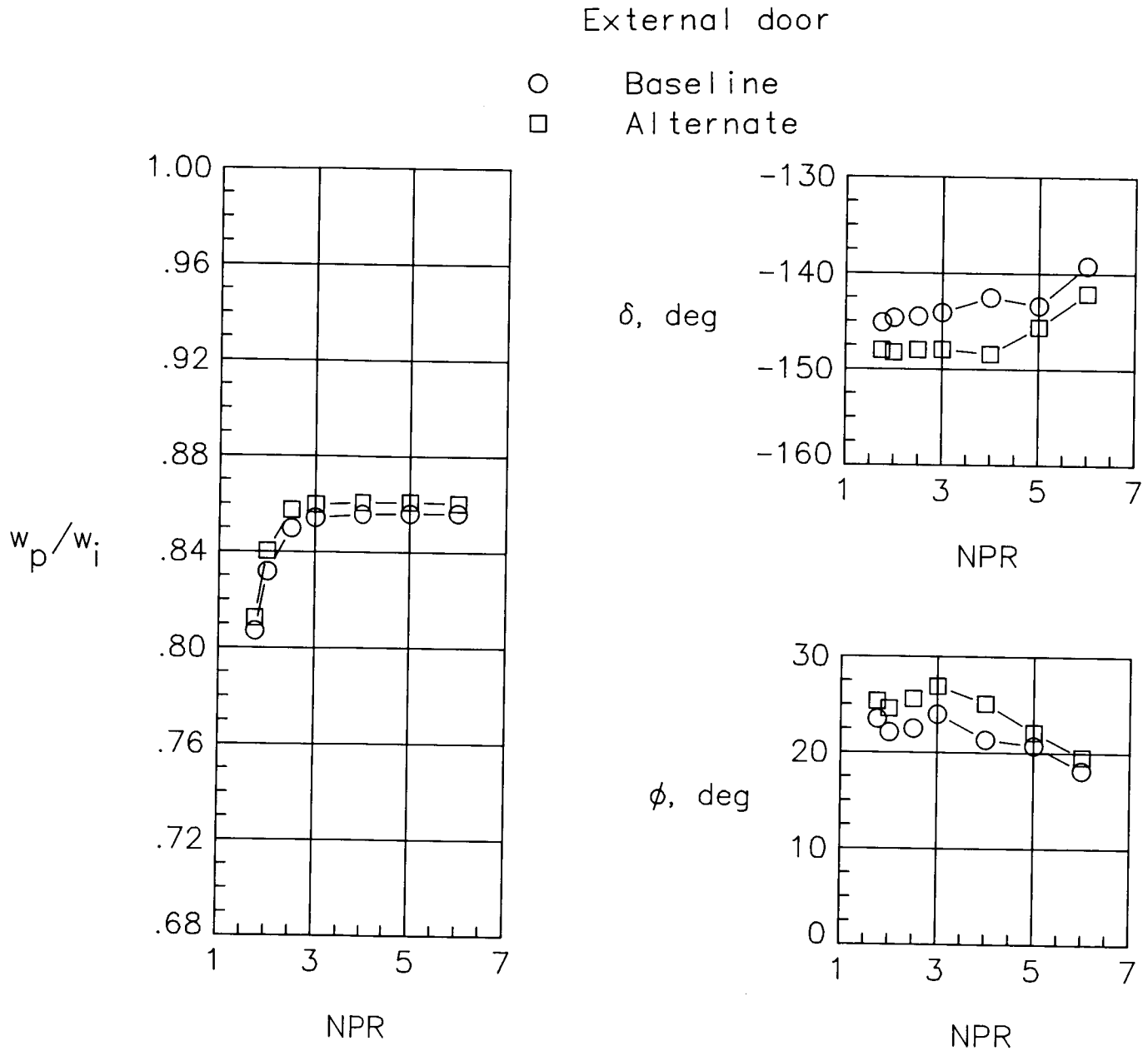

(b) Discharge coefficient and turning angles; top port.

Figure 15. Continued.

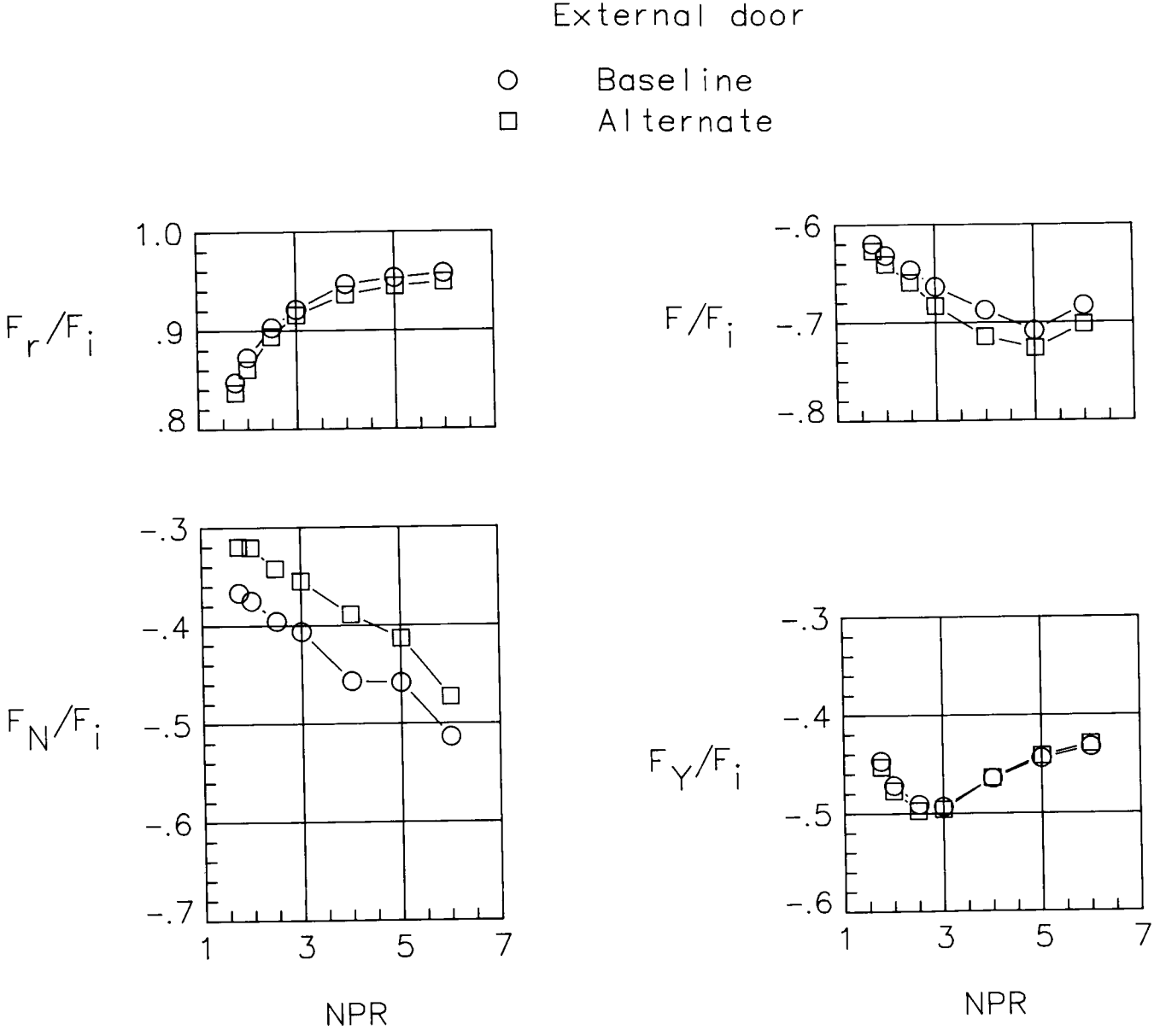

(c) Force data, bottom port.

Figure 15. Continued.

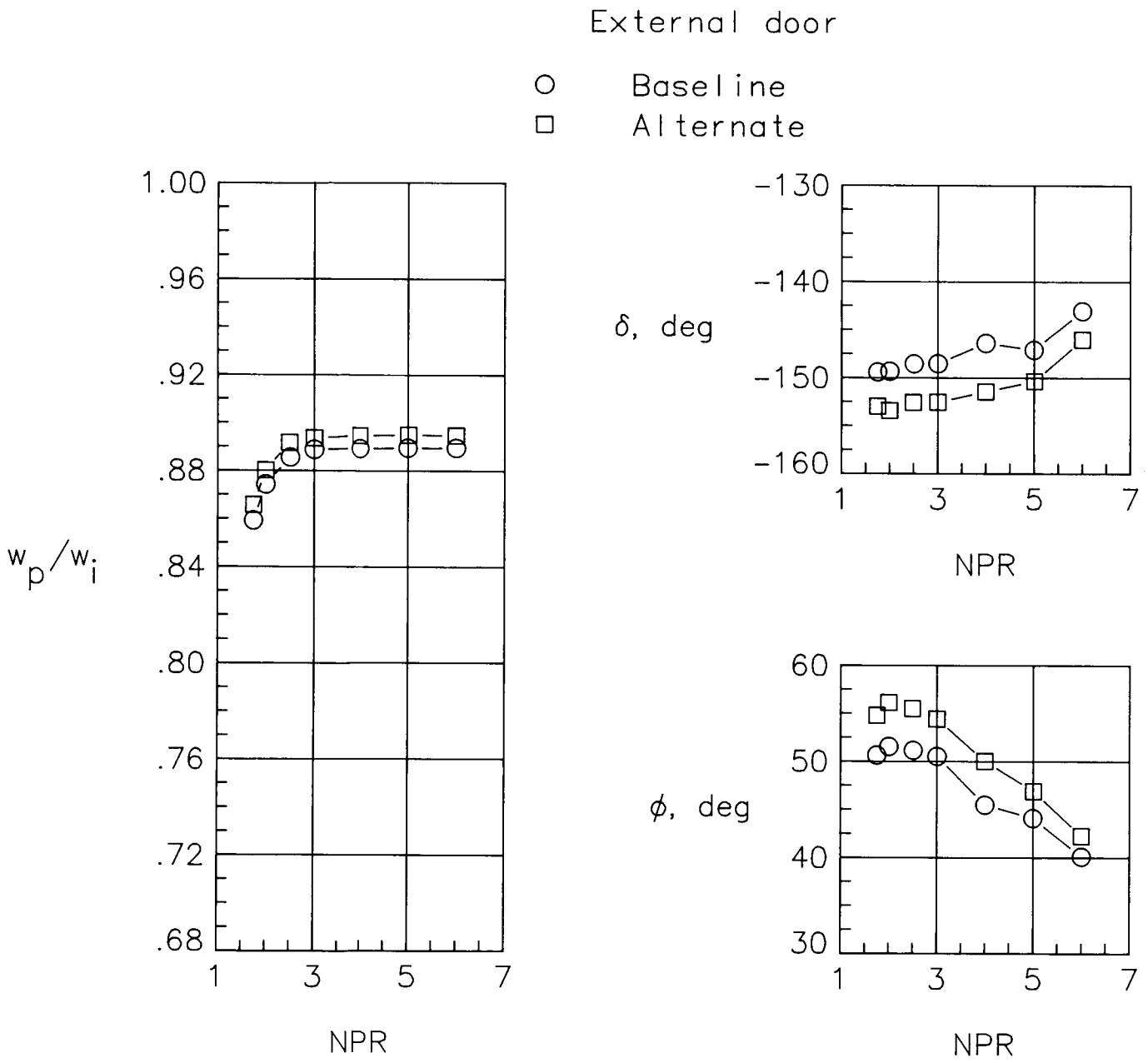

(d) Discharge coefficient and turning angles; bottom port.

Figure 15. Concluded.

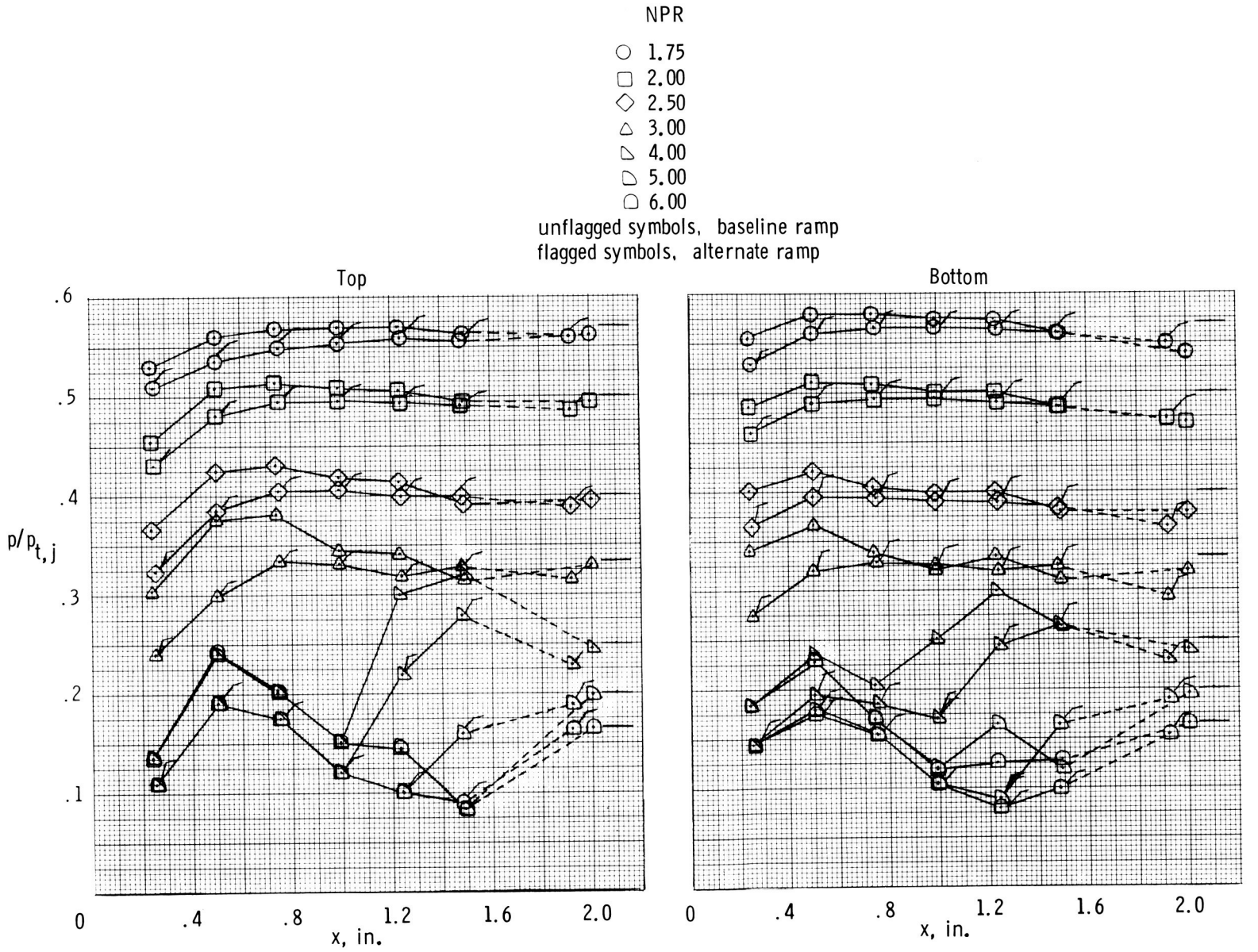

Figure 16. Effect of outer door position on static pressures. (See definition of x in fig. 4(h).)

NASA
National Aeronautics and Space Administration

Report Documentation Page

1. Report No.	2. Government Accession No.	3. Recipient's Catalog No.
NASA TP-2933		

4. Title and Subtitle	5. Report Date
Static Internal Performance of a Nonaxisymmetric Vaned Thrust Reverser With Flow Splay Capability	September 1989
	6. Performing Organization Code
7. Author(s)	8. Performing Organization Report No.
Linda S. Bangert and Laurence D. Leavitt	L-16552
9. Performing Organization Name and Address	10. Work Unit No.
NASA Langley Research Center Hampton, VA 23665-5225	505-62-71-01
	11. Contract or Grant No.
12. Sponsoring Agency Name and Address	13. Type of Report and Period Covered
National Aeronautics and Space Administration Washington, DC 20546-0001	Technical Paper
	14. Sponsoring Agency Code

15. Supplementary Notes

16. Abstract

An investigation was conducted in the static-test facility of the Langley 16-Foot Transonic Tunnel on a dual-port, nonaxisymmetric, block-and-turn type thrust reverser model with vane cascades in the reverser ports, which turned the flow in the splay direction and aided in turning the flow in the reverse direction. Splaying reverser flow is a method of delaying to lower landing ground roll speeds the reingestion of hot exhaust flow into the inlets. Exhaust flow splay can also help prevent the impingement of hot exhaust gases on the empennage surfaces when the reverser is integrated into an actual airframe. The vane cascades consisted of two sets of perpendicular vanes with a variable number of reversing and splaying vanes. A skewed vane cascade was also tested which had only one set of vanes angled to provide both reversing and splay. Vane cascades were designed to provide different amounts of flow splay in the top and bottom ports. Inner doors, trim tabs, and an orifice plate all provided means of varying the port area for reverser flow modulation. The outer door position was varied as a means of influencing the flow reverse angle. Nozzle pressure ratio was varied from 1.75 to approximately 6.00.

17. Key Words (Suggested by Authors(s))	18. Distribution Statement
Nonaxisymmetric nozzles Thrust reversers Internal flow Splay vanes Vaned reversers	Unclassified—Unlimited Subject Category 02

19. Security Classif. (of this report)	20. Security Classif. (of this page)	21. No. of Pages	22. Price
Unclassified	Unclassified	87	A05

For sale by the National Technical Information Service, Springfield, Virginia 22161-2171